HAMZA SHAFIQ
SUPERVISORS: YANYAN SHA (UNIVERSITY OF STAVANGER)
STIAN LALAND RASMUSSEN (IKM OCEAN DESIGN)

University of Stavanger

Dragged Anchors Interaction with Subsea Pipelines

Master Thesis, Spring 2024

Structural & Mechanical Engineering

Faculty of Science and Technology

Department of Mechanical and Structural Engineering and Materials Science

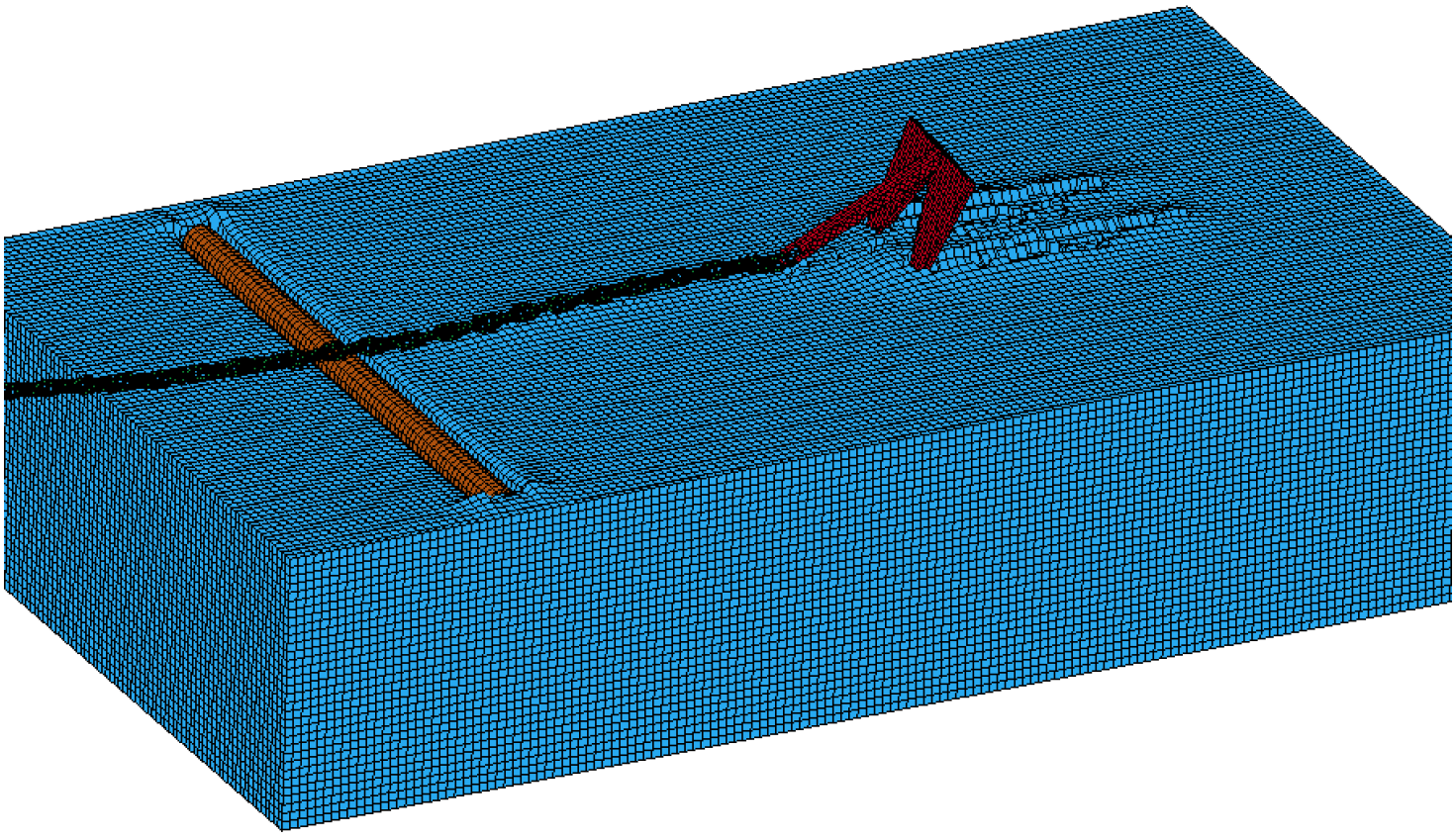

Abstract

Due to the extensive exploration of oil and gas reservoirs beneath the seabed, the installation of offshore oil and gas production systems has significantly increased. This surge necessitates an extensive network of pipelines on the seabed to transport crude oil and gas efficiently. Simultaneously, cargo ships and other vessels remain the most cost-effective means for bulk transportation of goods. According to *PARLOC 2001: The Update of Loss of Containment Data for Offshore Pipelines (Ltd et al., 2003)* there have been 44 recorded instances of interactions between anchors and subsea pipelines. These interactions underscore the critical need to study the dynamics of such interactions and explore preventive measures. One such measure is the use of rock berms to protect subsea pipelines and cables, offering a potential solution to mitigate the risks associated with anchor dragging incidents.

The scope of this thesis encompasses the development of a numerical model to comprehensively investigate the interaction dynamics between anchors and pipelines on the seabed. Specifically, the study focuses on analyzing the response of a 20 inches outer diameter rigid pipe to the dragging action of 3 and 5 tonnes anchors at speeds of 2 and 10 knots. Additionally, this thesis aims to construct a numerical model to predict the efficacy of utilizing rock berms as a protective measure for subsea pipelines. Through these numerical simulations, the current thesis endeavors to provide insights into the behavior of subsea pipelines under varying conditions of anchor dragging.

A Finite Element Method (FEM) based numerical model was established to study anchor-pipeline interaction on the plain seabed by using a Lagrangian mesh within the LS-Dyna modeling and analysis tool. To address the challenge of large deformation in soil, element erosion criteria were integrated based on predefined strain limits. The analysis model employed segment-based contact physics within the LS-Dyna software, surface to surface contacts facilitated interactions between all rigid components and erosion-based contacts between rigid parts and the soil.

Analysis of the model revealed a direct correlation between anchor mass and penetration depth. The study examined two distinct soil types: loose soil and stiff soil. Results demonstrated that loose soil facilitated deeper penetration of the anchor compared to stiff soil, highlighting the influence of soil properties on anchor-soil interactions.

The parametric case study highlights the significant impact of the dragged anchor's attack angle with respect to pipeline, on the interaction mode (hooking, sliding, and bouncing over) between dragged anchor and pipe. Cases involving a 45 degrees angle of attack tend to result in sliding or bouncing over the pipeline post-impact, whereas a 90 degrees angle increases the likelihood of hooking. Additionally, observations indicate that anchors dragging at 10 knots exhibit lower hooking probabilities compared to those at 2 knots.

This study explores literature associated with Smoothed Particle Hydrodynamics (SPH) and Discrete Element Method (DEM) numerical techniques for modeling seabed soil and rock berms, respectively. Extensive literature review and studies have been conducted to calibrate the rock berm dynamics using both DEM and Finite Element Analysis (FEA) methods, detailed in appendix.

Acknowledgement

I extend my sincerest gratitude to Professor Yanyan Sha for providing me with the invaluable opportunity to undertake this thesis. His unwavering support, guidance, and provision of essential resources have been instrumental throughout this endeavor.

Furthermore, I am deeply thankful to IKM Ocean Design for graciously providing me with the opportunity to immerse myself in a professional environment conducive to learning and growth. I am thankful to Stian Laland Rasmussen, Zhenguo Tu, and Moeen Nazari for their mentorship and unwavering support, as well as for furnishing the necessary data essential for the completion of this project.

My gratitude also extends to DYNAmore Nordic AB and Axel Hallen for their instrumental contributions. Their provision of initial training in LS-Dyna Software, coupled with ongoing support during my master's thesis, has been invaluable.

The simulations for this study were executed utilizing the resources of Sigma2, the National Infrastructure for High-Performance Computing and Data Storage in Norway (project number NN9721K). This support is gratefully acknowledged.

It is acknowledged that AI language models were utilized in this thesis to remove grammatical errors.

Table of Contents

List of Figures

List of Tables

Abbreviations

SDE: Spherical Discrete Element

DEM: Discrete Element Method

FEA: Finite Element Analysis

FEM: Finite Element Method

SPH: Smoothed Particle Hydrodynamics

CEL: Coupled Eulerian-Lagrangian

OD: Outer Diameter

LFRD: Load Factored Resistance Design

SLS: Serviceability Limit State Category

ULS: Ultimate limit state

FLS: Fatigue limit state

ALS: Accidental limit state

CEL: Coupled Eulerian-Lagrangian

EN: Equipment Number

EL: Equipment Letter

3D: Three Dimensional

w.r.t.: With respect to

1. Introduction

1.1 Motivation

According to the PARLOC (Ltd et al., 2003) database, 44 subsea pipeline accidents have been attributed to interactions with anchors. These incidents typically occur when ship captains are unaware of the presence of subsea pipelines or due to unsuccessful anchoring attempts. The outcomes of dragged anchor incidents can vary from minor to major, depending on the intensity of the interaction with pipelines, which, in turn, is influenced by the geometry and weight of the anchor. Major accidents can result in loss of life, harm to marine ecosystems, significant environmental damage, and economic losses, particularly considering that subsea pipelines often transport highly explosive hydrocarbons such as crude oil and gas.

As global exploration and extraction of crude oil and gas intensify, the demand for expensive subsea pipeline networks, essential for transporting hydrocarbons, correspondingly increases. This increased network density heightens the likelihood of interactions between anchors and pipelines. Therefore, it is imperative to conduct comprehensive studies on anchor-pipeline interactions and implement strategies to mitigate the probability of such incidents.

1.2 Objective

To comprehensively study the interaction between dragged anchors and subsea pipelines and to explore various scenarios, such as different angles of attack, speeds of dragged anchors, and burial conditions of pipelines. Additionally, investigating methods to protect pipelines, such as using rock berms.

1.3 Scope and limitations

Scope:

- Conduct a comprehensive literature review encompassing relevant research articles, thesis reports, and conference papers concerning anchor and subsea pipeline interactions.
- Establish a numerical model to study the interaction between dragged anchors and 20 inches outer diameter (OD) pipelines.
- Utilize CAD modeling techniques to create accurate representations of anchors and realistic chains.
- Develop numerical model within LS-Dyna software investigate the anchor-pipeline interaction.
- Conduct a parametric study investigating the interaction modes between anchors and pipeline, considering variables such as the angle of attack, anchor size, burial condition of the pipeline, and dragged anchor speed.

- Design rock berms and assess their effectiveness in protecting the pipeline from dragged anchors.

Limitations:

- **Pipeline Condition**: The study focuses on untrenched pipelines naturally settled with gravity, partially embedded in the seabed and subjected to flushing level w.r.t. seabed.
- **Soil Type**: The analysis is conducted using loose soil (sand) and stiff soil as the predominant soil type.
- **Anchor Size**: The investigation considered anchors of 3, 5, and 7.8 tonnes sizes.
- **Anchor Speed**: Anchor speeds of 2 and 10 knots are examined.
- **Pipeline**: This study is conducted using a 20 inches outer diameter (OD) fixed pipeline.
- **Mooring Chain Length**: This study involves mooring chains with a length of 14 meters (for 5 tonnes anchor).

1.4 Outline of thesis

Chapter 2: Theory and Background

This chapter presents a brief history of subsea pipeline accidents in the North Sea by using statistics from PARLOC (Ltd et al., 2003). It also covers relevant design codes, key sets of rules and design criteria as stipulated by DNV.GL.

Chapter 3: Literature Review

This chapter provides a concise literature review on anchor-soil-pipeline interactions. It explores various numerical methods applicable to the soil domain, numerical methods to design rock berms, and the test models required to calibrate these berms. Furthermore, it studies the FEA numerical method to investigate pipeline deformation under different conditions, particularly in relation to soil stiffness and burial depth.

Chapter 4: Methodology

It introduces numerical methods, detailing both mesh-based and mesh-independent methods employed in this study. Also, this chapter provides information about the physics behind the contact types utilized in the study's numerical model, ensuring accurate simulation of interactions between different components.

Chapter 5: Modeling and Analysis Setup

Chapter 5 explores the dynamics behind the soil material model used in this study to establish the seabed, specifically Mohr-Coulomb material model. Further it explains the numerical method used to design the anchor-pipeline interaction numerical model for analysis. Moreover, this chapter includes the standards

employed for the design of anchors and chains, and presents the 3D models for various parts, such as anchor, chain, rock berm, pipeline, and soil domain. It also details the boundary conditions implemented in the numerical models, ensuring near realistic circumstances. Further material properties for various parts and contact types used between parts are also discussed in this chapter.

Chapter 6: Results and Discussion

Chapter 6 discusses the mesh convergence of the soil domain, calibration, and validation of different numerical models, including pipe deformation and soil-anchor interaction. It examines the limitations associated with Lagrangian mesh fields and element erosion criteria. The chapter also analyzes the impact of dragged anchor on subsea pipelines at different speeds, angles of attack, and mooring chain inclination angles w.r.t. seabed. It also investigates the effect of anchor geometry on penetration depth in two different seabed soil types.

Chapter 7: Conclusion and Assumptions

This chapter summarizes the findings from the analysis models and outlines the assumptions made throughout the study and the analysis process.

Further Work Recommendations

This chapter offers the author's recommendations for further investigation, suggesting areas where additional research could enhance understanding and improve methodologies.

2. Theory and Background

2.1 Subsea Pipeline Accidents

In terms of the database pertaining to accidents in the North Sea, PARLOC 2001 (Ltd et al., 2003) stands out as a comprehensive resource providing detailed information about pipeline accidents. (Mustafina, 2015) compiled the data available in PARLOC 2001 and offered graphical representations of different accidents with clarity and detail in his master's thesis on the topic of "Anchor Damage Assessment of Subsea Pipelines - Optimization of Design Methodology".

An overview of the various incidents can be visualized through a flowchart (Figure 2.1) which indicates that out of a total of 542 incidents, 248 occurred under operational conditions. Further analysis reveals that out of these 248 incidents, 209 were associated with steel pipelines, while the remaining incidents were linked with flexible pipelines.

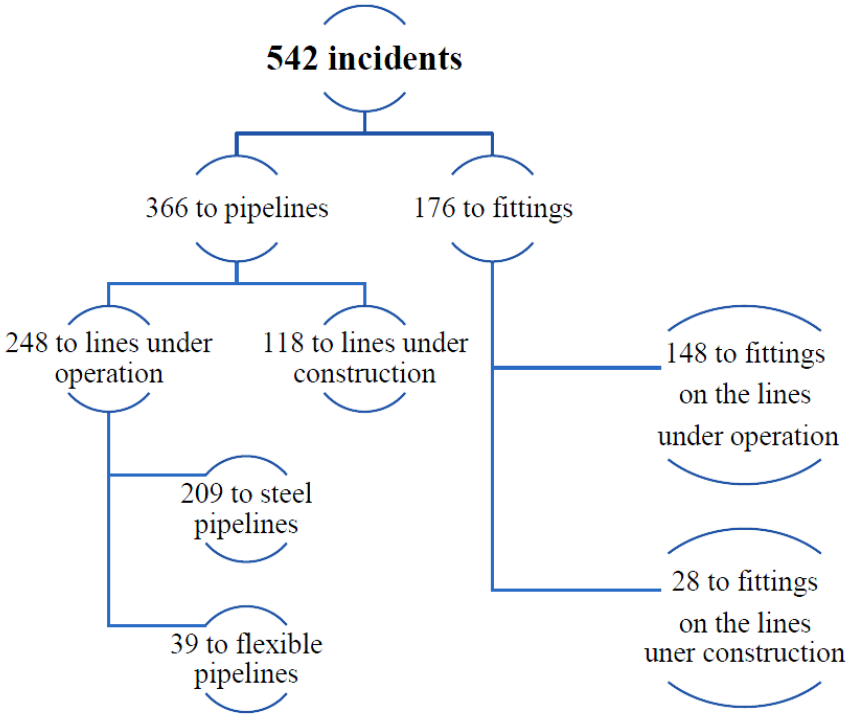

Figure 2.1: Accident database by PARLOC (Mustafina, 2015)

In (Mustafina, 2015) thesis, several detailed databases Figure 2.2 are provided, encompassing incidents involving anchors interaction with pipelines, dropped objects impact, and material failure due to corrosion. However, the focus of the present study is primarily on incidents caused by dragged anchor interaction with subsea pipelines. In A. Mustafina's work these incidents are analyzed and discussed in greater detail, shedding light on the specific challenges and implications associated with anchor-related accidents in subsea environments. Figure 2.2 illustrates that for steel pipelines, the majority of incidents were caused by impacts and anchors. This underscores the necessity of studying the interaction between

anchors and subsea pipelines and exploring strategies to mitigate the risk of such incidents in the future. Understanding how anchors interact with subsea pipelines is crucial for developing effective measures to protect pipelines and minimize the occurrence of accidents.

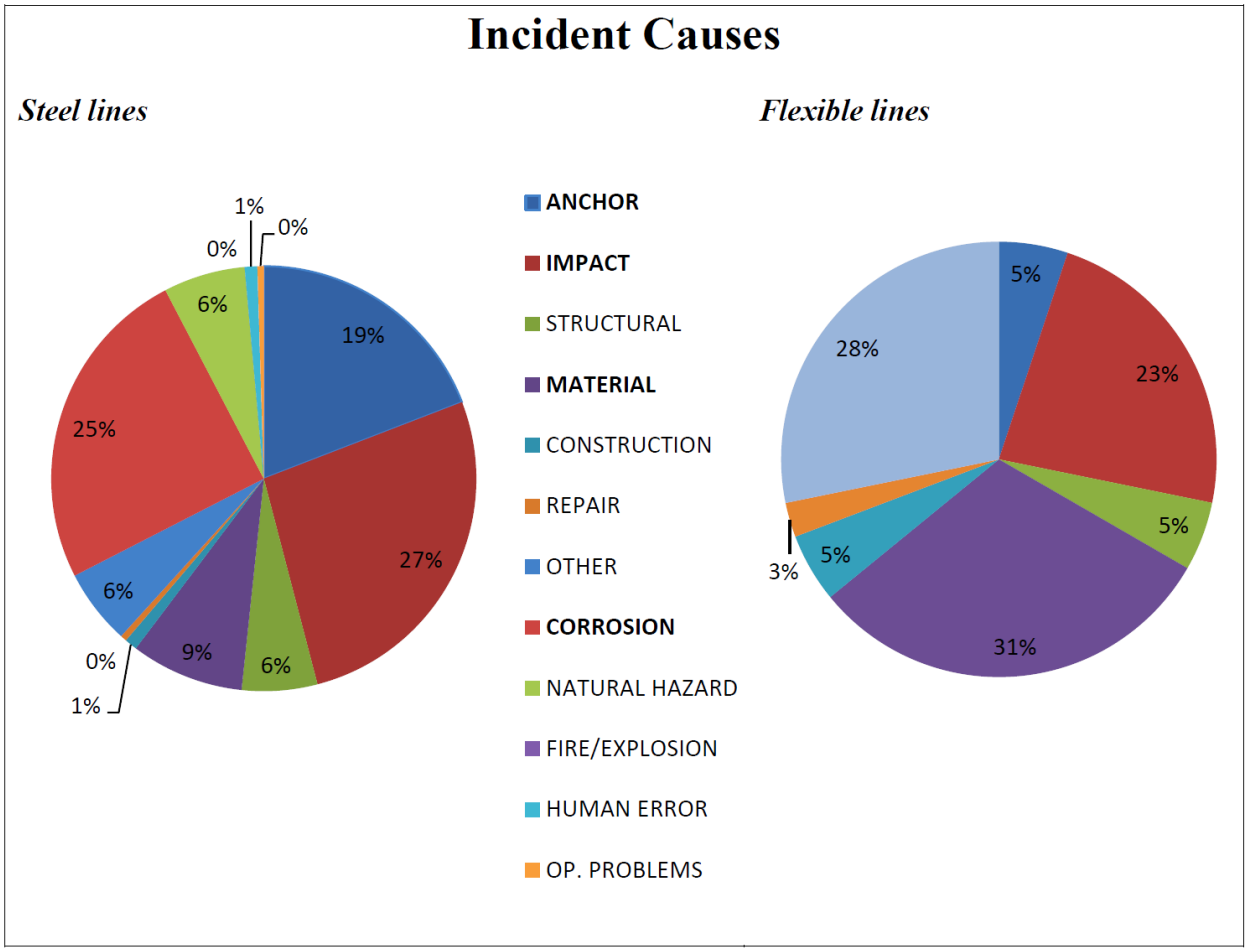

Figure 2.2: Incident causes database by PARLOC (Mustafina, 2015)

2.2 DNV.GL Recommended Practices and Standards

DNV.GL offers four distinct sets of recommended practices and standards for pipeline and subsea structures. Firstly, DNV-OS-F101 (Standard, 2013) establishes design limit states and scenario classifications for subsea pipelines, ensuring their security through a safety class methodology and limit state design. Secondly, DNV-OS-E301 (Standard, 2018) focuses on position mooring, categorizing anchors based on ship class to provide guidelines for anchor system design and classification. Thirdly, DNV-RP-F111 (Standard, 2014) outlines practices for minimizing risks associated with the interaction between trawl gear and subsea pipelines, covering aspects of design, installation, and operation. Lastly, DNV-RP-F107 (Standard, 2010) offers guidance on risk assessment pertaining to pipeline protection, addressing factors such as corrosion protection, coating, and cathodic protection systems.

The offshore standard for submarine pipelines and systems, described in DNV-OS-F101 (Standard, 2013), establishes criteria and recommendations for the conceptual development, design, construction,

operation, and abandonment of underwater pipelines. This standard ensures the security of pipelines below sea level by applying a safety class methodology and limit state design. It dictates the loads to be checked under limit states, requiring the examination of extreme and critical load values for all operational conditions and states. There are four primary types of loads that can affect pipelines: functional, environmental, interference, and accidental.

Accidental Load: These are unplanned and abnormal loads that are unpredictable. However, they have minimal probability of occurrence, typically around 10^{-2}.

Functional Load: This refers to the load expected on the system due to operational conditions.

Interference Load: These loads are imposed by third parties, such as those applied by trawling, falling objects, anchor hooking, or vessel impacts on the pipelines.

Environmental Load: This refers to loads applied by boundary conditions under certain environmental circumstances, such as deepwater pressure or sea waves.

There are two methods for designing a system against accidental loads: direct and indirect. Direct design involves dealing with exact values for the load, while indirect design considers tolerance for the accidental load.

Load Factored Resistance Design (LFRD) is a fundamental design principle within DNV standards, enabling designers to assess the pipeline's load-bearing capacity effectively. This principle ensures that the pipeline can withstand various loads, with the magnitude of the load effect contingent upon the chosen limit state. DNV standards recognize two primary types of limit states for pipeline design:

- Serviceability Limit State Category (SLS)
- Ultimate limit state (ULS)
    - Fatigue limit state (FLS)
    - Accidental limit state (ALS)

The determination of appropriate load effect factors relies on the specific limit state selected for the pipeline design, with detailed information provided by reference DNV-OS-F101 (Standard, 2013) illustrating the relationship between state limits and corresponding scenarios, as depicted in Table 2.1.

Table 2.1: Scenario vs limit state (Standard, 2013)

	Ultimate Limit State						**Serviceability Limit State**			
Scenario	**Bursting**	**Fatigue**	**Fracture**	**Collapse**	**Propagating buckling**	**Combined loading**	**Dent**	**Ovalisation**	**Ratchet**	**Displacement**
Wall thickness design	X			X	X					
Installation		X	X	X	X	X		X		X
Riser	X	X	X	X	X	X		X		X
Free span	X	X	X			X				
Trawling/3rd party	X	X				X	X			
On bottom stability	X	X	X			X	X	X		X
Pipeline Walking		X				X				
Global Buckling	X	X	X			X			X	

The formulation for the design and principle load effect is given by Equation 2.1 (Standard, 2013).

$$f((\frac{L_{Sd}}{R_{Rd}})_i) \leq 1 \tag{2.1}$$

Where:

R_{Rd} = Design Resistance

L_{Sd} = Design Load

Design load value must never exceed the design resistance value to ensure the safety and integrity of designed pipelines.

Equation 2.2 provides the formulation for the R_{Rd} design resistance value.

$$R_{Rd} = \frac{R_c(f_c t_c, f_0)}{\gamma_m \gamma_{SC}} \tag{2.2}$$

Where:

R_C = Characteristic resistance

f_c = Characteristic material strength

t_c = Characteristic thickness

f_0 = Initial ovality

$\gamma_m\gamma_{SC}$ = Partial resistance factor, depends on material and safety class

$$L_{Sd} = L_F\gamma_F\gamma_c + L_E\gamma_E + L_I\gamma_F\gamma_c + L_A\gamma_A\gamma_c \quad (2.3)$$

Equation 2.3 defines the design load, which relies on the combination of load effects multiplied by the load effect factor, dictated by the chosen limit state for pipeline design. These load effect factors, adapted to the scenario, are guided by provided guidelines, as depicted in Table 2.1. The load effects are the output cross sectional load in pipeline resultant of applied load.

Where:

L_F = Functional load effect

L_E = Environmental load effect

L_I = Interference load effect

L_A = Accidental load effect

γ_F = Functional load effect factor

γ_E = Environmental load effect factor

γ_I = Interreference load effect factor

γ_A = Accidental load effect factor

γ_c = Seabed topology factor

In cases where direct guidelines are absent, such as anchor hooking with the pipeline, the scenario is considered an interference load, akin to trawling. However, due to the low probability of anchor hooking incidents, it may also be interpreted as an accidental load (Pettersen et al., 2017).

Engineers may opt for either a direct or indirect design approach, each with its distinct methodology. The direct approach involves precise consideration of extreme design values, ensuring a robust safety margin. Conversely, the indirect approach employs a tolerance method during the design procedure, accommodating uncertainties in the operational environment (Pettersen et al., 2017).

3. Literature Review

3.1 Anchor Interaction with Soil and Pipeline

(Bartolini et al., 2018) investigated the interaction dynamics between dragged anchors and subsea pipelines through two distinct modeling methodologies: a simplistic global analysis and an advanced finite element (FE) analysis incorporating detailed local studies of anchor-soil interaction. Figure 3.1 elucidates the disparity between the simplified and advanced FEA models utilized in this study.

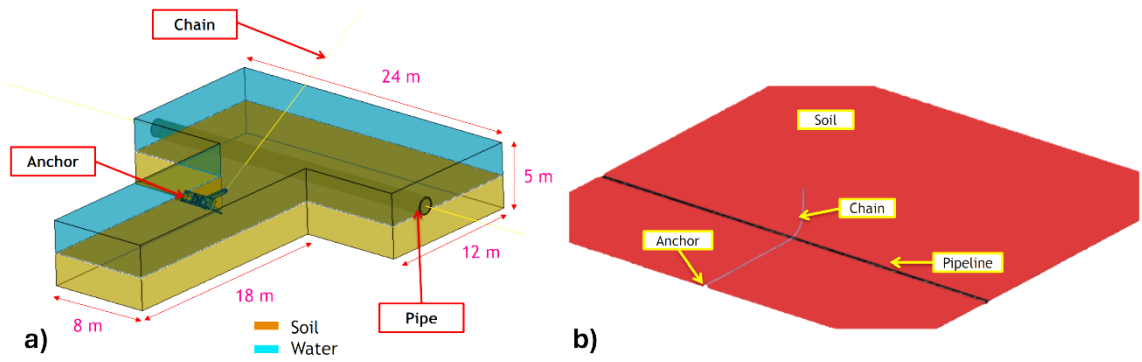

Figure 3.1:Models used by L. Bartolini, a) Advance FEA model, b) simplified numerical model (Bartolini et al., 2018)

An advanced CEL (Coupled Eulerian-Lagrangian) technique is utilized by using Abaqus analysis tool in advance FEA model (Figure 3.1(a)). The Drucker-Prager material model is used for the soil elements which also depicts the cap plasticity behavior of the soil (Bartolini et al., 2018).

A spectrum of anchor speeds of 1, 5, and 10 meters per second and interaction angles 30 and 90 degrees between the anchor and pipeline is scrutinized to encompass various scenarios. Moreover, anchor weights corresponding to different ship classes are employed to discern the influence of anchor geometry on subsea pipelines. The advanced FEA model in this article incorporates both soft and hard soil types, with undrained shear strength ranging from 1-10 (kPa).

Findings underscore the paramount importance of anchor geometry regarding ship class on pipeline hooking incidents. Specifically, ship class 5, coupled with a 90 degrees angle of attack between anchor and pipe, reveals notable hooking occurrences across different soil types at varying speeds.

This study offers invaluable insights into the complex interplay between dragged anchors and subsea pipelines, affirming the significance of adopting advanced FEA modeling techniques for robust analysis. The discernment of anchor-soil interaction dynamics and its correlation with anchor geometry elucidates crucial considerations for mitigating pipeline integrity risks in offshore environments.

In the conference proceeding (Wang et al., 2009), a comprehensive exploration of pipeline protection strategies utilizing a homogeneous rock berm is conducted. Employing a Lagrangian mesh coupled with damage criteria for elements, the study meticulously simulates anchor-soil interaction dynamics,

ensuring precise representation of behavior. Various configurations of rock berm were positioned around the pipeline, facilitating analysis to ascertain instances of anchor hooking or collision. Figure 3.2 illustrates the analysis model overview, encapsulating the sophistication of the employed methodology.

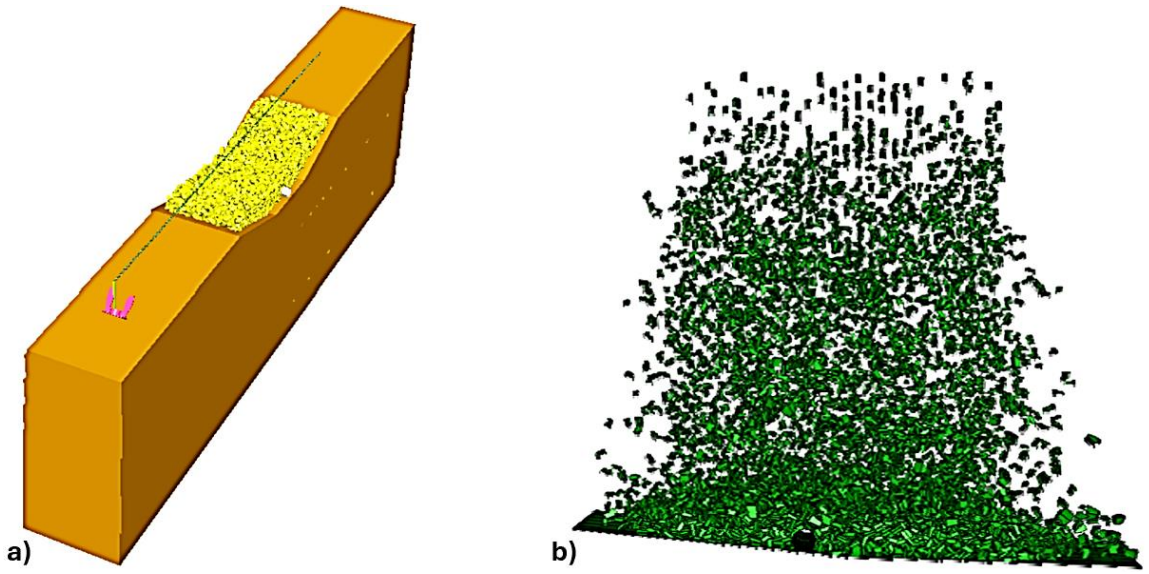

Figure 3.2: a) Analysis model used by L. Wang to study the rock berm efficacy against dragged anchors, b) rock dumping with help of gravity (Wang et al., 2009)

A consistent anchor speed of 2.5 meters per second is applied across diverse simulation scenarios. The utilization of soft clay substrate, characterized by an internal friction angle of 32°, 4 kPa cohesion, and an elastic modulus of 5 MPa, supplements the reliability of the analyses. Additionally, this conference proceeding advocates for a clearance of 300mm between subsea pipelines and dragged anchors, a critical parameter for optimal pipeline protection (Wang et al., 2009).

Notably, this study underscores the necessity of incorporating element erosion criteria when employing Lagrangian mesh in models characterized by high deformation. Figure 3.2 distinctly depicts the gravity-assisted deposition of the rock berm, representing the practical implementation of the proposed protection strategy.

Ultimately, this conference proceeding elucidates that FEA serves as a powerful tool for engineers to predict the impact of dragged anchors on pipelines fortified with rock berm protection. Furthermore, achieving an 800mm clearance between pipelines and dragged anchors surpasses the stipulated requirement of 300mm (Figure 3.3), affirming the efficacy of the proposed protective measures in ensuring pipeline integrity.

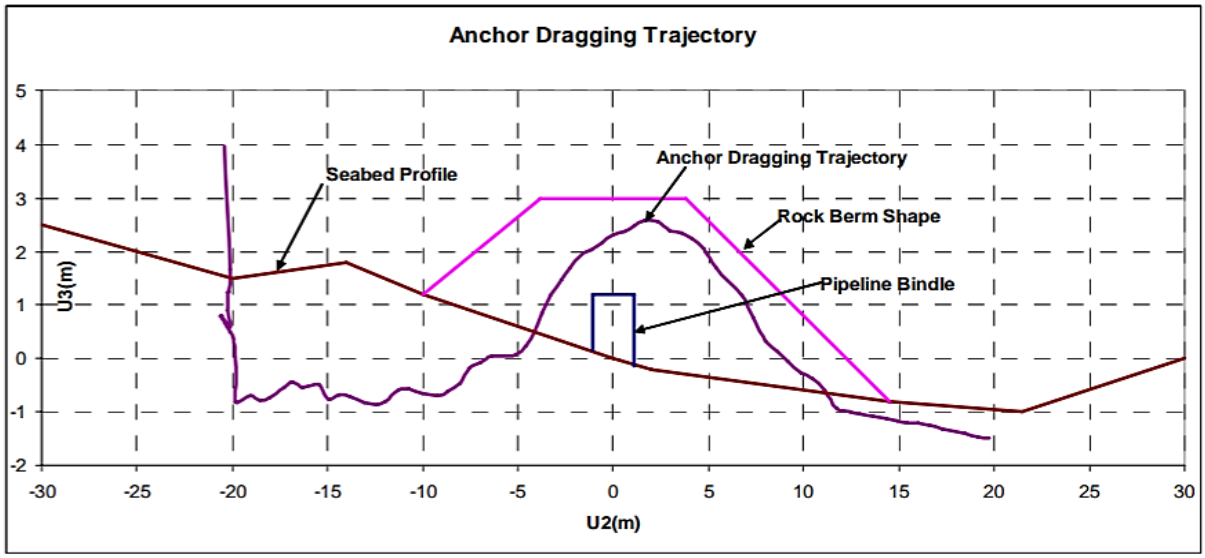

Figure 3.3: Anchor Dragging Trajectory (Wang et al., 2009)

(Selker et al., 2018) elucidated, as depicted in Table 3.1 and Figure 3.4, that the depth of the pipeline within the soil bed significantly influences its vulnerability to anchor-induced forces. Deeply buried pipelines are shown to be more susceptible to damage, as they absorb greater forces exerted by hooked anchors. This finding underscores the critical importance of considering pipeline burial depth as a key factor in mitigating the risks associated with anchor-pipeline interactions.

Table 3.1: Parametric study to investigate burial depth (Selker et al., 2018)

Case No.	Pipe Burial
1	1 m cover
2	flush
3	half-buried
4	on-seabed

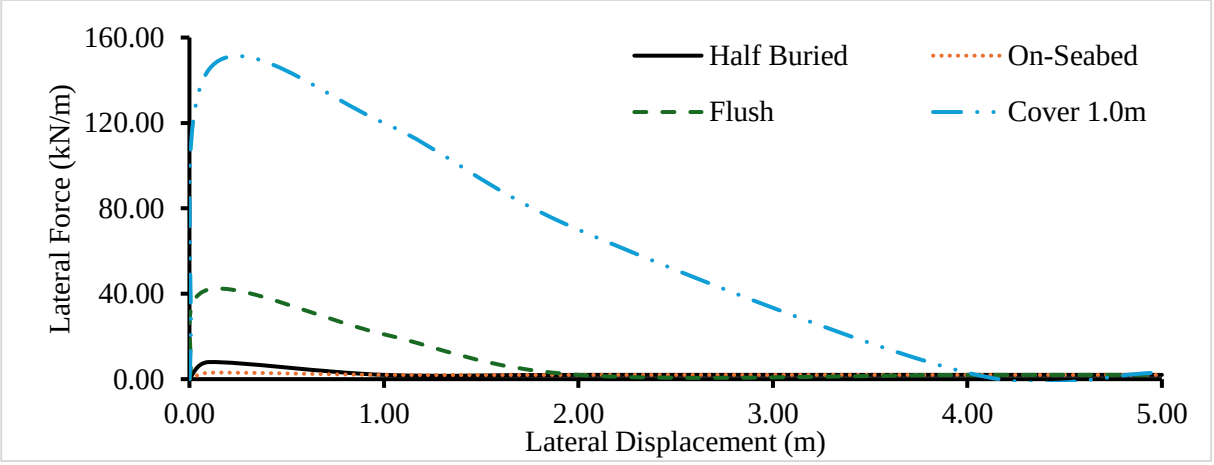

Figure 3.4: Forces absorbed by pipeline vs displacement (Selker et al., 2018)

In the investigated article (Selker et al., 2018), the significance of soil elastic stiffness in mitigating impact forces on pipelines is underscored. It is interpreted that soft soil exhibits a greater capacity to absorb impact energy compared to hard soil. Through the analysis of six distinct soil types, 5-230 kPa undrained shear strength (Table 3.2), predominantly clay-based soil, the research explores the varying effects of soil stiffness on pipeline damage resulting from impacts (Figure 3.5). This comprehensive examination highlights the pivotal role of soil characteristics in influencing the magnitude of forces transmitted to the pipeline during anchor interactions, emphasizing the necessity of accounting for soil properties in risk assessment and mitigation strategies for subsea pipelines.

Table 3.2: Seabed soil (Clay) (Selker et al., 2018)

Soil *ID*	***E* (MPa) 0 *m* / 15 *m***	***v***	***S_u* (kPa) 0 *m* / 15 *m***	***Y_{sat}* (kg/m³)**
S1	1.5 / 10.5	0.4995	5 / 35	1700
S2	4.5 / 13.5	0.4994	15 / 45	1700
S3	7.5 / 16.5	0.4992	25 / 55	1700
S4	15.0 / 24.0	0.499	50 / 80	1700
S5	30.0 / 39.0	0.498	100 / 130	1700
S6	60.0 / 69.0	0.497	200 / 230	1700

In the table above *E, v,* S_u, and Y_{sat} presents elastic stiffness, Poisson's ratio, undrained shear strength, and saturated soil density respectively.

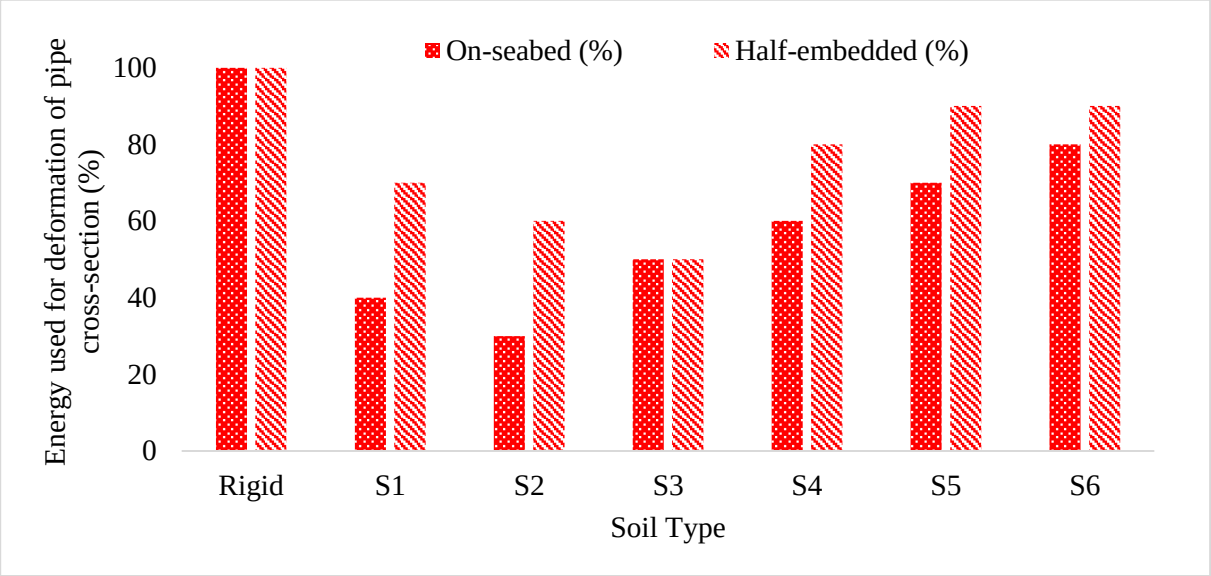

Figure 3.5: % Energy used to deform pipe on different soils (Selker et al., 2018)

(Naeij et al., 2023) conducted a comprehensive investigation into the interaction dynamics between dragged anchors and subsea pipelines, with a primary focus on safeguarding trenchless pipelines on the seabed. Employing a protective strategy involving the utilization of rock berm and sand backfill, the

study integrated analytical, finite element analysis (FEA), and experimental methodologies to validate the findings derived from analytical and FEA-based results.

The analytical approach adopted in the study is rooted in the assessment of passive pressure (Equation 3.1) exerted by the soil in front of the anchor (Figure 3.6). This methodology hinges on a fundamental assumption that the anchor is consistently fully penetrated in the soil. Notably, this formulation draws inspiration from the work (Reese et al., 1974), facilitating a structured and theoretically grounded analytical framework for evaluating the anchor-pipeline interaction dynamics.

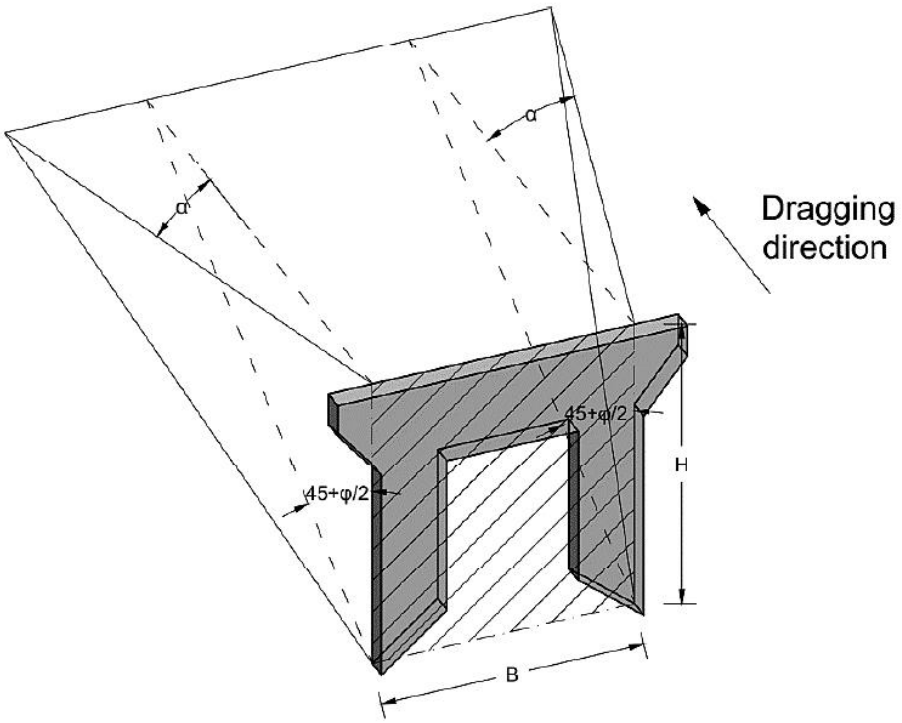

Figure 3.6: Passive wedge behind penetrated anchor in soil (Naeij et al., 2023)

$$F_{\text{passive}} = \gamma_s h^2 \left[\frac{K_0 h \tan\varphi \sin\beta}{3\tan(\beta-\varphi)\cos\alpha} + \frac{\tan\beta}{\tan(\beta-\varphi)} \left(\frac{B}{2} + \frac{h}{3}\tan\beta\tan\alpha \right) + \frac{K_0 h \tan\beta}{3} (\tan\varphi\sin\beta - \tan\alpha) \right] \quad (3.1)$$

$$K = 1 - sin\varphi \quad (3.2)$$

$$B = \frac{\pi}{2} + \frac{\varphi}{2} \quad (3.3)$$

Where φ represents internal friction angle, h, B, γ_s are soil height, anchor width, and soil density respectively.

Through a meticulous blend of theoretical analyses, numerical simulations, and experimental validations, (Naeij et al., 2023) studied to outline effective strategies for protecting subsea pipelines from the deleterious effects of dragged anchors. By leveraging insights from analytical solutions and FEA-based simulations, supported through experimental observations, the study contributes valuable insights

to the field of pipeline engineering, particularly in the context of mitigating risks associated with anchor interactions in offshore environments.

Furthermore, (Naeij et al., 2023) utilized a CEL (Coupled Eulerian-Lagrangian) based mesh, renowned for its robustness in handling analyses characterized by large deformations. In this analysis model, a simplified anchor with a 33 degrees fluke angle configuration was employed (Figure 3.7). To protect untrenched pipelines, a combination of sand and gravel, arranged in distinct layer configurations (Table 3.3), was utilized as protective measures.

The implementation of a CEL-based model is depicted in Figure 3.8, wherein the white domain signifies the void space. This sophisticated modeling approach enhances the fidelity of simulations, enabling a comprehensive evaluation of the protective efficacy of the sand and gravel layers surrounding the pipeline. Whereas values for loose and silty sand were acquired from (Imam et al., 2018) and (Look, 2007).

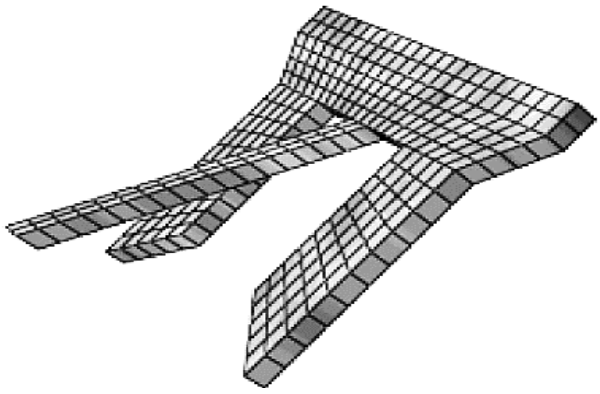

Figure 3.7: Simplified 7.8 tonnes anchor (Naeij et al., 2023)

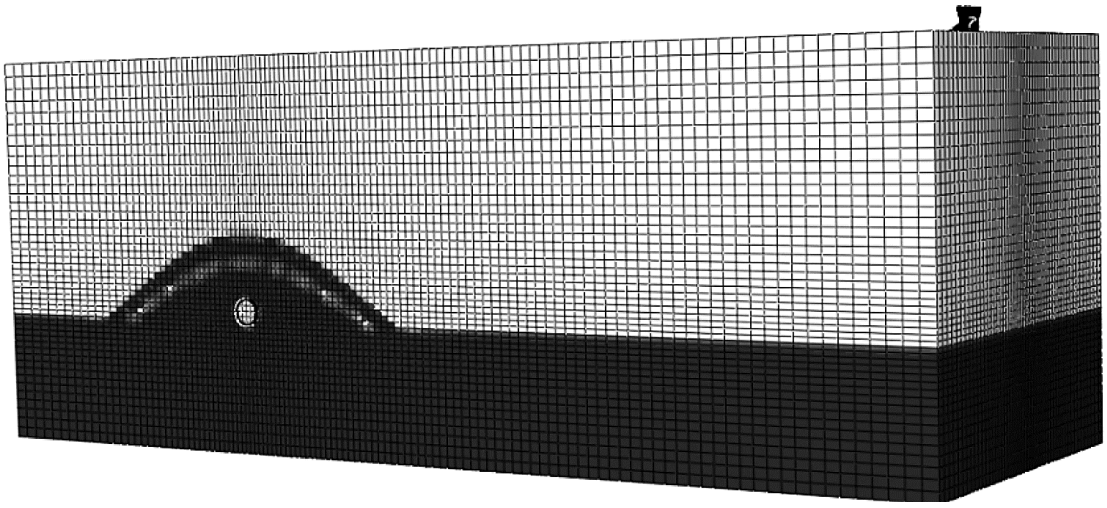

Figure 3.8: CEL based FEA model (Naeij et al., 2023)

In this article to validate the FEA model, an experimental setup was meticulously prepared, a scale factor of 1:20 was employed in the experimental setup in comparison to the FEA model. The experimental

setup involved the utilization of two anchors weighing approximately 7800 and 2000 kg, respectively. Firoozkooh sand#101 was selected as the medium for the experimental setup. Notably, it was observed that increasing the granular size in the sand led to an raise in both the shear strength and Young modulus values, which is in agreement with (Mirghasemi & Naeij, 2015). The experimental arrangement is depicted in Figure 3.9, providing a visual representation of the setup utilized to validate the FEA model.

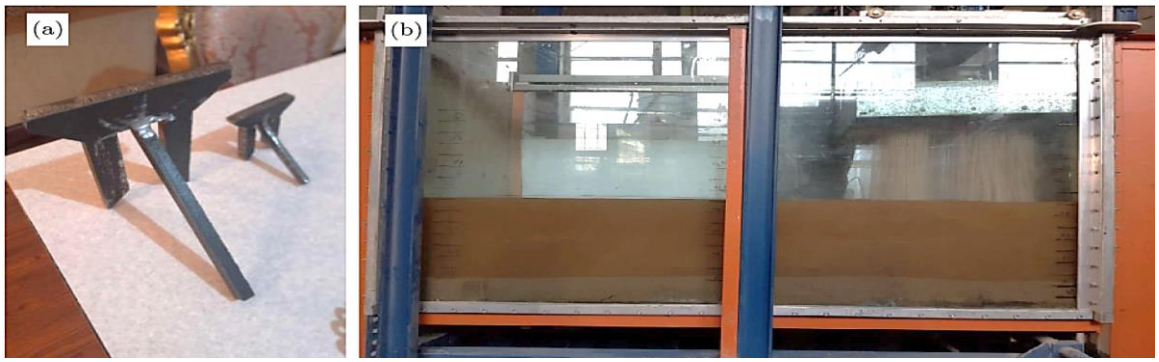

Figure 3.9: Experimental setup used by M. Naeij to study anchor interaction with trenchless pipeline covered with backfilled soil and rock berm (Naeij et al., 2023)

Figure 3.10 and Table 3.3 illustrates the comparison of traction forces between the dragged anchor and subsea soil, highlighting analytical, experimental, and FEA model results. Notably, all values exhibit strong agreement, affirming the efficacy of the FEA methodology employed by (Naeij et al., 2023). This congruence across analytical, experimental, and numerical analyses underscores the reliability and accuracy of the FEA-based approach in studying anchor-soil interactions, validating its utility for predictive modeling in subsea environments.

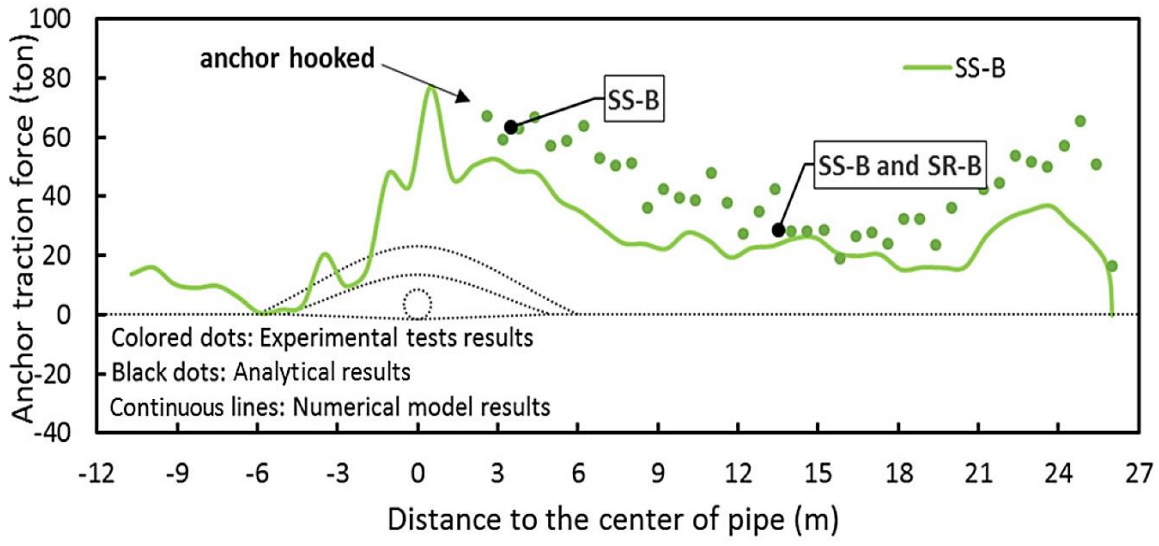

Figure 3.10: Comparison of analytical, experimental, and FEA-based anchor-soil traction forces between anchor and soil (Naeij et al., 2023)

Table 3.3: Test setups and detailed input for seabed formation (Naeij et al., 2023)

Test No.	Case (*ID*)	Pipe diameter (*cm*)	Height of first layer (*cm*)	Height of second layer (*cm*)	First layer material	Second layer material	Anchor type
1	SR-S	5	5	5	Fine sand	Gravel	Small
2	SS-S	5	10	0	Fine sand	—	Small
3	SR-B	5	5	5	Fine sand	Gravel	Big
4	SS-B	5	10	0	Fine sand	—	Big

3.2 Lagrangian vs Eulerian Mesh

Two prominent mesh formulations were examined for modeling the interaction between structures and soil by (Naeij et al., 2023), Lagrangian and Eulerian mesh. In Lagrangian mesh, as deformation occurs, elements undergo large deformations and mass is attached to nodes, potentially leading to unrealistic deformation outputs in case of large deformation. Conversely, in Eulerian mesh, mass being independent of mesh nodes, offers a distinct advantage. Figure 3.11 exemplifies the disparity between Lagrangian and Eulerian mesh behaviors under large deformation. In Lagrangian mesh, extreme deformation leads to mesh distortion, which may yield unexpected results. On the other hand, in Eulerian mesh, nodes of elements remain in position, facilitating the flow of mass within the mesh domain.

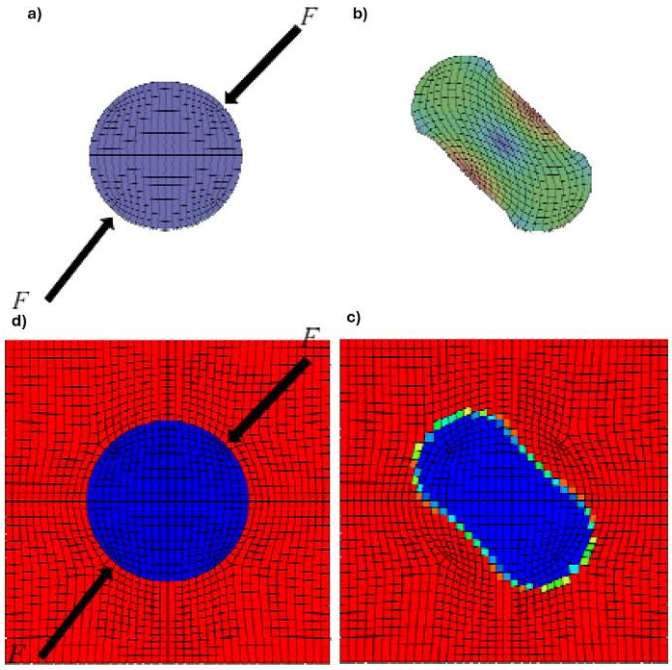

Figure 3.11: a,b) Lagrangian mesh before and after deformation correspondingly, c,d) Eulerian mesh before and after deformation respectively (Naeij et al., 2023)

Evident by Figure 3.11 the Eulerian mesh field emerges as more compatible for handling large deformations, as observed in scenarios such as the interaction of dragged anchors in subsea soil. This

mesh formulation offers a balanced approach, ensuring accurate representation of deformations while maintaining computational stability, thus enhancing the reliability of simulations in modeling complex phenomena like anchor-soil interactions.

3.3 Rock Berm Design

To assess the efficacy of rock berm protection on subsea pipelines, it's crucial to meticulously design each rock particle individually. Several master's theses have explored design of rock particles by using Spherical Discrete Elements (SDE) numerical method which lies under the category of Discrete Element Method (DEM) to represent the rock berm. (Larsson, 2014) specifically demonstrated the feasibility of modeling and simulating rock particles using SDE and with customized rock particles using Finite Element Analysis (FEA) methods. Figure 3.12 demonstrates the agreement between SDE and FEA numerical methods.

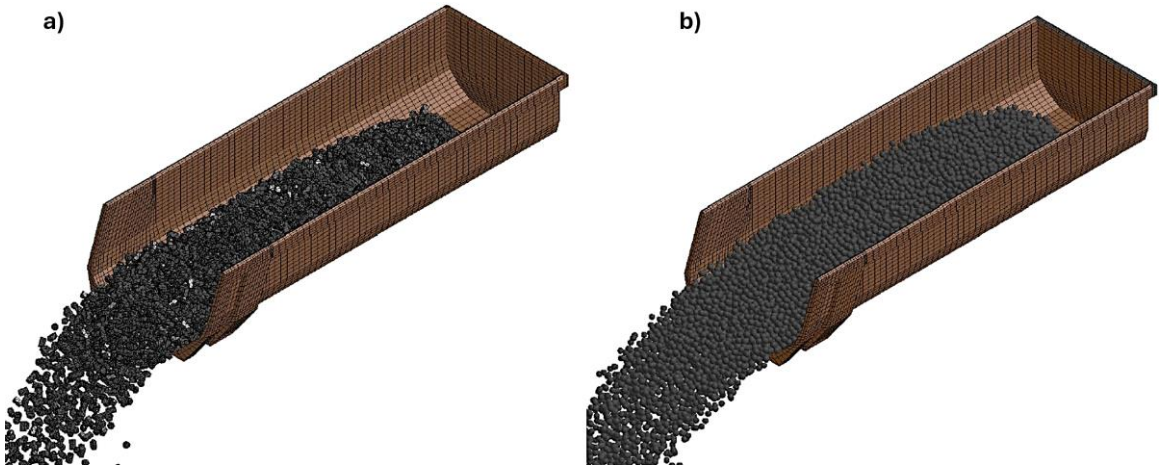

Figure 3.12: Comparison of SDE and FEA approach, a) FEM particles, b) SDE particles (Larsson, 2014)

It's worth noting that while Finite Element Method (FEM) and Discrete Element Method (DEM) both offer valuable insights into rock berm protection, there are differences in computational efficiency. For instance, in the case study depicted in Figure 3.12, FEM required 64 hours to compute, whereas DEM only took 17 hours (Larsson, 2014).

To accurately simulate rock particles, it is essential to have the correct shapes. (Huang, 2010) employed an advanced Aggregate Image Analyzer, as depicted in Figure 3.13, to achieve this precision. This analyzer captures 2D images of rocks from various angles, enabling the design of accurate 3D rock particles through a meticulous reconstruction process.

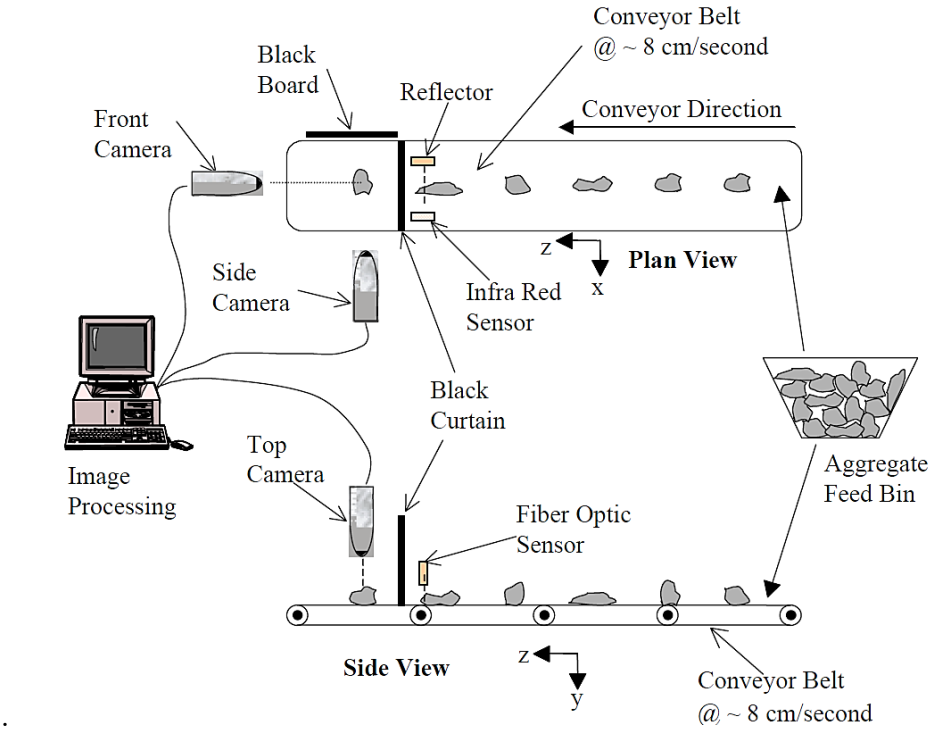

Figure 3.13: Aggregate image analyzer (Huang, 2010)

Direct 3D scanning offers a robust method for obtaining accurate representations of rock particles. (Latham et al., 2008) utilized a 3D scanner for this purpose, as depicted in Figure 3.14. This advanced technology enables precise capture of rock particle geometry, ensuring high detail and reliability in the resulting 3D images.

Figure 3.14: 3D image capture system for high resolution 3D images of rock (Latham et al., 2008)

Using accurate shapes for rock particles can be computationally expensive, especially when multiple shape and size libraries are incorporated into FEA models. This necessitates modeling and analysis computers with high specifications to handle large 3D models with higher number of nodes to achieve

accurate shape efficiently. However, to mitigate computational demands, it is possible to simplify rock particles by reducing them to a few nodes and elements.

Before integrating the customized rock berm into the model, it is imperative to calibrate its behavior using experimental results. For instance, (Zhong et al., 2022) conducted repose angle tests and slide calibration tests on the gravel, as depicted in Figure 3.15. Additionally, Huang Hai (Huang, 2010) performed shear box tests, shown in Figure 3.16, to calibrate the internal friction angle of rock particles. These experimental tests serve as crucial benchmarks for validating and fine-tuning the behavior of the customized rock particles within the FEA and DEM models.

(Huang, 2010) investigated shear box method to determine the internal friction angle of the rock particles, the slope of a linear line is utilized, representing the relationship between shear stress and normal stress at various normal stress values. This linear line is derived from multiple shear-box tests (Huang, 2010), which provide insights into the behavior of the rock particles under different loading conditions. According to (Marsal, 1973) article, friction angle can be found using same technique.

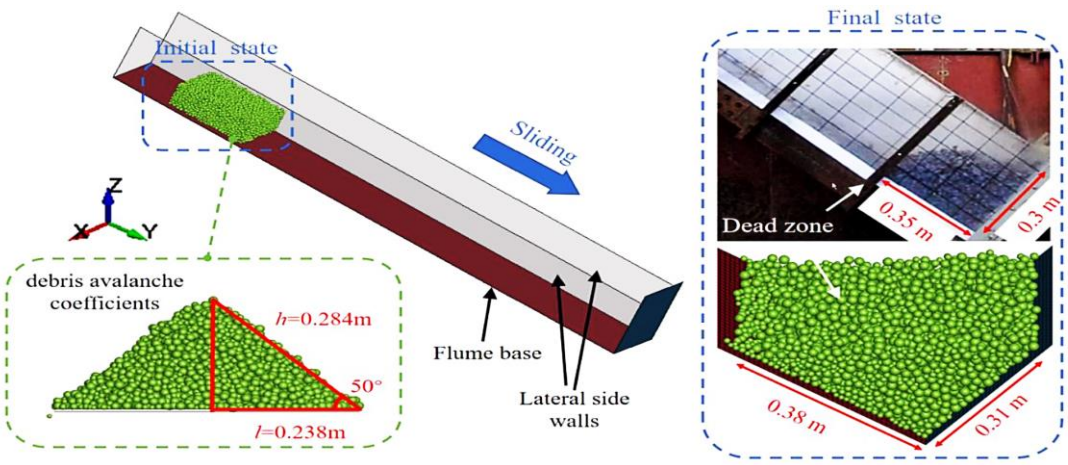

Figure 3.15: Calibration method of spherical DEM particles (Zhong et al., 2022)

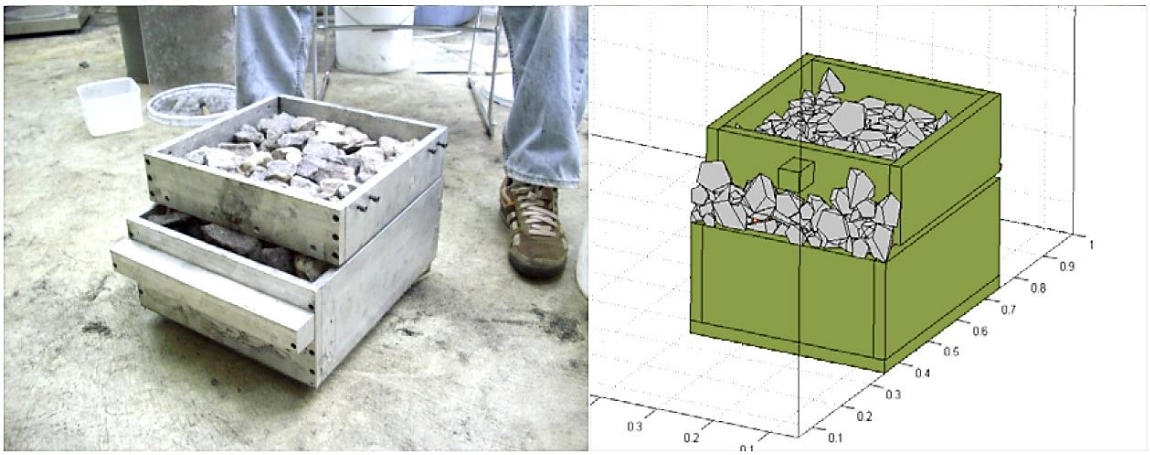

Figure 3.16: Shear-Box test to calibrate the internal friction angle of rock particles (Huang, 2010)

3.4 Pipe Deformation

(Zeinoddini et al., 2013) conducted both numerical and experimental tests to evaluate the influence of seabed stiffness and pipe's end boundary condition on pipe deformation under standard deformation tests. This investigation involved conducting various cases for instance with variable pipe's end boundary conditions, pipe embedment in soil, internal pressure magnitude, and bed stiffness. The indenter used in this study followed the design code outlined in DNV-RP-F111 (Standard, 2014), as depicted in Figure 3.17.

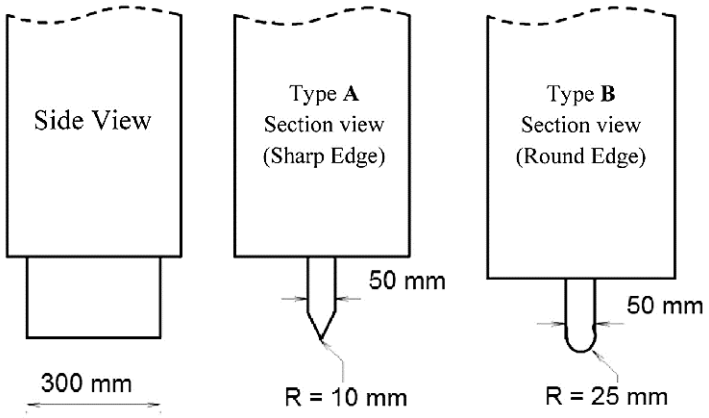

Figure 3.17: DNV-RP-F111 recommended indenter shapes (Standard, 2014)

Figure 3.18 illustrates the results from M. Zeinoddini's work, where energy is represented by the area under the load and indenter displacement curve, and normalized distance is compared with 0.5D (pipe diameter) of the pipe. It is evident that with a flexible bed, more energy is required to deform the pipe to the same extent as observed with a fixed bed. Furthermore, changes in soil bed stiffness affect the energy required to produce similar deformation. Whereas β and ϕ represents angle of friction and internal friction angle of soil.

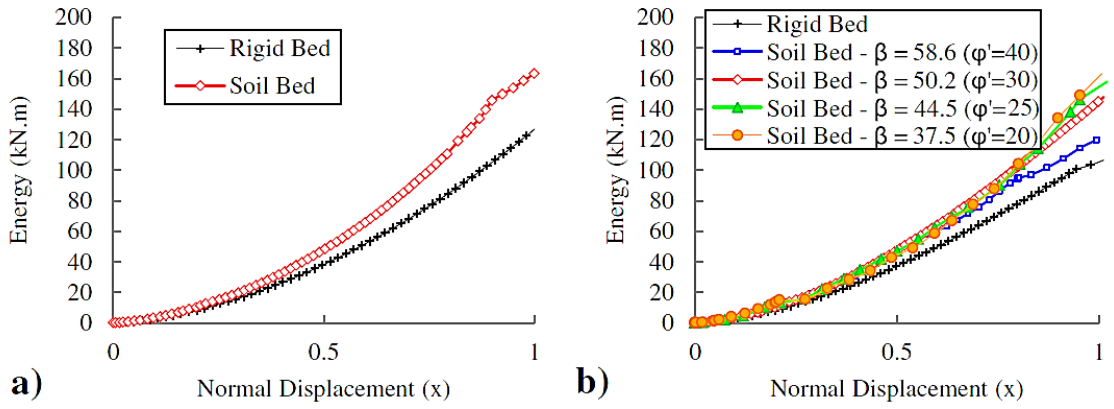

Figure 3.18: Effect of bed flexibility on deformation of pipeline, (a) pipes ends are free, (b) pipe ends are fixed, D/t=76, D=611mm, t=8mm, yield stress=517MPa (Zeinoddini et al., 2013)

4. Methodology

The LS-Dyna analysis software was utilized in this thesis's study, employing Finite Element Analysis (FEA) numerical method.

4.1 Numerical Methods

4.1.1 Finite Element Analysis

Finite Element Analysis (FEA) is a computational procedure used to predict the behavior of a model through the Finite Element Method (FEM), FEA allows engineers to analyze and predict the behavior of structures, heat transfer, fluid flow, biological cell growth, and many other physical phenomena (Simscale, 2023). Solving FEA models involves addressing partial differential equations (PDEs) using high-performance computing resources (Simscale, 2023). Through FEA, engineers can predict how structures will behave under various loads and conditions, optimize designs for cost-effectiveness and weight reduction, and enhance overall performance.

The FEA procedure consists of a series of steps, including:

1. Computer Aided Design (CAD) of the model/parts
2. Model simplification
3. Meshing of the model
4. Implementation of boundary conditions
5. Solving the FEA numerical model
6. Extraction of results

To obtain valid and trustworthy results from FEA, a converged mesh is essential. Convergence in FEA involves reducing the size of the mesh elements until the results become consistent and independent of mesh size, ensuring the accuracy and reliability of the simulation (Harish, 2024).

The "Review of Solid Elements Formulation in LS-Dyna" (Erhart, 2011; LS-DYNA, 2021) offers a comprehensive overview of solid elements and their underlying physics used in LS-Dyna tool. Solid elements are capable of modeling three-dimensional objects with solid geometries, providing a more realistic representation compared to shell and beam elements. However, they may not be as robust when used for thin surface bodies, where shell elements excel (Erhart, 2011; LS-DYNA, 2021). Solid elements also require more memory due to the additional segments and nodes they entail.

In LS-Dyna, various formulations of solid elements exist, each with its own set of advantages and disadvantages. In this current study, the reduced integration formulation is employed for solid elements, characterized by only one integration point, as depicted in Figure 4.1(a). This formulation is referred to as the "Constant stress solid element" in LS-Dyna. This formulation requires hourglass control which is an extra step to control this type of formulation.

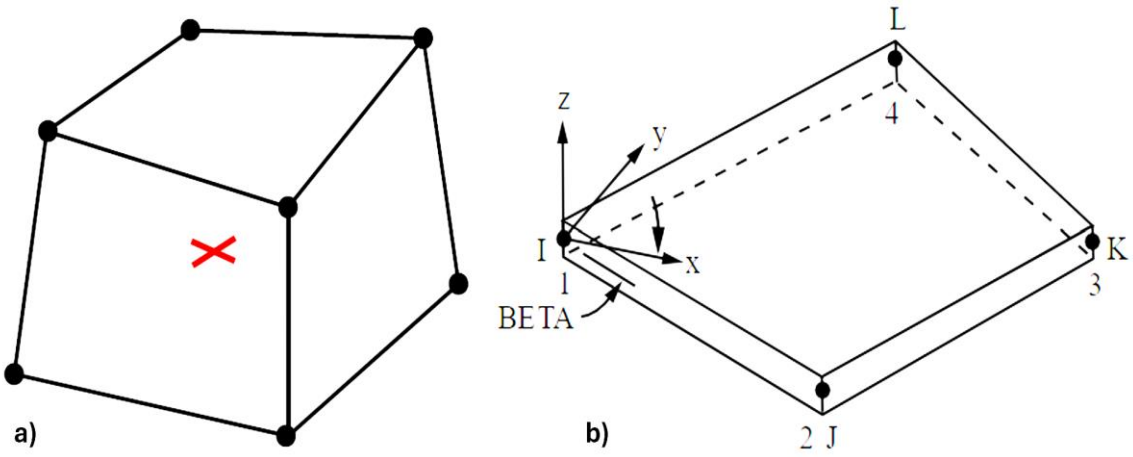

Figure 4.1: Element visual formulation, a) constant stress solid element (Erhart, 2011), b) shell element (Ansys)

Shell elements are ideal for modeling thin parts and help reduce the number of nodes and elements in a simulation model. In Figure 4.1(b) the formulation of a shell element is illustrated. Each node in a shell element has 12 degrees of freedom, encompassing translation, acceleration, and velocities along three axes. The nodes are labeled I, J, K, and L, and BETA represents the material angle (Ansys).

4.1.2 Smoothed Particles Hydrodynamics (SPH) and Discrete Element Method (DEM)

Smoothed Particle Hydrodynamics (SPH) is a mesh-independent Lagrangian method specifically designed to handle large deformations that conventional solid mesh techniques struggle to accurately represent (Svenning). It is particularly well-compatible for scenarios involving high-speed impacts (Figure 4.2(a)), such as bird strikes with planes, large-scale shear cutting of metals, and plowing analysis. Notably, SPH can only be solved using an explicit solver due to its inherent characteristics and computational requirements (Lacome, 2000).

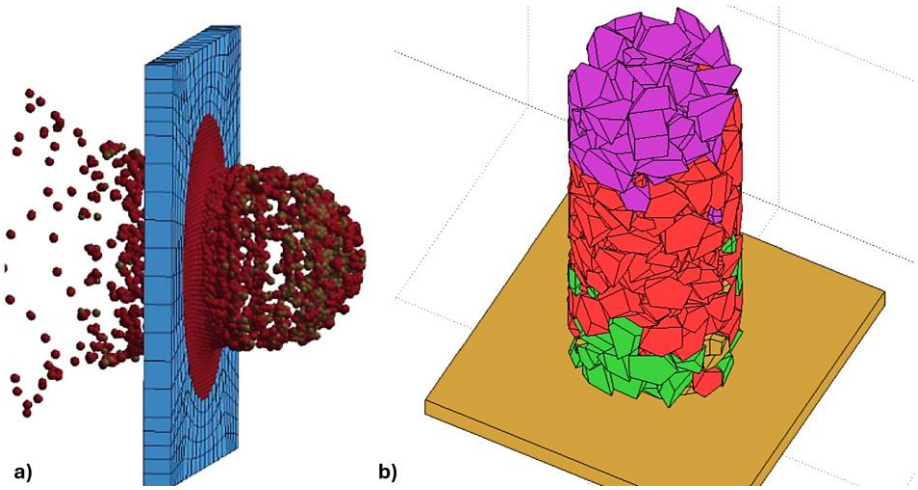

Figure 4.2: Mesh-independent numerical methods, a) High velocity impact analysis using SPH method (Svenning), b) rock particles modeling by using DEM (Huang, 2010)

Granular materials pose challenges for definition within confined solid meshes or fluid simulations. To address this, a unique technique called the discrete element method (DEM) is employed in Figure 4.2(b) (Aspenberg, 2018). In LS-Dyna, this formulation is referred to as discrete element spheres (DES), and it is specifically designed for spherical discrete elements. DEM is particularly valuable for analyzing granular flow, granular bodies impacts, bulk granular shape objects in production lines, sand, and rock debris (Figure 4.2(b)).

4.2 Contacts Physics

The penalty-based contact method is a widely employed technique in LS-Dyna. It operates on the principle of simulating linear springs between nodes, surfaces, and segments of elements. When a slave node penetrates a master segment or surface, a force is applied to the slave node to push it away from master surface (Owen, 2020).

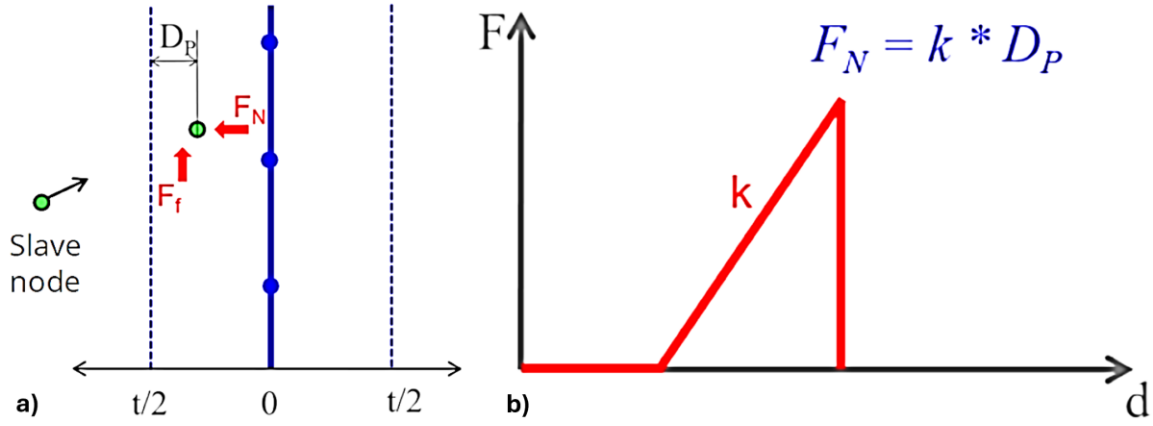

Figure 4.3: Penalty based contact depiction (Owen, 2020)

Figure 4.3 illustrates this physical phenomenon, depicting the interaction when a slave node penetrates a master boundary. F_n represents the normal force and F_f represents the friction force applied on the slave node, with their magnitudes dependent on the depth of penetration D_p and the stiffness K.

To manage an analysis model with bodies that exhibit significant differences in density magnitudes, it is advisable to utilize the *SOFT=2* contact formulation. This setting enables segment-based contact stiffness, in this contact method, the stiffness k is calculated based on Equation 4.1.

$$k = SLFAC(SFS\ or SFM)\left(\frac{m_1 m_2}{m_1 + m_2}\right)\left(\frac{1}{\Delta t}\right)^2 \tag{4.1}$$

SLFAC serves as the global scale factor for stiffness, whereas *SFS* or *SFM* represent scale factors applicable to individual parts within the model. Here, m_1 and m_2 denotes the masses of the segments to be in contact, while Δt represents the global timestep utilized in the analysis.

Figure 4.4 presents a crucial part of the contact control card interface in LS-Dyna, where the *SOFT=2* contact option is controlled. Within this interface, the SBOPT and DEPTH options are particularly

significant. The SPOBT=3 parameter facilitates checks for wrapped segments, aiding in the identification of segments that are not normal to each other. Meanwhile, the *DEPTH* option governs segment-based contact physics. LS-Dyna's user manual (LS-DYNA, 2024) recommends setting *DEPTH=35*, as this enables the option for segment-to-segment and edge-to-edge contact physics, as illustrated in Figure 4.5.

10	SOFT	SOFSCL	LCIDAB	MAXPAR	SBOPT	DEPTH	BSORT	FRCFRQ
	2	1.0000000	0	1.0250000	3.0	35	0	1

Figure 4.4: Contact card from LS-Dyna

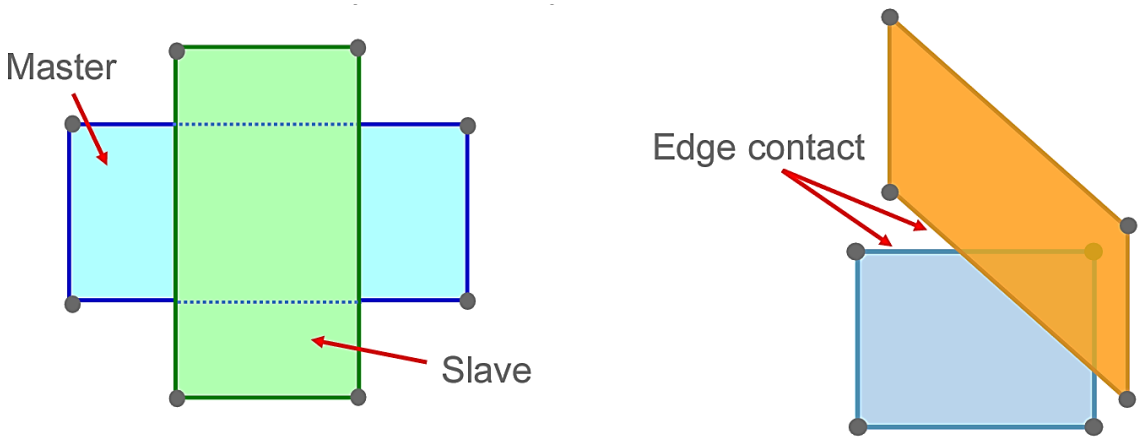

Figure 4.5 SOFT=2 contact depiction (Owen, 2020)

5. Modeling and Analysis Setup

Table 5.1 provides essential information about the types of elements and material models utilized in LS-Dyna software for all parts in the model.

Table 5.1: Parts used in anchor-pipe interaction model and their specifications

Part Name	Element Type	Material Model
Chain	Shell	Mat_020 and _220: Rigid + Discrete Rigid
Anchor	Shell	Mat_020: Rigid
Rock Berm	Shell	Mat_220: Discrete Rigid
Soil	Solid	Mat_173: Mohr and Coulomb

5.1 Materials

5.1.1 Soil

The Mohr-Coulomb material model is extensively utilized to simulate the behavior of cohesive, sandy, and granular soils (LS-DYNA, 2024). This model incorporates a yield surface that is dependent on the Mohr-Coulomb failure criteria, as depicted in Figure 5.1.

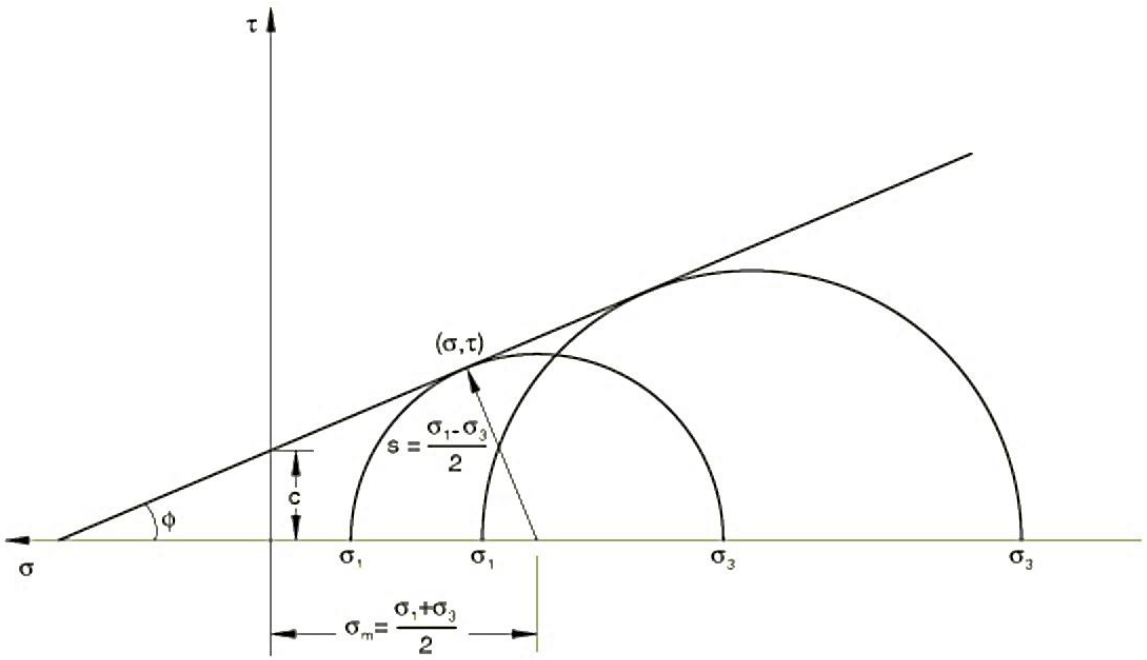

Figure 5.1: Mohr-Coulomb failure criteria (ABAQUS)

The failure criteria of the Mohr-Coulomb material model is governed by a linear relationship between shear stress and normal stress, which can be represented by Equation 5.1 (LS-DYNA, 2024).

$$\tau = c - \sigma . tan\,(\varphi) \quad (5.1)$$

Where τ, c, σ, and φ represents shear stress, cohesion, normal stress, and internal frictional angle respectively. Equation 5.1 describes that shear failure can be experienced with different combinations of internal friction angle and cohesion value of soil, also Figure 5.1 illustrates that shear failure can be predicted using this criterion by analyzing different combinations of minimum and maximum principal stresses.

From Figure 5.1 expressions for τ, σ, and s can be extracted as (equations 5.2, 5.3 and 5.4).

$$\tau = s . cos(\varphi) \quad (5.2)$$

$$\sigma = \sigma_m + s . sin\,(\varphi) \quad (5.3)$$

$$s = \frac{1}{2}(\sigma_1 - \sigma_3) \quad (5.4)$$

Where σ_1 and σ_3 represent the maximum and minimum principal stress, respectively. By substituting equation 5.2 and 5.3 in equation 5.1 becomes:

$$s + \sigma_m . \sin(\varphi) - c . \cos(\varphi) = 0 \quad (5.5)$$

Where $$\sigma_m = 1/2(\sigma_1 + \sigma_3) \quad (5.6)$$

This material model is specified as *MAT_173 (MAT_MOHR_COULOMB)* in LS-Dyna.

5.1.2 Other Materials

Below material models information is adapted from LS-Dyna user's manual 2024 (LS-DYNA, 2024).

MAT_RIGID or *MAT_020* is a commonly utilized material model for rigid bodies in LS-Dyna. It offers cost-effectiveness by bypassing element processing, and it does not store history variables within the FEA software memory. However, it is crucial to assign realistic values for parameters such as elastic modulus, Poisson's ratio, and density, as these values significantly impact the calculation of contact stiffnesses.

Serving as an advanced iteration of *MAT_020, MAT_RIGID_DISCRETE*, also known as *MAT_220*, is an invaluable material model that facilitates the assignment of material properties to disjoint pieces of a body. This model is particularly useful for simulating granular materials and rigid structural components with uniform material properties.

MAT_024, also known as *MAT_PIECEWISE_LINEAR_PLASTICITY*, is a commonly employed material model for elasto-plastic materials. In this material model, stress is determined by the strain curve, which may be influenced by the strain rate. This model offers a versatile approach for simulating materials with nonlinear stress-strain behavior, allowing for a more accurate representation of elasto-plastic deformation under varying loading conditions.

NB. In this thesis work *MAT_024* is only used for pipeline deformation model's validation, it's not included in the final model.

Table 5.2 and Table 5.3 furnish the requisite input parameters for all components in the analysis model. Scaled densities are employed for both the anchor and chain, and shell elements are utilized instead of solid elements for these parts to minimize the number of elements in the model. Employing scaled masses is imperative to attain masses conforming to SOTRA (SOTRA, 2014a) standards and to ensure realistic masses for the anchor and chain.

Table 5.2: Material properties for different parts (MAT_RIGID and DISCRETE_RIGID)

Part Name	Density (Kg/m^3)	Poisson's Ratio	Elastic Modulus (*GPa*)
Anchor	7800	0.33	210
Chain	7800	0.33	210
Rock Berm	2700	0.25	50
Rigid Pipe	7800	0.33	210

Table 5.3: Material properties for soil (MAT_MOHR_COULOMB) (Chen et al., 2024; Naeij et al., 2023)

Soil Type	Density (Kg/m^3)	Poisson's Ratio	Elastic Shear Modulus (*Pa*)	Cohesion (*kPa*)	Internal Friction Angle (*Degree*)
Loose Soil (sand)	1550	0.25	1.2E+6	0	26
Stiff Soil	1923	0.2	2.08+6	0	50.2

5.2 Anchor and Chain Design

5.2.1 Anchor

Stockless anchors are extensively employed in the shipping industry owing to their practicality (Sriskandarajah & Wilkins, 2002). There are three main types of stockless anchors: Hall, Spek, and Spek-M anchors. Each of these anchors comprises components such as fluke, shackle, forerunner, and shank. In this thesis, three varied sizes of anchors are modeled, weighing approximately 3, 5, and 7.8 tonnes, respectively. SOTRA mooring (SOTRA, 2014b) equipment manufacturing company provides detailed information about the shapes and dimensions of these anchors. Importantly, the geometries of these anchors are contingent upon the Equipment Number (*EN*) of the vessel.

$$EN = \Delta^{\frac{2}{3}} + A_c \tag{5.7}$$

EN stands for Equipment Number, representing a parameter used to determine the dimensions and characteristics of various ship equipment. Additionally, A_c denotes the projected area of wind-exposed surfaces, providing insight into the vessel's susceptibility to wind forces. Moreover, Δ represents the sea water displacement by the ship, typically measured in tonnes, which is a crucial parameter for assessing the vessel's buoyancy and stability characteristics. Table 5.4 and Figure 5.2 illustrates the detailed relationship between *EN* (Equipment Number), Equipment Letter (*EL*), anchor weight, and chain link diameter. Similarly, these standards can also be found in DNV.GL standard for position mooring DNVGL-OS-E301 (Standard, 2018).

Table 5.4: Relation between Equipment Number and mooring equipment (SOTRA, 2014a)

Equipment Number	**Equipment Letter (DNGVL)**	**Anchor Weight (Kg)**	**Chain Diameter "*D*" (mm)**	**A (mm)**	**B (mm)**	**C (mm)**	**D (mm)**	**E (mm)**	**F (mm)**
980-1059	w	3060	56	2058	1578	748	365	1133	1114
1670-1789	E	5250	73	2405	1846	888	450	1325	1338
2530-2699	K	7800	90	2757	2112	1015	514	1518	1533

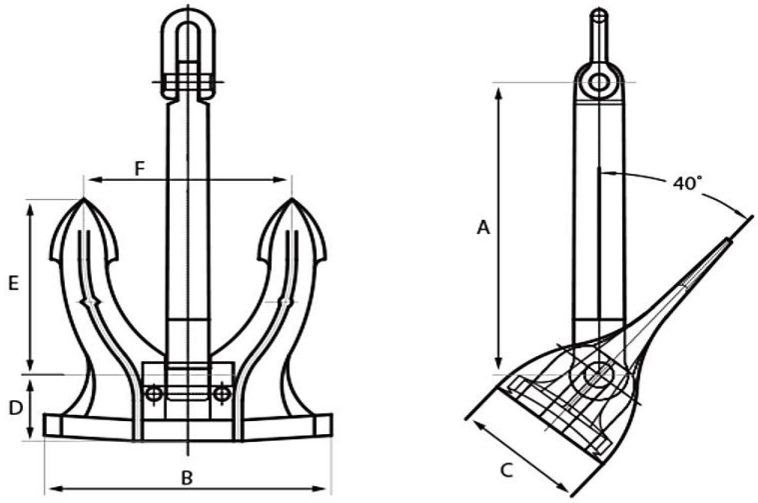

Figure 5.2: Spek-M anchor dimensions (SOTRA, 2014b)

Autodesk Inventor 3D modeling software was utilized to create the 3D parts of the analysis model. Two distinct 3D models have been prepared for the anchor: one fully realistic and one simplified. The realistic model (Figure 5.3) is adapted from (Shin et al., 2020), adhering to the Korea Standards Association's "SPS-KSA0127-V3311-5978; 2014". The standard dimensions are provided in Table 5.5.

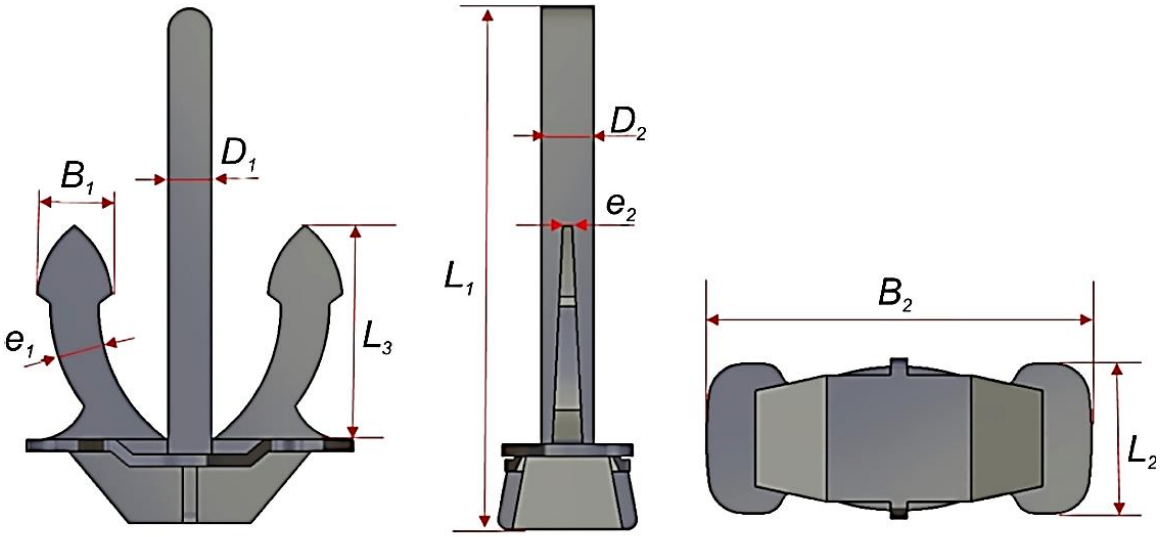

Figure 5.3: Guidelines for dimensions of anchor (Shin et al., 2020)

Table 5.5: Stockless anchor dimensions (Shin et al., 2020)

Weight (tonnes)	B_1 (mm)	B_2 (mm)	D_1 (mm)	D_2 (mm)	L_1 (mm)	L_2 (mm)	L_3 (mm)	e_1 (mm)	e_2 (mm)
5.25	460	2000	268	318	3140	780	1308	302	56
10.5	580	2520	338	400	3958	980	1644	380	71
15.4	660	2860	383	455	4486	1120	1864	432	80

In accordance with the above standards Table 5.5, a realistic 3D model weighing 5.25 tonnes was prepared, featuring 40 degrees opening between the fluke and shank, as depicted in Figure 5.4. As the anchor and chain are modeled as rigid bodies, a reasonable mesh size was applied to maintain shape integrity and ensure low computational cost. Anchor and chain mesh were generated using the *Auto-Mesher* tool available in LS-Dyna.

Complex and realistic shapes result in unnecessarily complex and computationally expensive mesh. To address this issue, a simplified anchor model (Figure 5.5) was modeled, adhering to the standards provided by SOTRA, Table 5.4 (SOTRA, 2014b).

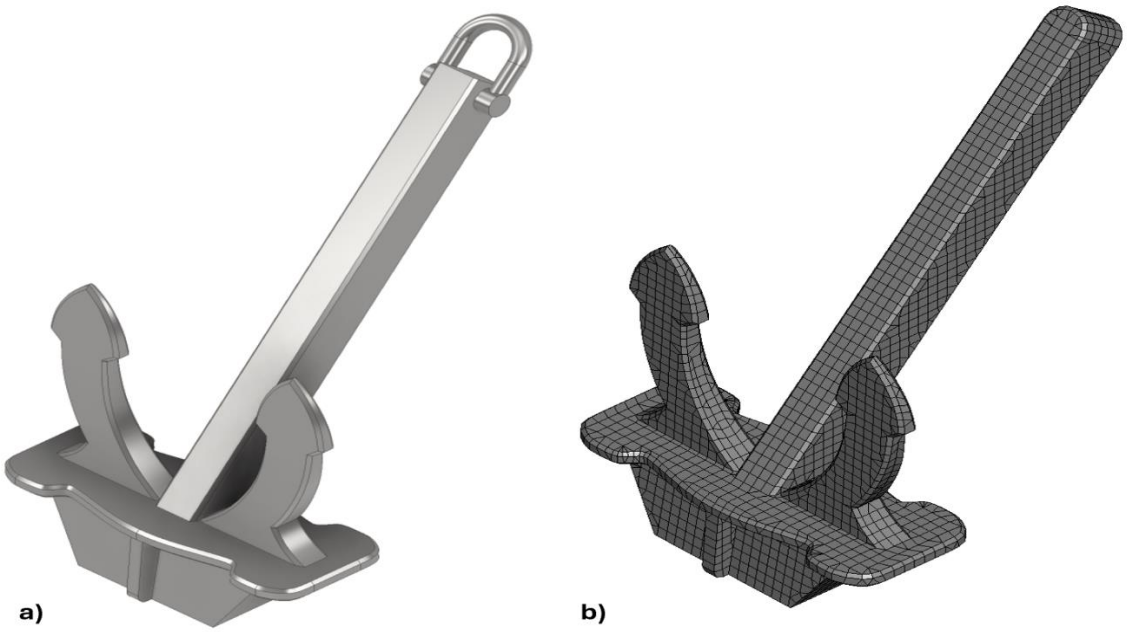

Figure 5.4: Realistic 5.25 tonnes stockless anchor, a) CAD model, b) anchor's mesh for FEA model

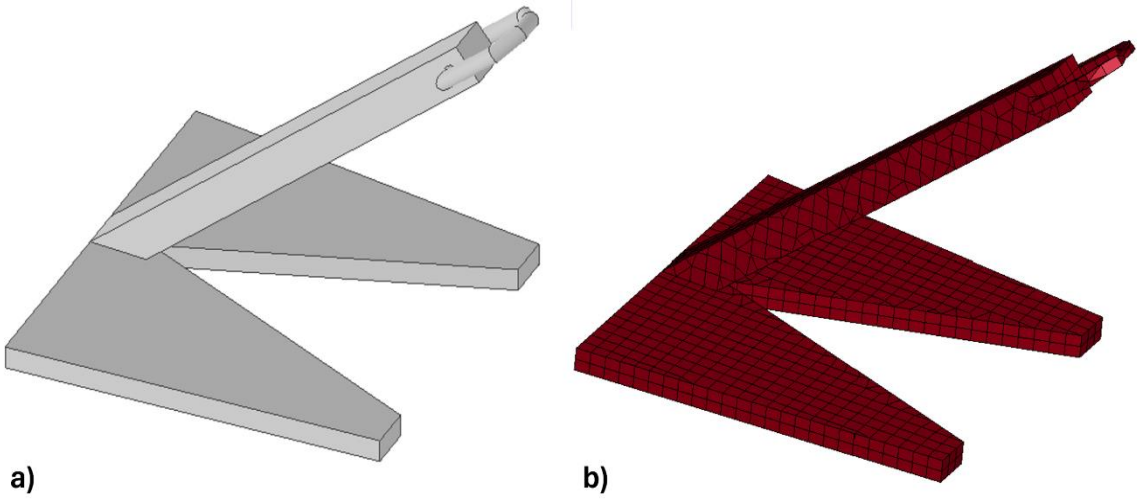

Figure 5.5: 5 tonnes simplified stockless anchor, a) CAD model, b) anchor's mesh for FEA model

5.2.2 Chain

Typically, two primary types of mooring lines are utilized in conjunction with anchors: steel or fiber ropes and chains. Ropes offer greater flexibility, while steel chains are known for their robustness and widespread use (Sriskandarajah & Wilkins, 2002). Within the realm of chains, two common types are employed: stud link and stud-less, chosen based on the nature of the anchoring requirements. Stud-less chain is predominantly used for permanent anchoring applications, whereas stud link chains are preferred for temporary purposes. Figure 5.6 illustrates the standard dimensions for the stud link of mooring chain, which is contingent upon the diameter (D) of the steel rod used to manufacture the stud links. This diameter (D) statistics can be obtained from equipment Table 5.4.

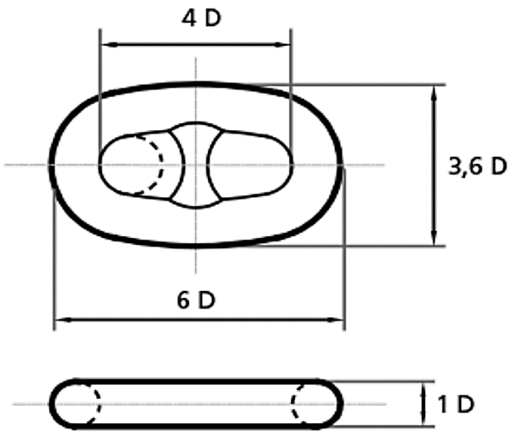

Figure 5.6: General stud link (SOTRA, 2014c)

(Jónsdóttir & Sævik, 2016) conducted a detailed analysis to determine the minimum chain length required for a vessel to touch a 200 meters deep seabed at speeds of 2 and 10 knots. This study evaluated the chain length necessary for different anchor sizes, ranging from 3 to 15 tonnes. For this current thesis's study, only the angle between the chain and seabed is obtained from (Jónsdóttir & Sævik, 2016), corresponding to the vessel's speed. Figure 5.7 illustrates the hanging shape of the chain at 2 knots for a 7.8 tonnes anchor, further values of the angle between chain and seabed is present in Table 5.6.

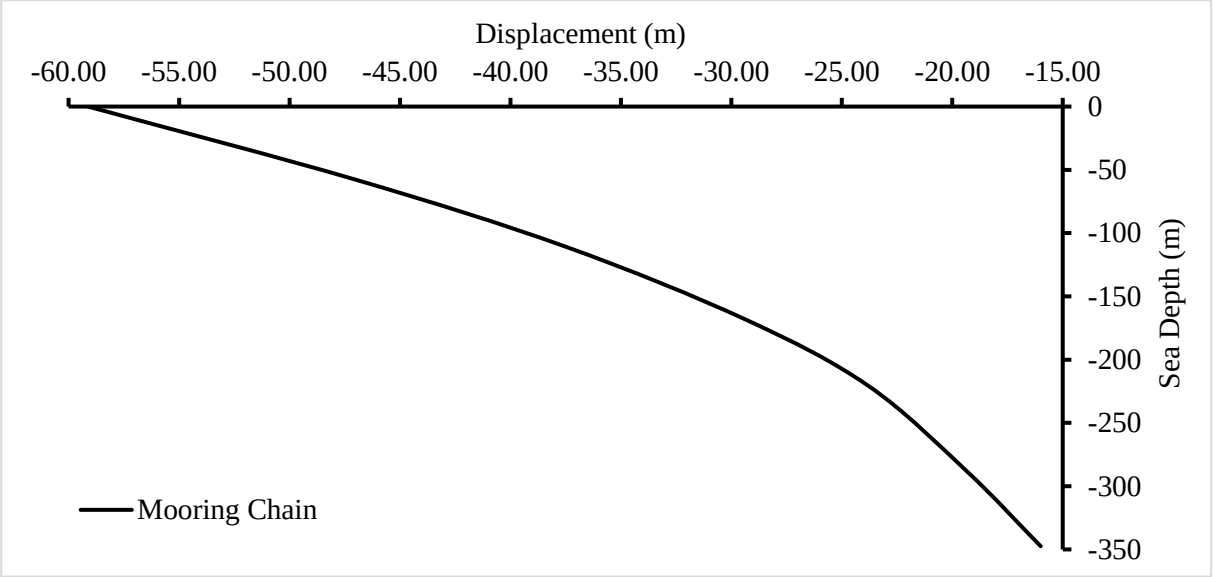

Figure 5.7: Minimum chain length required to touch the 200m deep seabed, 7800kg anchor, speed 2 knots, chain length used 350m (Jónsdóttir & Sævik, 2016).

Table 5.6: Chain angle with seabed (Jónsdóttir & Sævik, 2016)

Speed (*knots*)	**Chain angle with seabed (*Degrees*)**
2	80
10	33

The steel mooring chain was modeled in accordance with (SOTRA, 2014a) standards for a 5 tonnes anchor. The diameter value of "grade 1" chain links was obtained from Table 5.4, where value of chain diameter is 73mm and the weight of a single chain link is approximately 37 kg for 5 tonnes anchor. Utilizing the standard chain link shape depicted in Figure 5.6, a single chain link was 3D modeled (Figure 5.8) and subsequently assembled to achieve a length of 14 meters (for 5 tonnes anchor).

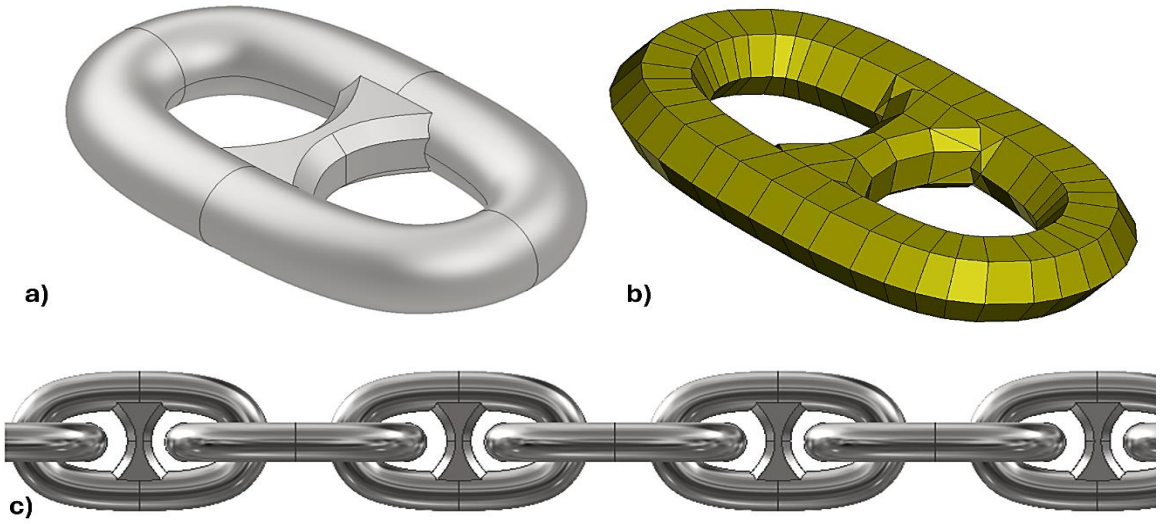

Figure 5.8: Chain stud link for 5 tonnes anchor, 37 kg each link, a) CAD model, b) chain's mesh for FEA model, c) chain assembly

5.3 Rock Berm

To represent the rock berm, a single shape was designed with a mean diameter of 75 mm. Initially, a single rock particle was designed using Autodesk Inventor and then assembled into groups of 9 stones (Figure 5.9(a)). This assembly of rock particles was further multiplied in LS-Dyna to create the rock berm particles according to requirement.

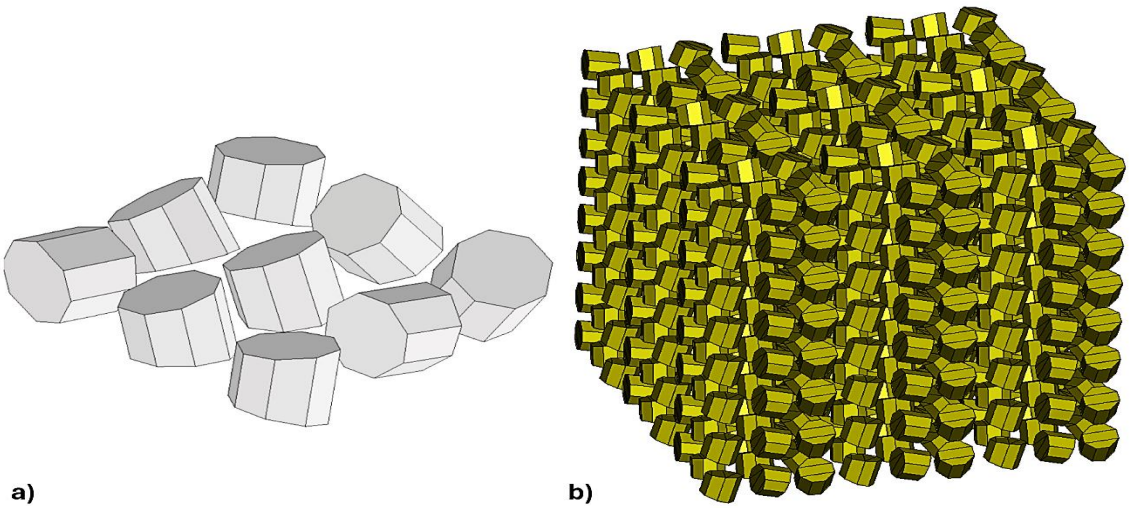

Figure 5.9: Rock particle modeling, a) Group of 9 rock particles modeled in Inventor, b) rock's mesh in LS-Dyna

For calibrating the internal friction angle of the rock debris, a shear box test was modeled (Figure 5.10), described in section 3.3. This test setup consists of two boxes and a lid for applying the normal force. All components of the shear box test model were constructed using shell elements to ensure computational efficiency.

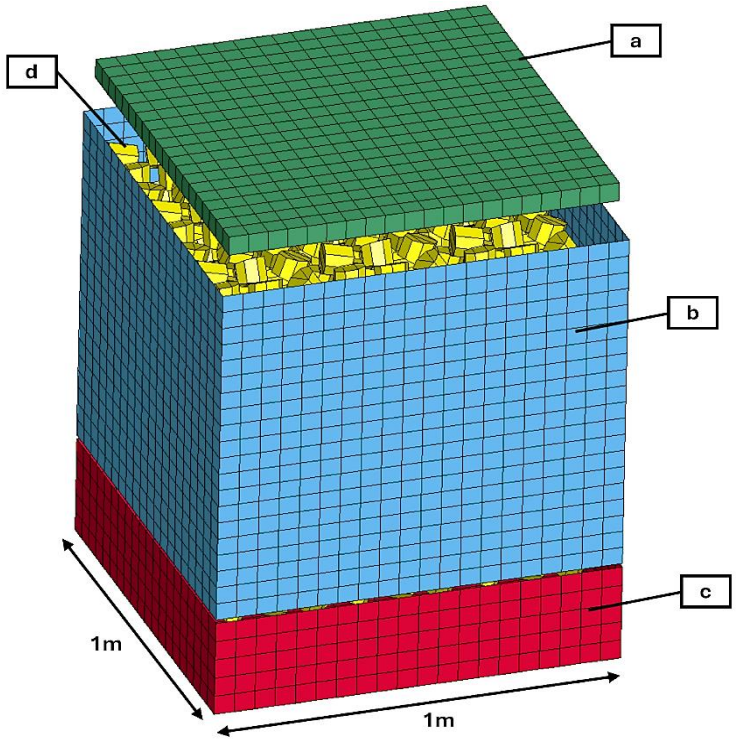

Figure 5.10: Shear box test model, a) green lid for normal force application, b) blue box is allowed to move in one direction. c) bottom red box is fixed, d) rock berm

5.4 Contacts

All surface to surface contacts within the model are modeled using the *SOFT=2* option, as extensively detailed in section 4.2 of the report.

Table 5.7 provides the values for coefficient of friction between various components within the analysis model. Additionally, the exponential decay coefficient and viscous damping coefficient were set to 0.2 and 20%, respectively, in accordance with the recommended values outlined in the LS-Dyna user manual (LS-DYNA, 2021).

Table 5.7: Values for coefficient of friction between parts

Part 1st Name	Part 2nd Name	Coefficient of Friction
Anchor	Chain	0.55
	Pipe	0.5-0.55
Soil	Chain, Anchor, and Pipe	0.6 (Veritas, 2012)

Rock Berm	--	0.6

Table 5.8 presents the details of various contact options along with the parts where these contact types are utilized. A *SINGLE_SURFACE* contact option enables the self-contact of multiple FEA-based discrete bodies. This option is utilized for contacting chain links and the rock debris in the analysis model. *AUTOMATIC_SURFACE_TO_SURFACE* contact is the most widely used and robust contact type in LS-Dyna (LS-DYNA, 2021). *AUTOMATIC_ERODING_SURFACE_TO_SURFACE* contact identifies new surface segments when element erosion occurs after reaching erosion criteria, making it essential to include this contact option with element erosion criteria in the model. Lastly, *ERODING_SINGLE_SURFACE* contact is advantageous for internal contact within a part. When elements erode, it facilitates the identification of new segments within the internal structure of a part, which may be challenging to visualize from the exterior.

Table 5.8: Contact types used in analysis model

Contact Type	1st Part (Name)	2nd Part (Name)
SINGLE SURFACE	Chain links	--
	Rock berm	--
AUTOMATIC ERODING SURFACE TO SURFACE	Anchor, chain, pipe	Soil
AUTOMATIC SURFACE TO SURFACE	Chain	Pipe and Anchor
	Anchor	Chain and Pipe
ERODING SINGLE SURFACE	Soil	--

5.5 Soil Domain

Following extensive analysis and testing, a soil domain measuring 4*10.5*19-meter (Figure 5.11) was modeled to accommodate the stable penetration depth of 7800kg anchor traveling at speeds of 2 knots and 10 knots before interacting with the pipeline. This bed was constructed using solid elements as detailed in section 4.1.1, and hourglass control measures were implemented to address any unrealistic behavior exhibited by the reduced integration formulated solid elements. Hourglass control can be effectively managed through the *HOURGLASS* option available in the LS-Dyna keyword manager.

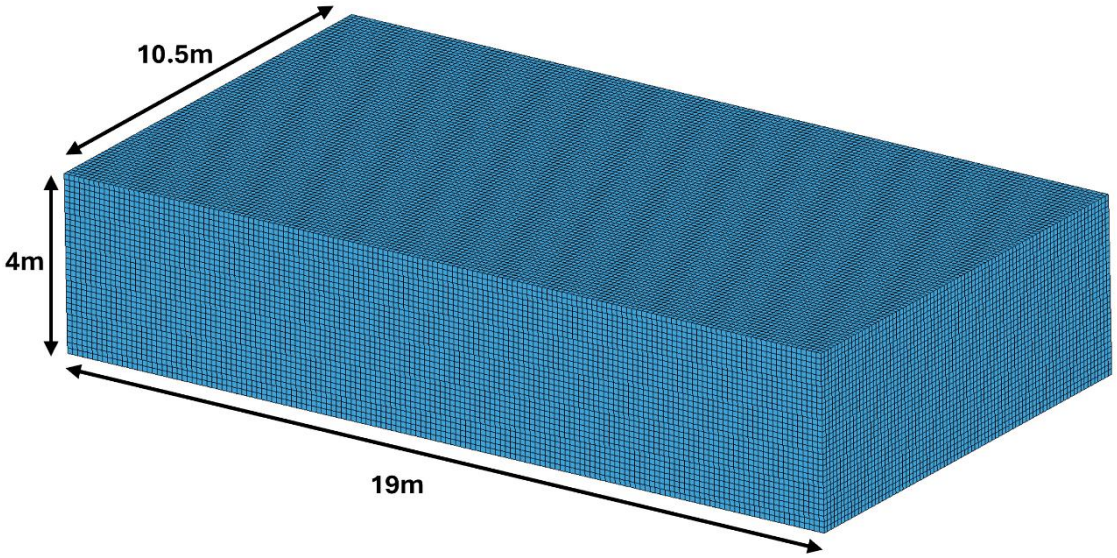

Figure 5.11: Soil domain

5.6 Anchor Soil Interaction Method

In the interaction method between the dragged anchor and soil, a Lagrangian mesh with element erosion criteria is employed. In thus study element erosion criteria is set to remove elements experiencing large deformations while maintaining the interaction forces between dragged anchor and soil according to reference values (discussed in section 6.2.1). The criteria can be defined based on maximum or minimum stress, strain, or pressure values within elements. When elements meet the defined erosion criteria, they get deleted from the mesh. In LS-Dyna, this erosion card can be activated using *MAT_ADD_EROSION*.

In the conference proceeding authored by LeQin Wang (Wang et al., 2009), this technique was utilized to simulate the interaction between soil and anchor. Figure 5.12 illustrates the element deletion after reaching the erosion criteria.

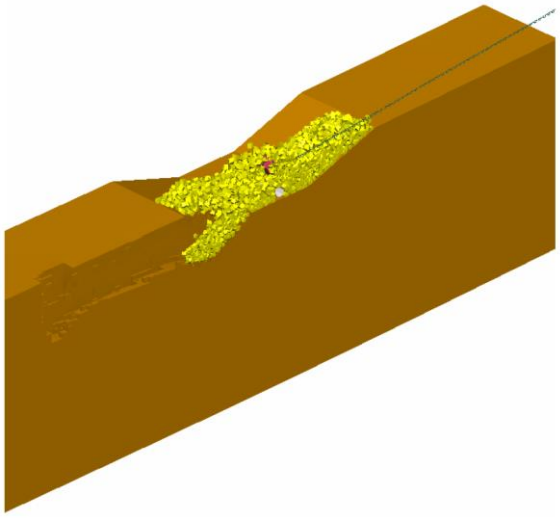

Figure 5.12: Analysis model based on element erosion criteria (Wang et al., 2009)

5.7 Boundary and Initial Conditions

To ensure the accuracy of the simulation model, it is essential to establish realistic boundary conditions. All numerical models are allowed to settle under gravity before applying any dynamic boundary conditions. Typically, 5-10 seconds are allocated in soil-anchor interaction models to achieve a static condition before proceeding with further analysis.

Further, all sides of the soil are fixed, except the top side, to provide support to the soil. This fixed boundary condition setup is achieved using the *BOUNDARY_SPC_SET* option in LS-Dyna, as illustrated in Figure 5.13.

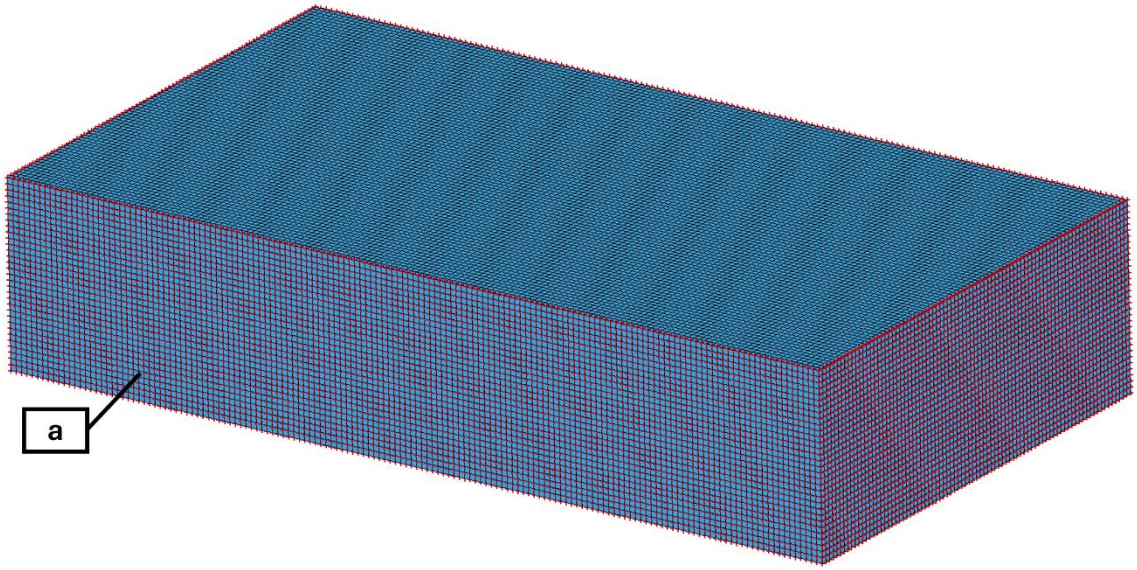

Figure 5.13: Illustration of fixed boundary condition in soil domain, a) fixed nodes

Regarding the anchor and chain configuration, all chain links except the last chain link are configured to be free to move and rotate in all axes and planes. An overview of the anchor chain setup is depicted in Figure 5.14. Notably, the last link of the chain is modeled as a separate rigid body using the *MAT_020* material model. This choice is made because the *MAT_220* material model does not support dynamic boundary conditions.

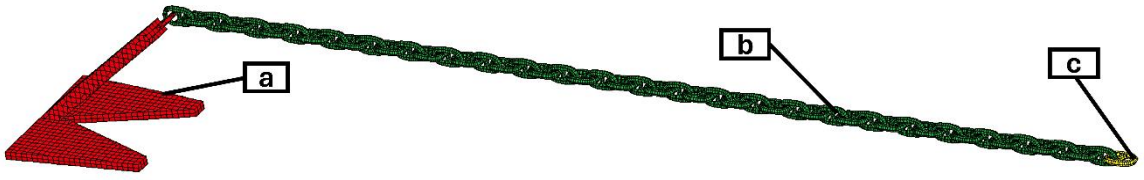

Figure 5.14: Configuration of anchor and chain, a, b, and c illustrate anchor, discrete rigid chain, and last link respectively

5.7.1 Gravity

Gravity is the fundamental force that bodies experience on earth. In this analysis model, the gravitational force is applied using the *LOAD_BODY_Z* option in LS-Dyna, which directs the gravitational force in the negative Z-direction. To mitigate any instability arising from rapid acceleration, a smooth gravitational force curve is defined using the *DEFINE_CURVE* tool. This curve is represented in Figure 5.15.

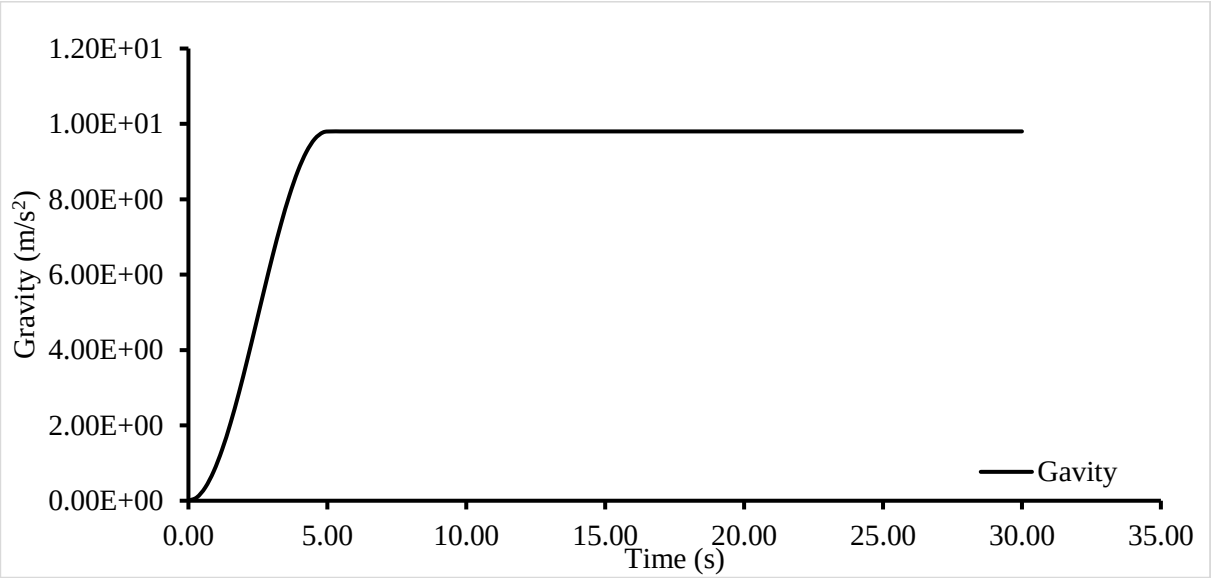

Figure 5.15: Gravity force over the time

6. Results and Discussion

6.1 Mesh Convergence

Mesh convergence is a crucial step in the Finite Element Analysis (FEA) procedure. Without a converged mesh, the results obtained can be ambiguous and unreliable. To achieve mesh convergence, a 7.8 tonnes anchor is pulled at a speed of 2 knots, this constant speed is applied to first link of chain opposite to anchor in loose soil. A snapshot of the analysis simulation capturing this process is depicted in Figure 6.1.

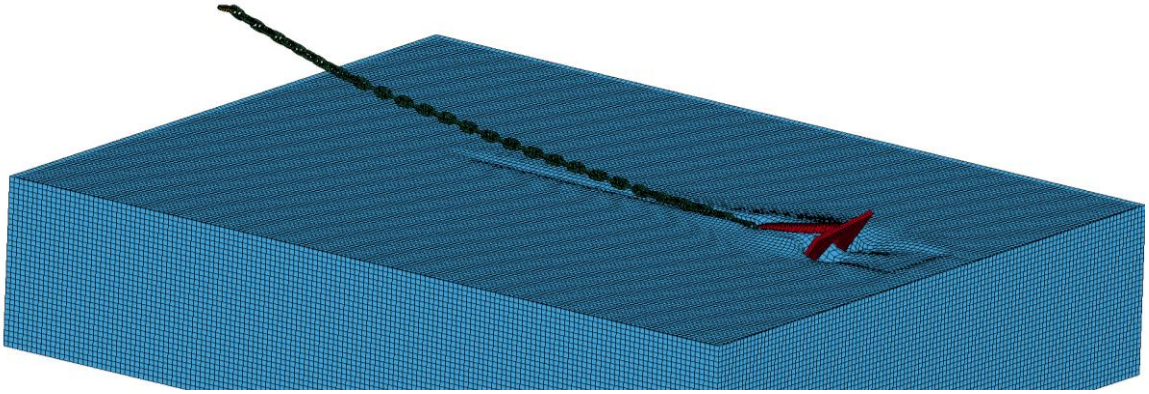

Figure 6.1: Snapshot of anchor soil interaction during convergence test (125mm soil mesh)

In the convergence test, three different mesh sizes were examined for soil domain: 250 mm, 125 mm, and 62.5 mm. The mesh converged with an element size of 125 mm for the soil. Figure 6.2 illustrates the convergence results, indicating that both the 125 mm and 62.5 mm element sizes yield approximately similar resultant forces of traction between the anchor and soil. The resultant force is the force experienced between dragged anchor and soil.

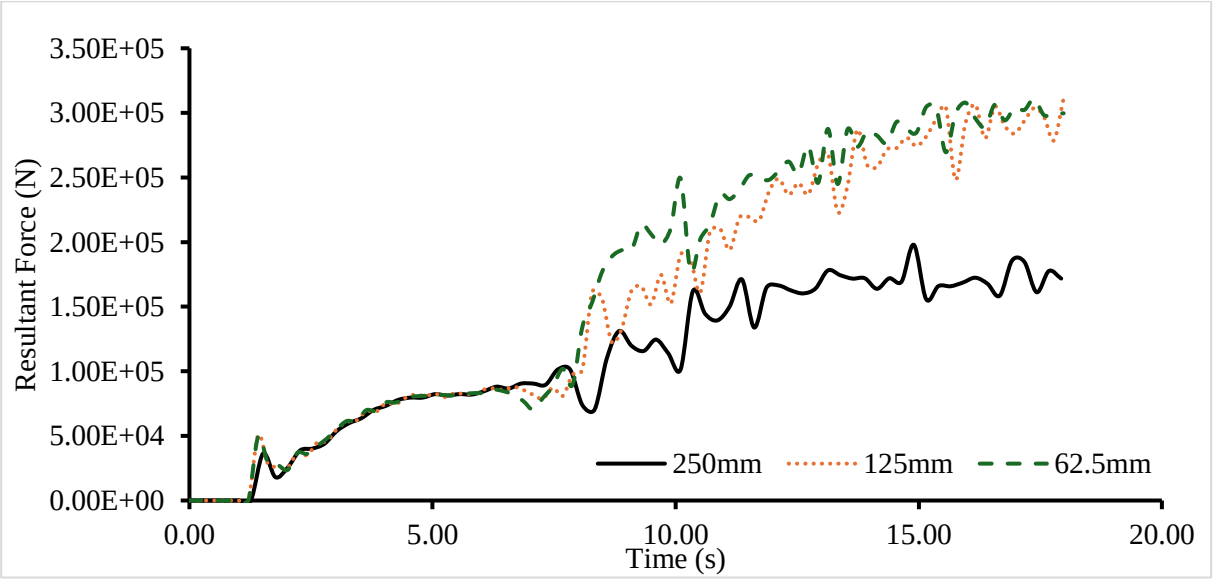

Figure 6.2: Mesh convergence test results, loose soil, 2 knots

Reducing the CPU hours required for computing an analysis model is vital, especially considering that decreasing the mesh size increases the number of elements, thereby affecting CPU hours. In Figure 6.3, detailed information regarding the CPU hours utilized for three different mesh sizes for the soil domain is provided. The 125 mm element size was found to be converged, requiring 43.2 CPU hours to compute the analysis model. In comparison, the 250 mm and 62.5 mm element size mesh consumed 6.8 and 672 CPU hours, respectively.

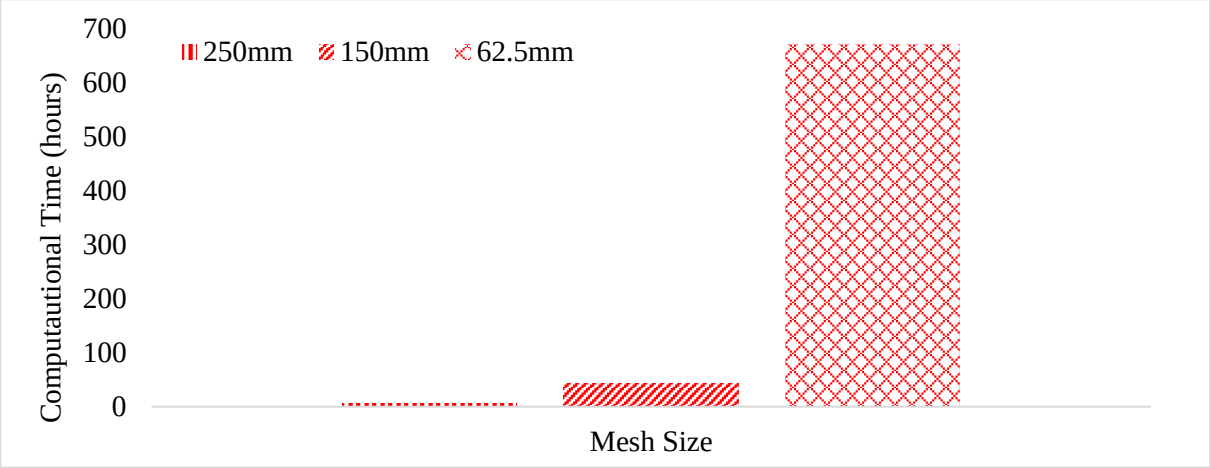

Figure 6.3: CPU hours taken to complete the convergence analysis

6.2 Numerical Models Validation

6.2.1 Anchor-Soil Interaction Force

For calibrating the FEA model of dragged anchor in soil, anchor-soil interaction force is calibrated with the reference values, reference values for soil-anchor interaction force were obtained from (Naeij et al., 2023), with detailed information available in section 3.1. Table 5.3 provides the essential values for soil properties utilized in this model. Furthermore, both studies (reference model and model in this thesis) employ a 7.8 tonnes anchor. These forces are calibrated once the anchor is fully penetrated into the soil. It is important to note that the dimensions of the anchor are not provided in the reference article. Hence, a simplified anchor used in this thesis adheres to the standard dimensions depicted in Table 5.4. After extensive investigation into the element erosion criteria to calibrate interaction forces between dragged anchor and soil, the erosion criteria were set based on three parameters: volumetric strain, plastic strain, and effective strain. The input parameters for these element erosion criteria are detailed in Table 6.1.

Table 6.1: Parameters for element erosion criteria

Parameter	Value
Volumetric Strain	0.6
Plastic Strain	1
Effective Strain	1

Figure 6.4 represent the good agreement between model used in this thesis and experimental model used in reference article (Naeij et al., 2023).

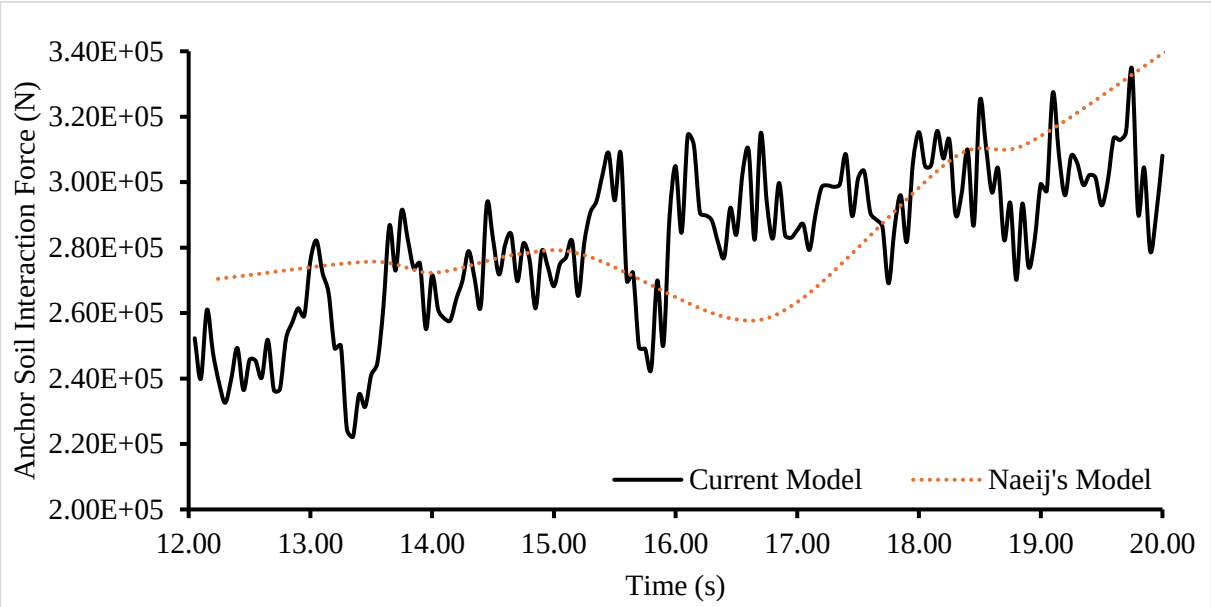

Figure 6.4: Calibration of soil-anchor interaction FEA numerical model, loose soil, 7.8 tonnes anchor, speed 2 knots

6.2.2 Steel Pipe Deformation

To validate the pipe deformation model, reference values were taken from article (Zeinoddini et al., 2013) which is detailed in section 3.4. To validate the steel pipe deformation only rigid bed is considered in this model. The rest of the properties and geometries are taken from reference article (Zeinoddini et al., 2013), where for steel pipe D/t=76, D=611mm, t=8mm, and yield stress= 517MPa. Whereas vertical speed of 70mm/s was applied to the indenter. The model for the steel pipe deformation validation can be seen in Figure 6.5.

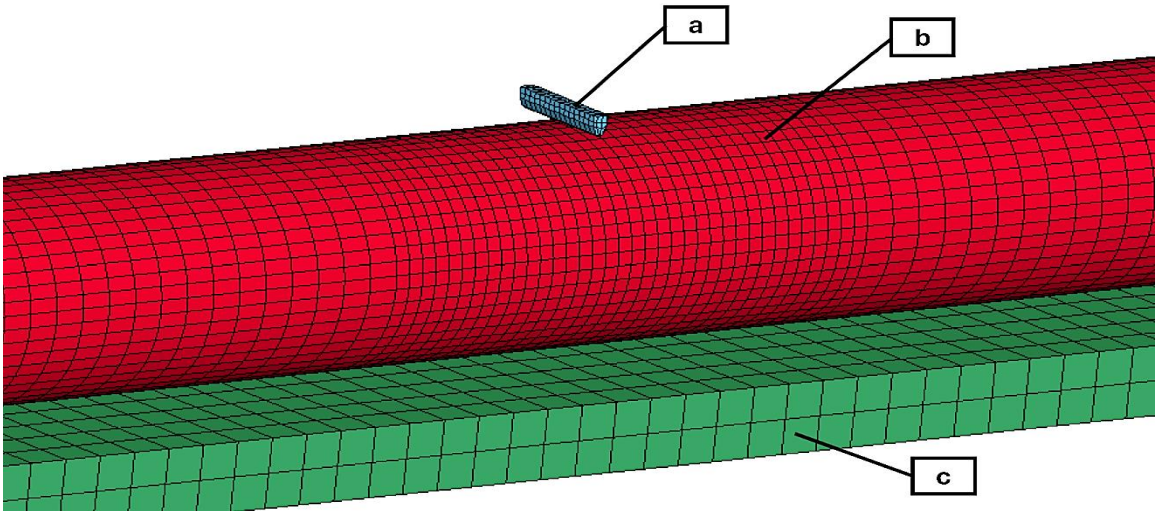

Figure 6.5: Pipe deformation validation model in LS-Dyna, a) blue part represents rigid indenter, b) red part indicates pipe, c) green part is depicts rigid bed

In Figure 6.6 and Figure 6.7 it can be seen that results from the validation model are in good agreement with reference values from (Zeinoddini et al., 2013). The energy term represents the area under the force-displacement curve between the indenter and the pipe, it quantifies the work done during the deformation process. Normalized deformation, on the other hand, is calculated by dividing the magnitude of the largest displaced node by 0.5D of the pipe, where D represents the diameter of the pipe. This normalization allows for a comparison of deformation across different pipe sizes.

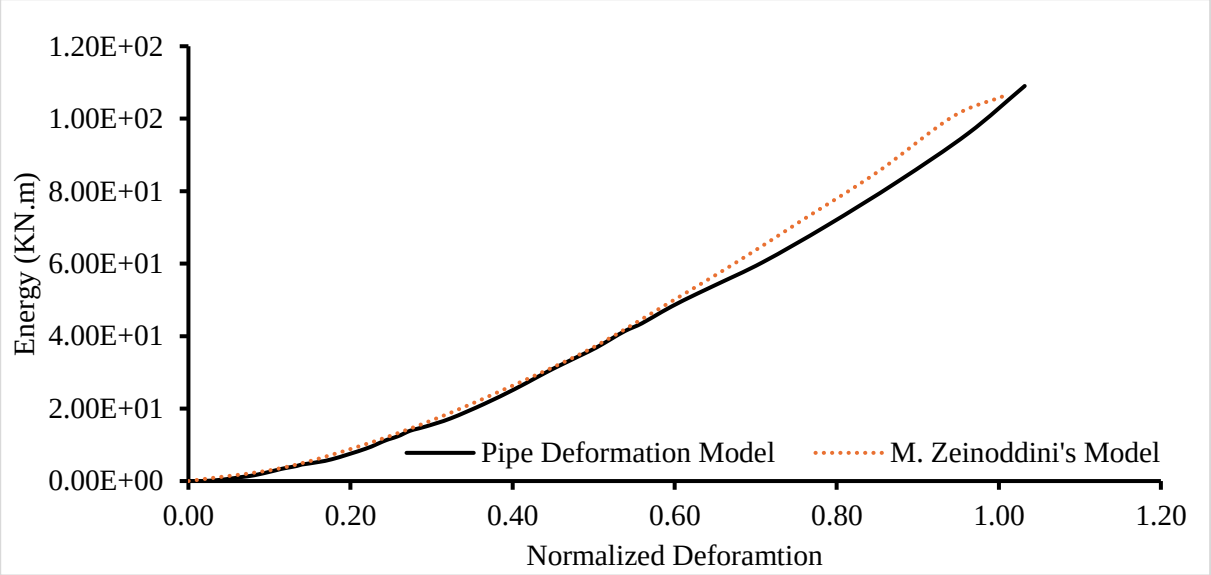

Figure 6.6: Pipe deformation validation, free ends (Zeinoddini et al., 2013)

It is noteworthy that the pipe with fixed ends required more force to achieve the same deformation compared to the model with free ends. This observation indicates the influence of boundary conditions on the deformation behavior of the pipe.

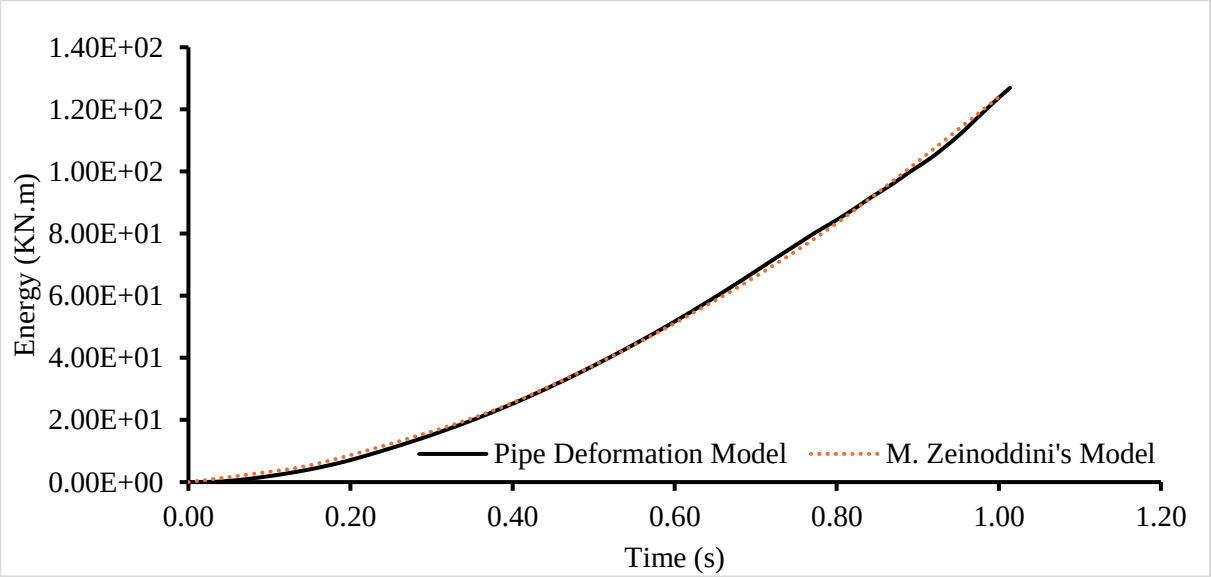

Figure 6.7: Pipe deformation validation, fixed ends (Zeinoddini et al., 2013)

Figure 6.8 depicts a snapshot of deformation and stress distribution during quasi-static analysis for FEA model validation purpose.

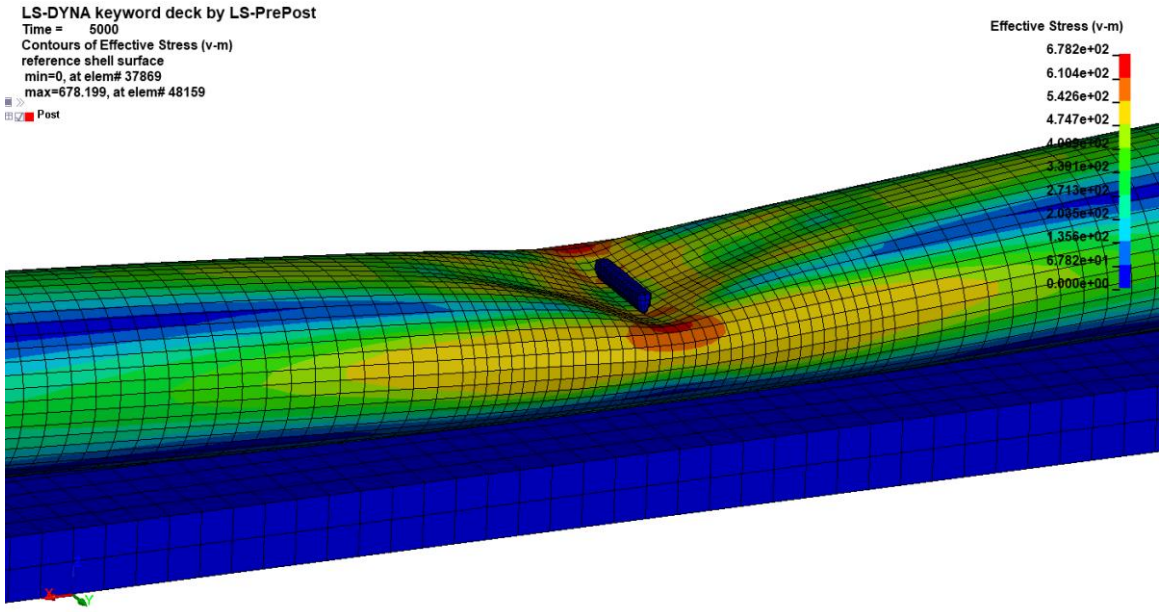

Figure 6.8: Snapshot of pipe deformation and stress distribution during pipe FEA model validation, fixed ends and rigid bed

NB. In the final model for the anchor interaction with soil and pipeline, pipeline is modeled as rigid body to reduce the complexity and computational time of model.

6.3 Hourglass Sensitivity

To calibrate the anchor-soil-pipeline analysis, element erosion criteria are used with a Lagrangian mesh field to address the unrealistic behavior of element deformation. An example of large deformation can be seen in Figure 6.9.

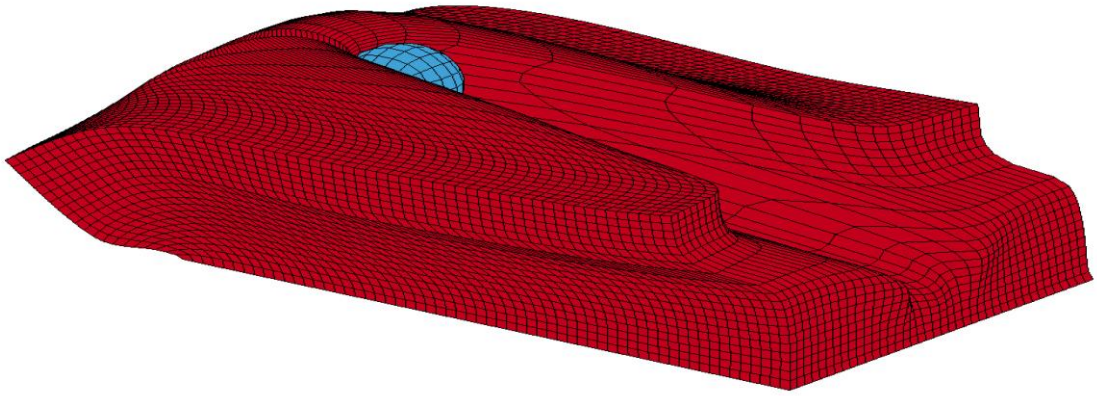

Figure 6.9: Test model for soil deformation and hourglass analysis, extreme deformation of loose soil, Hourglass formulation #5, Hourglass coefficient 0.05, no element erosion criteria

In Figure 6.9, it is evident that the elements deform as the rigid ball passes through the soil, causing soil elements to stretch significantly in response to the ball's displacement. This extreme deformation of elements is unrealistic and unacceptable in finite element analysis (FEA) based on Lagrangian mesh field, that's why erosion criteria was must have with soil material.

After extensive investigation into soil behavior under different Hourglass formulations and coefficients, a formulation was selected based on the "Flanagan-Belytschko with exact volume integration" model, with the hourglass coefficient set at 0.05. Despite this, significant shear deformation led to hourglass energy levels constituting 10-18% of the total internal energy of the model, which is considered excessively high in engineering practice.

Additionally, in Figure 6.10 it can be observed that hourglass energy is dependent on the element size in the soil domain. This data was extracted from the mesh convergence tests.

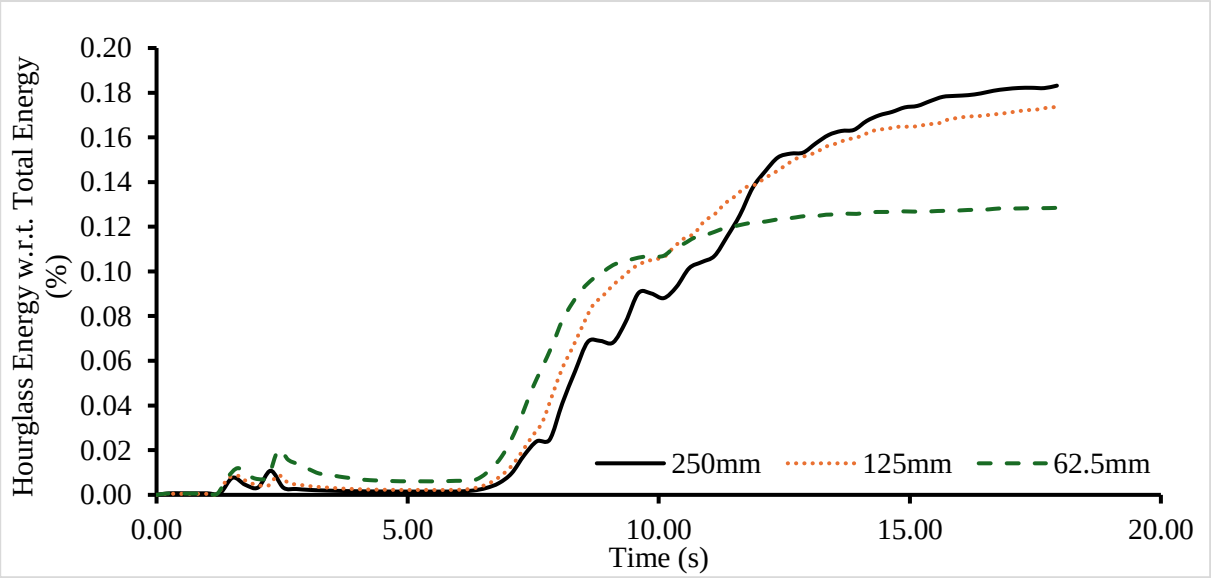

Figure 6.10: Relation between hourglass energy and soil mesh element size

6.4 Mesh Size & Element Erosion Criteria vs Anchor Penetration

Element erosion criteria is sensitive to large forces acting on a Lagrangian mesh domain. For instance, the pressure on a surface with a constant force change with the change in area on which the force is acting. In the context of soil, the force exerted by a dragged anchor affects the soil elements. As the element size decreases, the pressure on the soil elements increases, causing the elements to meet the erosion criteria more quickly compared to larger element sizes.

A similar scenario was observed during the mesh convergence study. As the element size decreased, the anchor penetrated deeper into the soil. This increased penetration was due to the higher pressure exerted on smaller elements, which have a smaller area. Figure 6.11 illustrates this phenomenon observed during the mesh convergence tests.

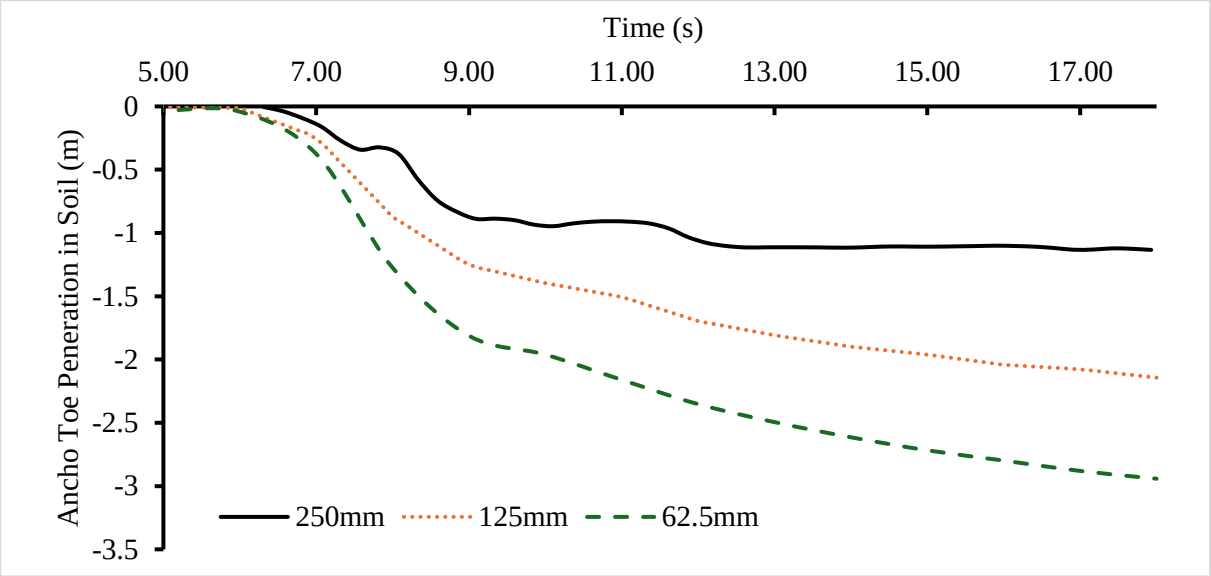

Figure 6.11: Effect of element size on anchor penetration in soil, 7.8 tonnes anchor, 2 knots, loose soil

The statements made above are also supported by the energy eroded (Figure 6.12) from the FEA model due to the element's erosion. Where mesh with the minimum size has the largest values for the eroded energy from the model.

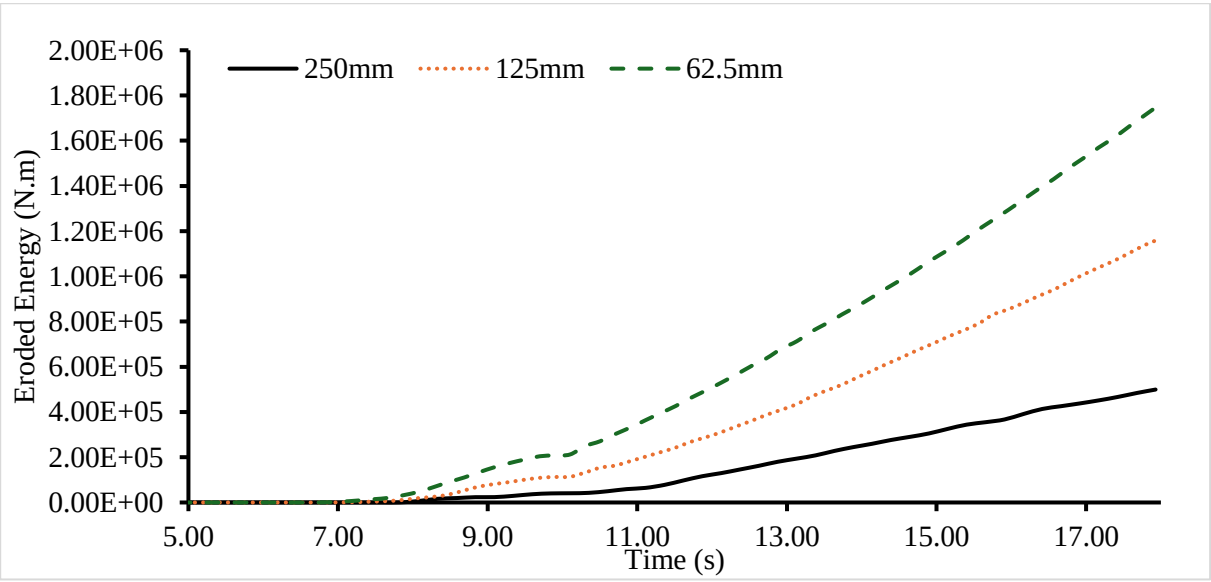

Figure 6.12: Eroded energy vs element size, 7.8 tonnes anchor, 2 knots, loose soil

6.5 Contact Sensitivity

SOFT=2 contact methods is employed in FEA model, detailed in section 4.2. In this contact type, stiffness between two parts is dependent on segments masses, scale factors, and the global timestep. Since the anchor exerts extreme forces during dragging, sufficient stiffness between parts is required to withstand these forces. As the densities of the materials cannot be altered, the only options left to manage

the contact stiffness between parts are scale factors or the global timestep. Both options are utilized to achieve sufficient stiffness to bear the extreme forces between the chain, anchor, and soil.

To reduce the global timestep, the *TSSFAC* scale factor option in LS-Dyna is used, set to 0.4. *TSSFAC* is a scale factor for the global timestep. *SFSA* and *SFSB*, the scale factors for slave and master segments in contact, are both set to 100 (in 5 tonnes anchor cases) for chain-anchor contacts.

In cases of lower stiffness, element segments penetrate each other, as shown in Figure 6.13. Conversely, setting the scale factor too high to achieve greater stiffness between element segments can result in abrupt ejection of chain links (Figure 6.14).

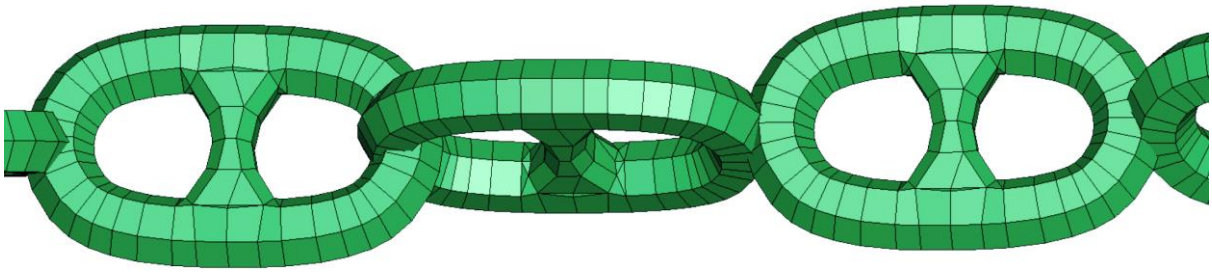

Figure 6.13: Segments penetration due to low contact stiffness

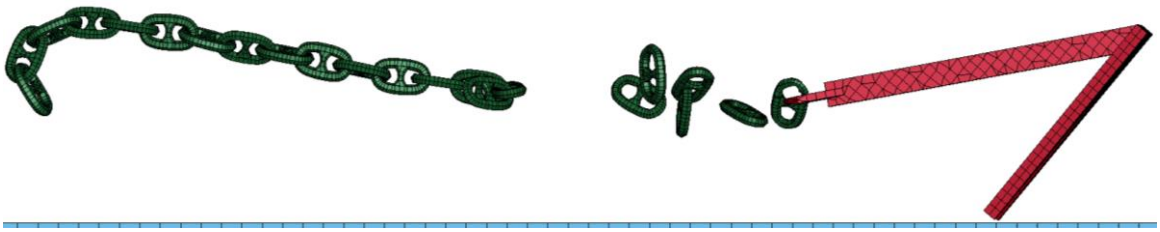

Figure 6.14: Ejection of chain links due to high contact stiffness

Thus, controlling this contact behavior is quite sensitive. With the current contact stiffness control, there is a limit of approximately 775 KN pulling force between chain links.

6.6 Anchor Penetration Depth in Soil

The penetration of the anchor into the soil was observed decidedly dependent on the weight of the anchor. In this thesis, three anchor sizes were analyzed: 3, 5, and 7.8 tonnes anchors. The results indicate significant differences in penetration depths for different anchor sizes in loose soil, as illustrated in Figure 6.15. It can be observed that the 3 tonnes anchor achieved its stable penetration depth after a 10-meter displacement. In contrast, the 5 tonnes anchor reached stable penetration after approximately 12 meters. The 7.8 tonnes anchor, however, did not achieve a stable depth in the soil even after being dragged for 14 meters.

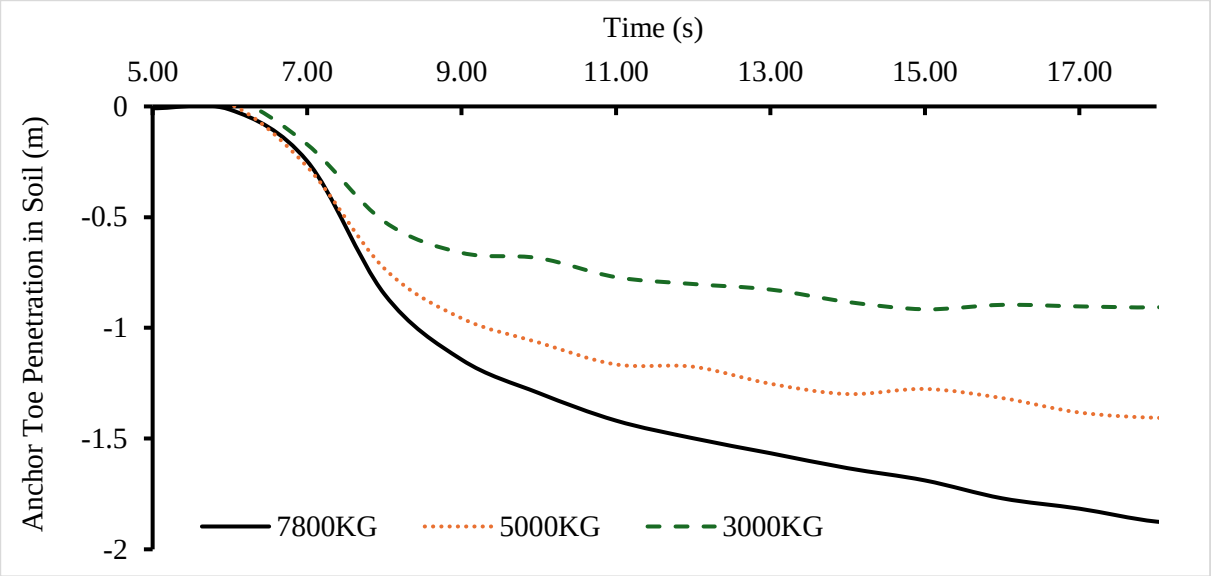

Figure 6.15: Effect of anchor size on the penetration depth in the soil, loose soil, 2 knots

Data from Figure 6.16 suggests that loose soil facilitates deeper anchor penetration into the seabed compared to stiff soil. This is evidenced by the penetration depths of 1.14 meters and 0.21 meters for loose soil and stiff soil, respectively. Table 5.3 provides the specific soil properties used in the study. Notably, the anchor only began dragging after reaching a stable state under gravitational forces at $t=10$ seconds.

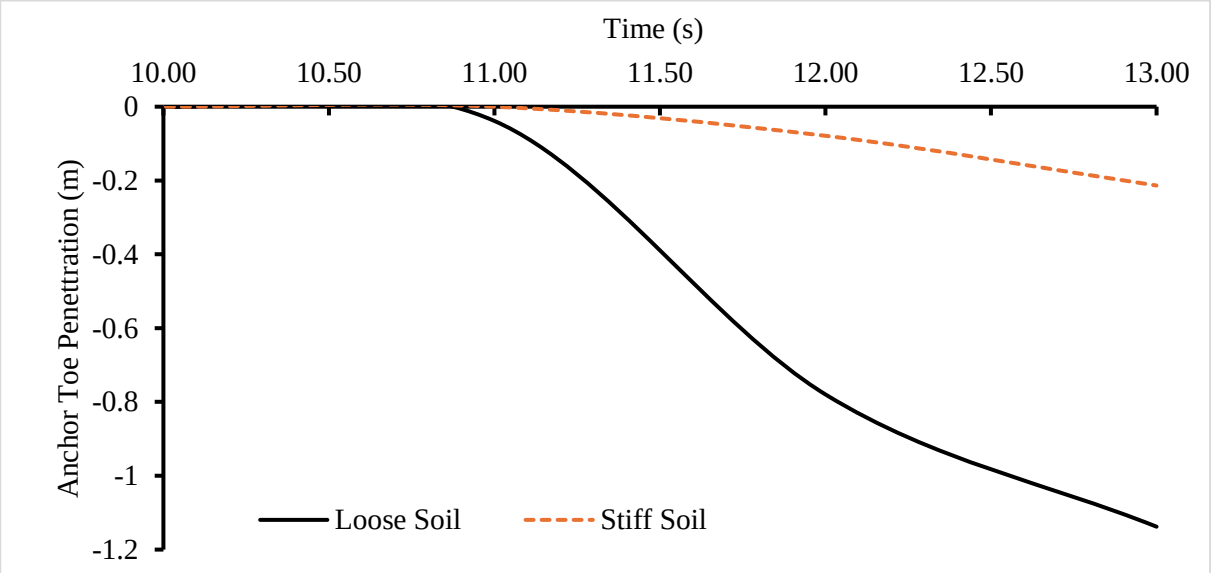

Figure 6.16: Comparison of anchor penetration in different soil types, 5 tonnes, 10 knots

6.7 Dragged Anchor, Soil, and Pipeline (Parametric Study)

A finalized FEA model to study the interaction between a dragged anchor and a subsea pipeline can be seen in Figure 6.17. In this model, a rigid 20-inch (OD) pipeline with a length of 9 meters investigated against dragged anchor. The angle of attack between the pipe and the anchor is set to 90 degrees.

Additionally, a separate model examines the interaction when the dragged anchor attacks the pipeline at an angle of 45 degrees.

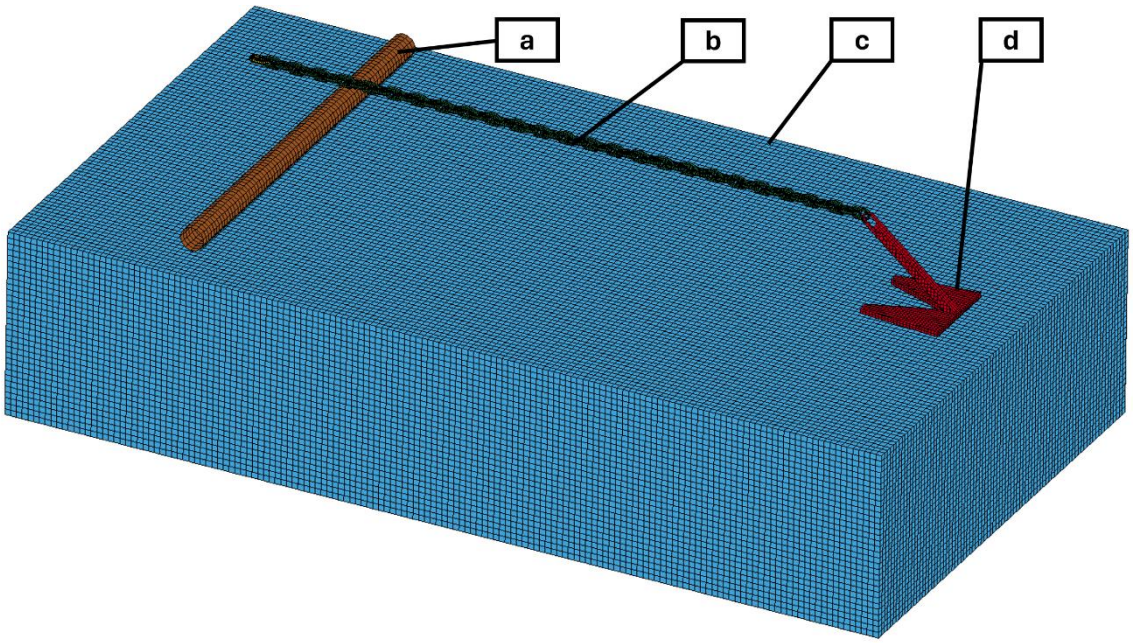

Figure 6.17: FEA model to investigate the interaction between dragged anchors and subsea pipelines, angle of attack=90 degrees, chain length=14m, a, b, c, and d represents rigid pipe, chain, seabed, and anchor respectively

Figure 6.18 depicts the configuration of ID (identification) for the parametric case study, Where *D* is outer diameter of pipe and *C* represents the chain's angle with seabed.

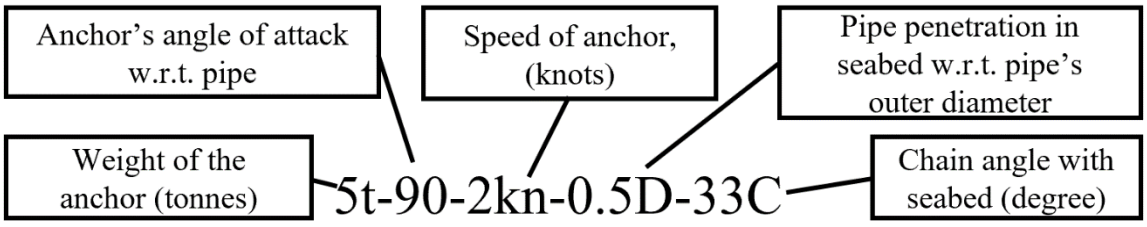

Figure 6.18: Configuration of case ID for parametric study, example ID

Three distinct modes of interaction between the anchor and the pipeline on the seabed were observed during the parametric study of different cases outlined in Table 6.2: hooking, sliding, and bouncing over, Figure 6.19, Figure 6.20, and Figure 6.21 depict these phenomena, respectively. Figure 6.19 illustrates the hooking interaction, where the anchor engages with the pipeline. Figure 6.20 shows the sliding interaction, where the anchor glides along the pipeline. Figure 6.21 demonstrates the bouncing over interaction, where the anchor moves over the pipeline without significant engagement.

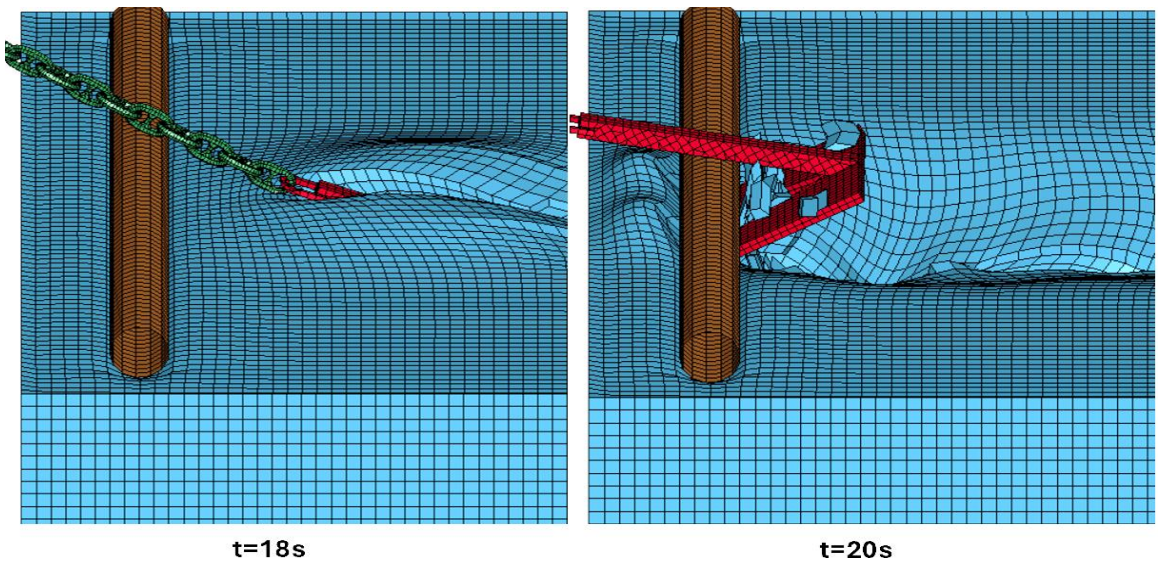

Figure 6.19: Hooking contact between anchor and pipe, side view, case ID:5t-90-2kn-0D-33C

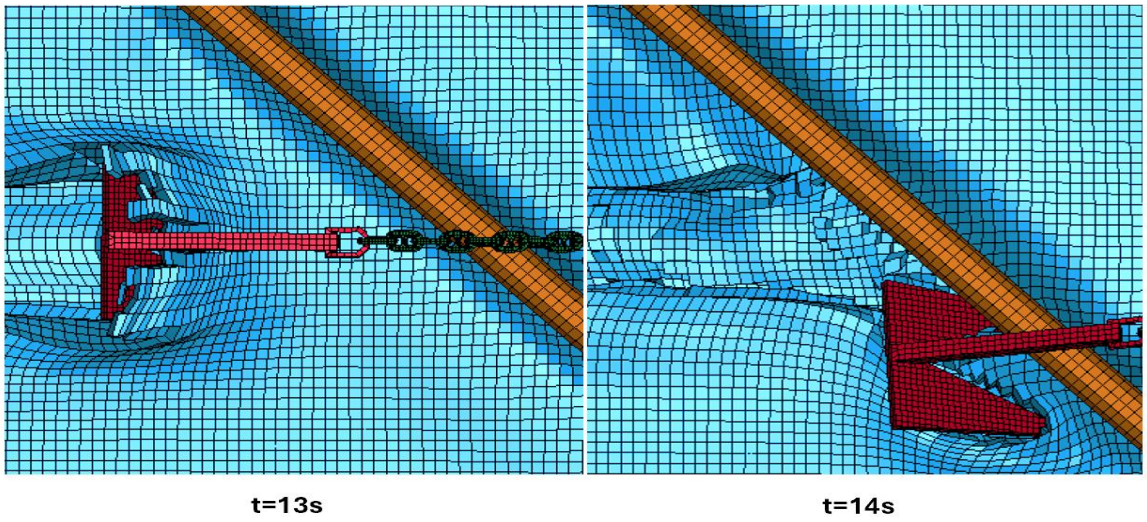

Figure 6.20: Sliding contact between anchor and pipe, top view, case ID: 5t-45-10kn-D-33C

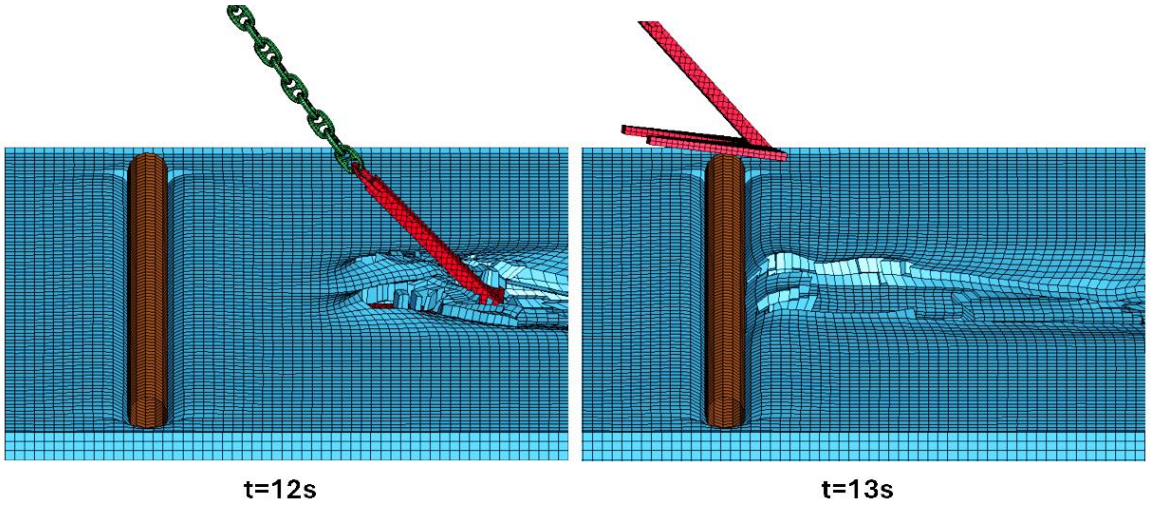

Figure 6.21: Bouncing over contact between anchor and pipe, side view, case ID: 5t-90-10kn-0.5D-80C

Table 6.2: Parametric study of dragged anchor interaction with subsea pipe, loose soil

Case Number	Case ID	Anchor-pipe interaction mode
1	5t-90-2kn-0D-33C	Hooked
2	5t-90-2kn-0.5D-33C	Hooked
3	5t-90-2kn-D-33C	Hooked
4	5t-45-2kn-0D-33C	Sliding
5	5t-45-2kn-0.5D-33C	Sliding
6	5t-45-2kn-D-33C	Sliding
7	5t-90-10kn-0D-80C	Hooked
8	5t-90-10kn-0.5D-80C	Bounced over
9	5t-90-10kn-D-80C	Bounced over
10	5t-45-10kn-0D-80C	Bounced over
11	5t-45-10kn-0.5D-80C	Bounced over
12	5t-45-10kn-D-80C	Bounced over
13	5t-90-10kn-0D-33C	Hooked
14	5t-90-10kn-0.5D-33C	Hooked
15	5t-90-10kn-D-33C	Hooked
16	5t-45-10kn-0D-33C	Hooked
17	5t-45-10kn-0.5D-33C	Sliding
18	5t-45-10kn-D-33C	Sliding
19	5t-45-10kn-0D-4C	Sliding
20	5t-45-10kn-0.5D-4C	Sliding
21	5t-45-10kn-D-4C	Sliding

Table 6.3: Parametric study of dragged anchor interaction with subsea pipe, Stiff soil

Case Number	Case ID	Anchor-pipe interaction mode
1	3t-90-2kn-0D-4C	Hooked
2	3t-90-10kn-D-4C	Bounced over
3	3t-90-10kn-0.5D-4C	Bounced over
4	5t-90-2kn-D-4C	Hooked
5	5t-90-10kn-0D-4C	Hooked
6	5t-90-10kn-D-4C	Bounced over

6.7.1 Loose soil

A parametric study (Table 6.2) was conducted to investigate the behavior of an anchor, pipeline, and seabed under varying conditions. A total of 21 different cases were considered for loose soil. The

mooring chain's angle with the seabed was a key factor, with 12 cases analyzing 33 degrees angle, 6 cases focusing on an 80 degrees angle, and 3 cases examining a 4 degrees angle (refer to section 5.2.2 for detailed explanations of the 33 and 80 degrees scenarios). The 4 degrees angle case was specifically chosen to study the interaction between the anchor, soil, and pipeline when the mooring chain moves nearly parallel to the seabed. Speed was another variable considered in the study. Out of the 21 cases, 6 employed a speed of 2 knots, while the remaining 15 cases were analyzed at a speed of 10 knots.

Figure 6.22 illustrates the relationship between the number of distinct interaction modes and the mooring chain's angle relative to the seabed. Notably, the 45 degrees attack angle scenario in most cases resulted in the anchor either bouncing over or sliding along the pipe. This observation aligns well with real-world practices, highlighting the strong agreement between the FEA model developed in this thesis and practical applications.

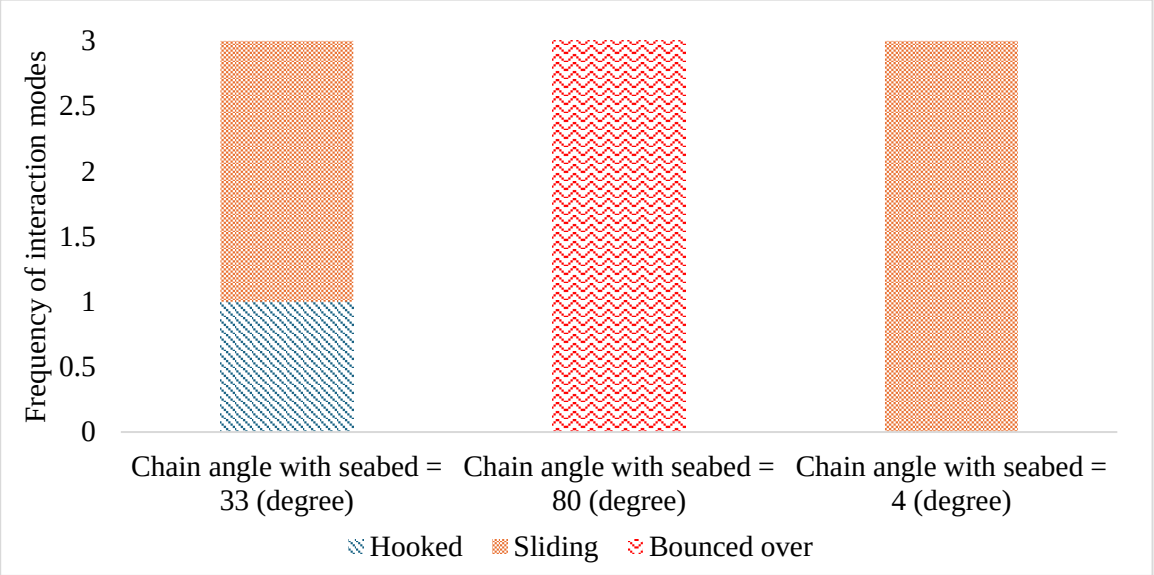

Figure 6.22: Anchor-pipe interaction modes, frequency of different interactions mode with 10 knots speed and 45 degrees angle of attack between anchor and pipe

Figure 6.23 presents the frequency of various interaction modes for different attack angles in 21 cases. The analysis focuses on the relationship between interaction mode and angle of attack. As the figure illustrates, cases with a 45 degrees attack angle predominantly resulted in either sliding or bouncing events between the anchor and pipeline. Notably, only one instance exhibited hooking behavior at this angle. In contrast, analyses involving a 90 degrees attack angle primarily yielded hooking or bouncing events, with no observations of sliding contact, this outcome is in strong agreement with the research article (Bartolini et al., 2018).

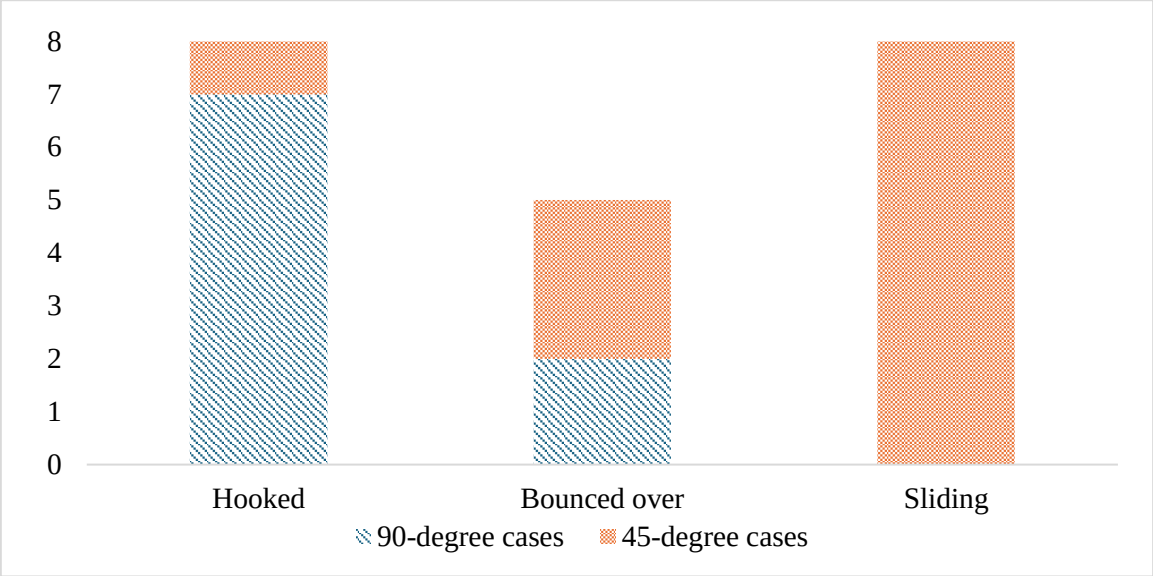

Figure 6.23: Anchor-pipe interaction modes in different angles of attack

7. Conclusion and Assumptions

7.1 Conclusion

The primary objective of this study was to build upon existing research and develop a numerical model to predict the interaction between dragged anchors and pipelines on the seabed, as well as to evaluate the effectiveness of rock berms as a preventive measure for pipeline protection. An FEA-based numerical model was established utilizing Autodesk Inventor and LS-Dyna tools, employing a Lagrangian mesh with element erosion criteria. The modeling process encompassed CAD modeling, FEA model setup, and thorough validation. The significant findings are summarized below:

- Extensive literature review has been conducted to explore numerical methods aimed at predicting the behavior of anchor-pipeline interactions and designing rock berms within numerical models to attain realistic simulations.
- The study successfully demonstrated that large deformations can be managed in FEA models using a Lagrangian mesh, provided that element erosion criteria are implemented to mitigate unrealistic extreme deformations. However, due to substantial deformations in the reduced integrated elements, the hourglass energy remained between 10-18% of the total internal energy of the model.
- For the interaction between a 20-inch (OD) pipeline and a 5 tonnes anchor on loose soil, the following observations were made:
    - The angle of attack between the anchor and the pipeline significantly impacts the interaction mode, determining whether the anchor hooks, slides, or bounces over the pipeline. According to the parametric study, a 45 degrees attack angle tends to result in sliding or bouncing over, while a 90 degrees attack angle is more likely to produce hooking or bouncing over anchor interaction mode with pipe.
    - It has also been observed that anchors moving at higher speeds are less likely to hook the pipeline, as anchors moving at higher velocities achieve less penetration in the soil compared to those moving at lower speeds.
    - Anchor mass is a major factor affecting penetration depth in the seabed. According to the analysis results, the 3, 5, and 7.8 tonnes anchors with 2 knots speed achieved penetration depths of approximately 0.9 meters, 1.4 meters, and around 2 meters, respectively.
- A considerable difference was noted during the comparison of anchor penetration in stiff and loose soils. For stiff soil, the 5 tonnes anchor with 10 knots speed penetrated approximately 0.21 meters, while in loose soil, it penetrated approximately 1.14 meters.
- Validation of pipeline deformation FEA models was conducted, and the results were found to be in good agreement with reference study.

7.2 Assumptions and Simplifications

Assumptions and simplifications made in the thesis:

- Soil is homogeneous regardless of depth effect, and the seabed is plain.
- A constant speed is applied to the dragged anchors.
- No water depth effect is taken into account.
- A linear line is considered for the chain's free shape between the vessel and anchor.
- Sea water isn't taken into account, so there is no effect of seawater movement in the analysis model.
- Shell elements with scaled masses are used instead of solid bodies to reduce the number of elements.
- A simplified anchor is utilized to minimize the complexity of a realistic anchor shape.
- The pipeline is considered a rigid body, and deformation of the pipeline due to anchor interaction isn't studied in this thesis.
- Anchor is dropped on the seabed from a height of approximately 0.5 meters with the help of gravity.
- No initial penetration of anchor in the soil is counted due to drop effect, anchor is penetration due to the dragging process only.

Further Study Recommendations

It would be interesting to investigate the further work recommended below:

- Design a similar analysis model using a CEL mesh domain, which does not require erosion criteria for large deformations. Use solid elements instead of shell elements for the anchor, chain, and rock berm to avoid the usage of scaled masses which then affect the behavior of contact's stiffness.
- Consider the effect of depth on soil properties to achieve a more realistic representation of the actual seabed.
- Incorporate the drop effect of the anchor on the seabed from realistic heights before anchor dragging.
- It will be interesting to see the effect of different shapes of anchor on the penetration depth in soil.
- Explore Smoothed Particle Hydrodynamics (SPH) and Discrete Element Method (DEM) for anchor-soil interaction, as these mesh-independent methods are more robust for handling such scenarios with large deformations.

Appendix A: Mesh-Independent Numerical Methods provides details of the work done to model the rock berm and soil domain using SPH and DEM. This information could be valuable for further development in the field. Appendix B: Rock Berm details the efforts made to design and analyze rock berm in FEA model.

References

ABAQUS. *Mohr-Coulomb Material Model*. https://classes.engineering.wustl.edu/2009/spring/mase5513/abaqus/docs/v6.6/books/stm/default.htm?startat=ch04s04ath117.html

Ansys, I. *Explicit Thin Structural Shell - Shell 163*. BME - Department of Applied Mechanics. https://www.mm.bme.hu/~gyebro/files/ans_help_v182/ans_elem/Hlp_E_SHELL163.html

Aspenberg, D. (2018). *Performing simulations in LS-DYNA using Discrete Element Spheres (DES)*. DYNAmore Nordic AB.

Bartolini, L., Marchionni, L., Parrella, A., & Vitali, L. (2018, 2018). Advanced FE Modelling Approach for Pipeline Hooking Interaction of Dragged Anchors.

Chen, W., Wan, F., Guan, F., Liu, X., Yang, Y., & Zhou, C. (2024). The effect of seabed flexibility on the impact damage behavior of submarine sandwich pipes. *Applied Ocean Research*, *142*, 103838.

Erhart, T. (2011). *Review of solid element formulations in LS-Dyna*. Dynamore.de. https://www.dynamore.de/de/download/papers/forum11/entwicklerforum-2011/erhart.pdf

Harish, A. (2024). What is Convergence in Finite Element Analysis. https://www.simscale.com/blog/convergence-finite-element-analysis/

Huang, H. (2010). *Discrete element modeling of railroad ballast using imaging based aggregate morphology characterization*. University of Illinois at Urbana-Champaign.

Imam, R., Fotowat, A., Ng, C., Leung, A., Chiu, A., & Zhou, C. (2018). Numerical modelling of stone columns in unsaturated silty sand. Seventh International Conference on Unsaturated Soils (UNSAT2018),

Jónsdóttir, K. E., & Sævik, S. (2016). Simulation of Anchor Loads on Pipelines. In: NTNU.

Lacome, J. L. (2000). Smooth particle hydrodynamics (SPH): a new feature in LS-DYNA. 6th International LS-Dyna Users Conference, Detroit, USA,

Larsson, S. (2014). Characterization and modeling of rock impact on steel plates. In.

Latham, J.-P., Munjiza, A., Garcia, X., Xiang, J., & Guises, R. (2008). Three-dimensional particle shape acquisition and use of shape library for DEM and FEM/DEM simulation. *Minerals Engineering*, *21*(11), 797-805.

Look, B. G. (2007). *Handbook of geotechnical investigation and design tables*. Taylor & Francis.

LS-DYNA. (2021). *LS-DYNA Keywords User's Manual Volume I*.

LS-DYNA. (2024). *LS-DYNA Keywords User's Manual Volume II*.

Ltd, M. M. I., Health, G. B., Executive, S., Association, U. O. O., & Petroleum, I. o. (2003). *PARLOC 2001: The Update of Loss of Containment Data for Offshore Pipelines*. Energy Institute. https://books.google.com.pk/books?id=TNsAkAEACAAJ

Marsal, R. J. (1973). Mechanical properties of rockfill. *Publication of: Wiley (John) and Sons, Incorporated*.

Mirghasemi, A. A., & Naeij, M. (2015). The effect of initial elongation of elliptical particles on macro–micromechanical behavior during direct shear test. *Procedia engineering*, *102*, 1476-1483.

Mustafina, A. (2015). Anchor damage assessment of subsea pipelines - optimization of design methodology. In: University of Stavanger, Norway.

Naeij, M., Ghafarian, D., Ghasemi, H., & Javanmardi, Y. (2023). Experimental and Numerical Study on the Dragged Anchor–Trenchless Rock Berm Interaction. *International Journal of Ocean and Coastal Engineering*, *5*(01n04), 2340001.

Owen, E. (2020). *LS-Dyna Introduction to contacts*. Oasys Software. https://www.oasys-software.com/dyna/wp-content/uploads/2020/01/Intro-to-Contacts.pdf

Pettersen, T. O., Sævik, S., & Levold, E. (2017). Simulation of Anchor Loads on Pipelines. In: NTNU.

Reese, L. C., Cox, W. R., & Koop, F. D. (1974). Analysis of laterally loaded piles in sand. Offshore Technology Conference,

Selker, R., Liu, P., Karras, D., Bijker, R., & Aktan, O. (2018). Impact of dropped objects and anchor dragging on pipeline integrity. ISOPE International Ocean and Polar Engineering Conference,

Shin, M.-B., Park, D.-S., & Seo, Y.-K. (2020). Response of subsea pipelines to anchor impacts considering pipe–soil–rock interactions. *International journal of impact engineering*, *143*, 103590.

Simscale. (2023). *What Is FEA | Finite Element Analysis*. SIMSCALE. https://www.simscale.com/docs/simwiki/fea-finite-element-analysis/what-is-fea-finite-element-analysis/

SOTRA. (2014a). *Equipment Table*. https://www.sotra.net/?produkter=equipment-table

SOTRA. (2014b). *Stockless Anchors - Spek M*. https://www.sotra.net/?produkter=spek-m

SOTRA. (2014c). *Stud link chain*. https://www.sotra.net/?produkter=stud-link-chain

Sriskandarajah, T., & Wilkins, R. (2002). Assessment of anchor dragging on gas pipelines. ISOPE International Ocean and Polar Engineering Conference,

Standard, D. O. (2010). DNV-RP-F107 - Risk assessment of pipeline protection In. Høvik.

Standard, D. O. (2013). DNV-OS-F101 - Submarine Pipeline System In. Høvik.

Standard, D. O. (2014). DNV-RP-F111 - Interference Between Trawl Gear and Pipelines. In. Høvik.

Standard, D. O. (2018). DNV-OS-E301 - Position Mooring In. Høvik.

Svenning, E. *Modeling Splashing and Sloshing in LS-Dyna using Smoothed Particle Hydrodynamics (SPH)*. DYNAmore Nordic AB.

Veritas, D. N. (2012). Design and installation of fluke anchors. *Offshore Standard DNV-RP-E301*.

Wang, L., Chia, H., Wei, J., & Chen, Q. (2009, 2009). FEA-Based Study of Pipeline Protection From Anchors.

Zeinoddini, M., Arabzadeh, H., Ezzati, M., & Parke, G. A. R. (2013). Response of submarine pipelines to impacts from dropped objects: Bed flexibility effects. *International journal of impact engineering*, *62*, 129-141. https://doi.org/10.1016/j.ijimpeng.2013.06.010

Zhong, H., Yu, Z., Zhang, C., Lyu, L., & Zhao, L. (2022). Dynamic mechanical responses of reinforced concrete pier to debris avalanche impact based on the DEM-FEM coupled method. *International journal of impact engineering*, *167*, 104282.

Appendix

Appendix A: Mesh-Independent Numerical Methods

The Discrete Element Method (DEM) and Smoothed Particle Hydrodynamics (SPH) are advanced, mesh-independent techniques within advanced numerical methods, offering significant advantages for modeling complex interactions in subsea environments. DEM is particularly effective for simulating the behavior of granular materials such as rock berms, while SPH excels in fluid dynamics and soil interaction modeling.

The initial two months of this thesis were dedicated to an in-depth study and rigorous testing of these advanced methods. Several hundred test simulations were conducted to explore their potential in addressing the problems outlined in the thesis scope. Despite promising preliminary results, time constraints necessitated the final model to be developed using conventional FEA techniques. Below is a summary of the key findings and analyses related to the use of SPH and DEM:

The subsequent sections provide a detailed account of the preliminary studies and analyses involving SPH and DEM/SDE techniques. These initial findings can form a solid foundation for future research aimed at leveraging advanced mesh-independent methods to address complex subsea engineering challenges.

To validate the effectiveness of the spherical discrete elements technique employed by (Zhong et al., 2022), slide and repose angle tests were conducted, as detailed in section 4.1.2. For the slide test, a similar model (Figure A.1) was constructed in LS-Dyna and subsequently calibrated by adjusting the variables specified in the *CONTROL_DISCRETE_ELEMENT* card (Figure A.2).

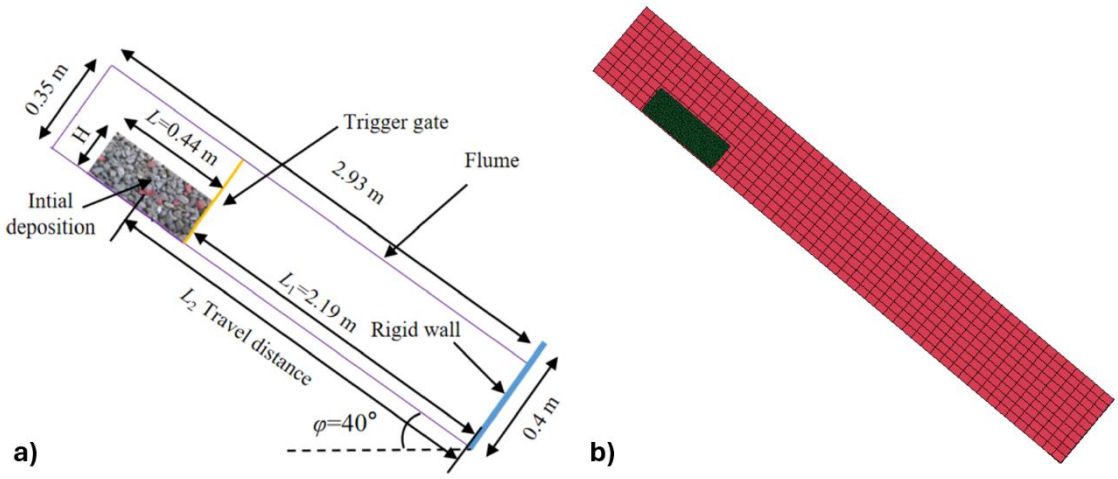

Figure A.1: a) Dimension for the model (Zhong et al., 2022), (b) LS-dyna model for calibration

NDAMP	TDAMP	FRICS	FRICR	NORMK	SHEARK	CAP	VTK
0.9000000	0.3000000	1.4000000	0.1200000	0.0100000	0.0029000	0	0

Figure A.2 : Control card for spherical discrete elements

Figure A.3 illustrates a comparison of the dead zone observed in the slide test, where discrete elements come to rest after sliding due to gravitational force alone. Remarkably, there is a strong agreement between the reference experimental and numerical models and the model utilized in this thesis, affirming the accuracy and reliability of the approach.

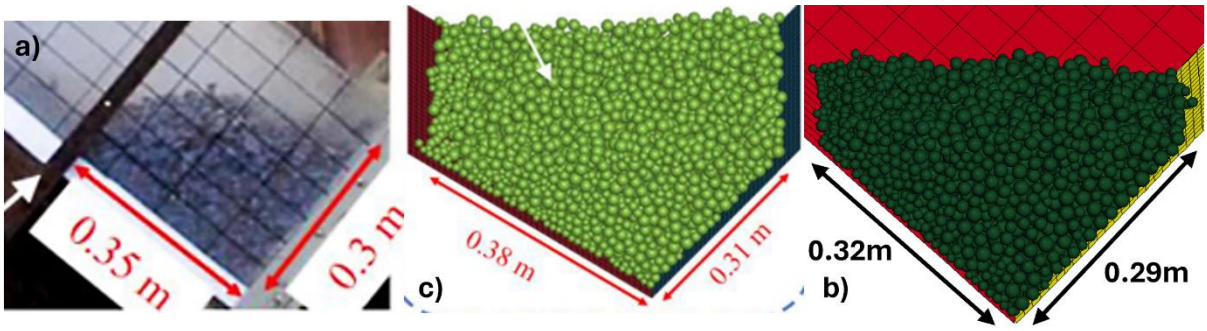

Figure A.3: Calibration of spherical discrete elements, (a) H. Zhong's experimental model (Zhong et al., 2022), (b) H. Zhong's numerical model (Zhong et al., 2022), (c) current study's model

Likewise, the repose angle can be calibrated by adjusting the control variables in the control card (Zhong et al., 2022). In this case, spherical discrete elements were evenly distributed within the range of 10-20mm (Zhong et al., 2022). The input parameters for the control card for discrete elements are depicted in Figure A.4.

The reference repose angle was set at 50° (Zhong et al., 2022). However, with the specified inputs in the control card, the model achieved a repose angle of around 45° (Figure A.5). Further calibration would have been necessary to align the model results more closely with the reference angle.

NDAMP	TDAMP	FRICS	FRICR	NORMK	SHEARK	CAP	VTK
0.7000000	0.3000000	1.4000000	0.1000000	0.0100000	0.0	0	0

Figure A.4: Input parameters for repose test, spherical discrete elements

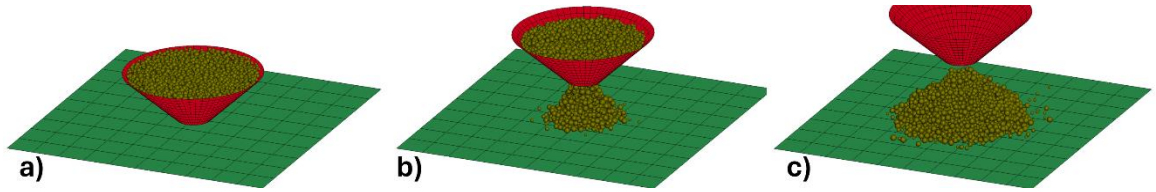

Figure A.5: Repose angle test for discrete elements, (a) initial model for repose test, (b) snapshot of SDE falling due to gravity, (c) final shape of SDE

NB. However, due to time constraints, this validation process was halted, as spherical discrete elements were eventually excluded from the final analysis model.

In this thesis, significant effort has been dedicated to designing the soil domain using the SPH method. Given that SPH is a different numerical approach compared to conventional FEM, it demanded more time than the thesis submission deadline allowed. Consequently, this approach was abandoned for modeling the soil domain. Below snapshots (Figure A.6) presents the effort made into the SPH-based soil domain.

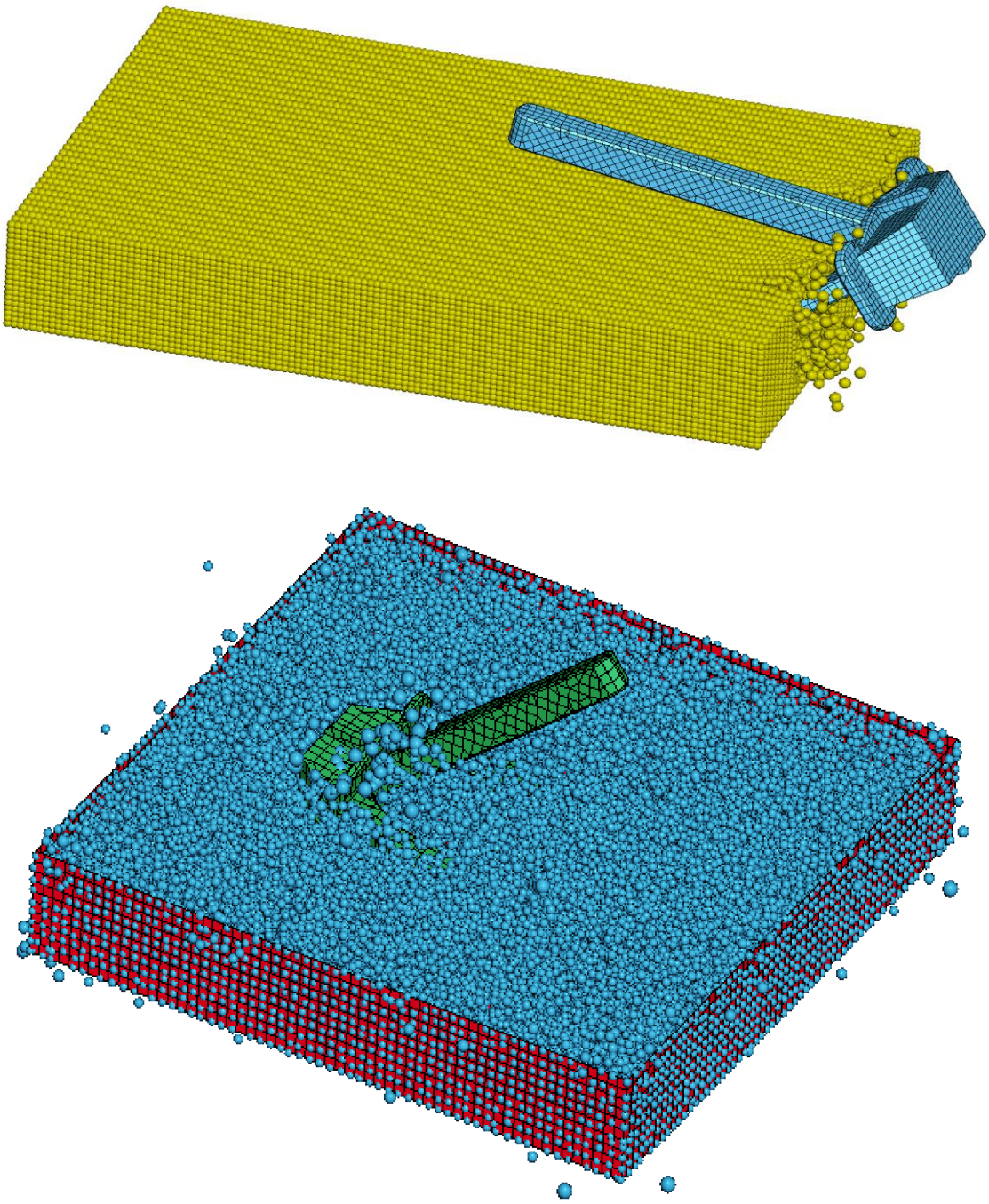

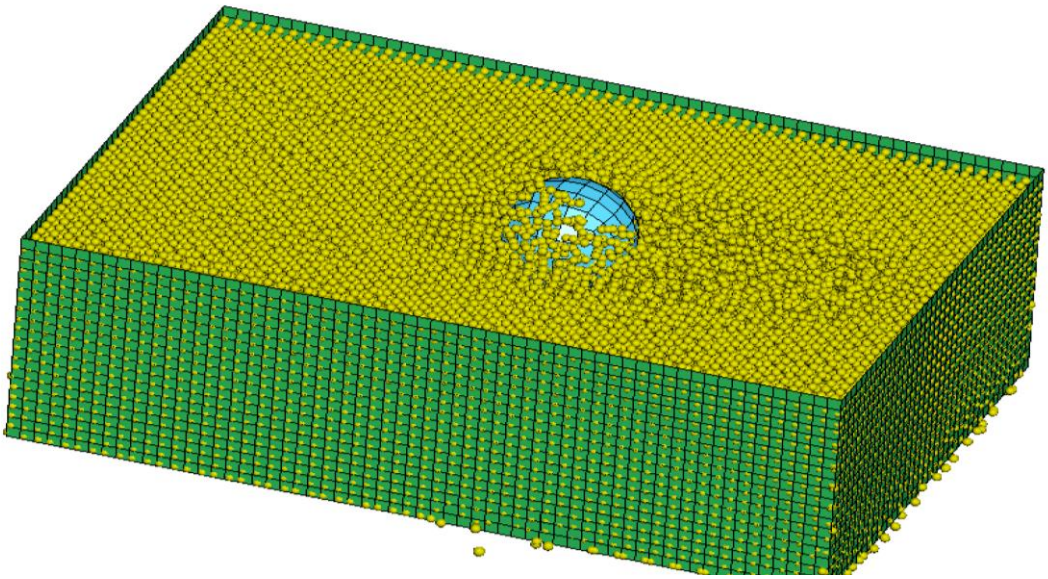

Figure A.6: Snapshots of test models for SPH-based soil domain

Appendix B: Rock Berm

Rock berms are used to protect subsea pipelines from various unforeseen events, such as strong sea waves and potential impacts from dropped or dragged objects like anchors. This protective measure is crucial to ensure the integrity and safety of the pipelines.

Figure B.1 represents the shear-box test procedure, where known normal force is applied to rock particles and upper box is forced to move at fixed speed in one direction, this modal is utilized for the calibration of internal friction while using a method described in section 5.3.

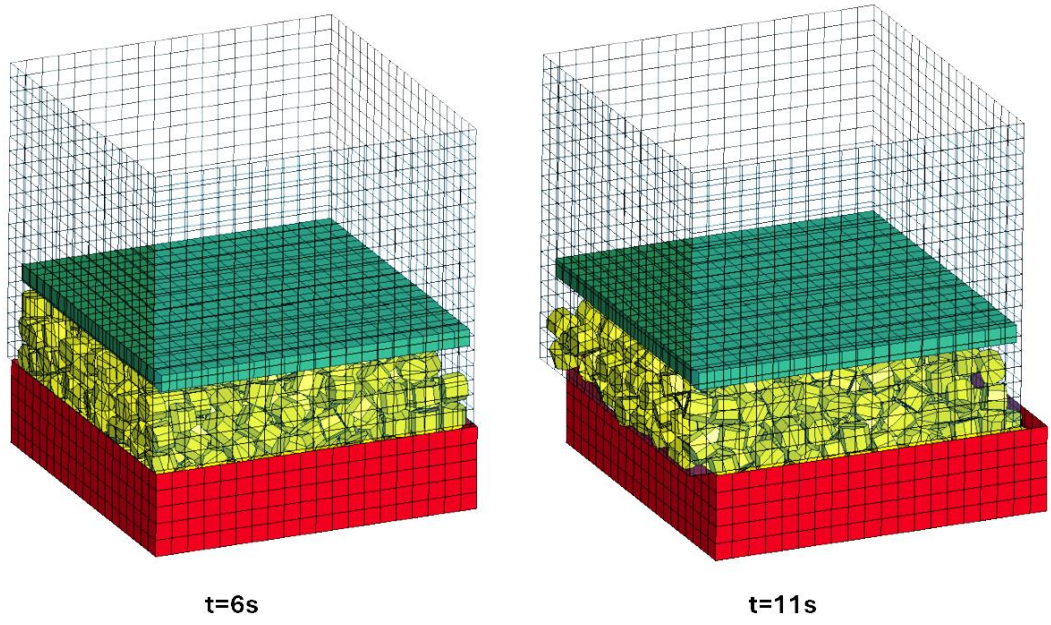

Figure B.1: Shear-box test, FEA model

In Figure B.2, the process of rock berm dumping is illustrated. In this analysis model, rocks are allowed to fall onto the seabed solely under the influence of gravity, and a stabilization period of 5 seconds is provided for the rocks to settle into a stable condition. This approach is adopted from conference proceeding (Wang et al., 2009).

Figure B.3 shows the final shape of the rock berm, which has a width of 10 meters and a height of 1.5 meters at the center of the pipeline. This configuration ensures that the pipeline is adequately covered and protected from potential impacts and environmental forces.

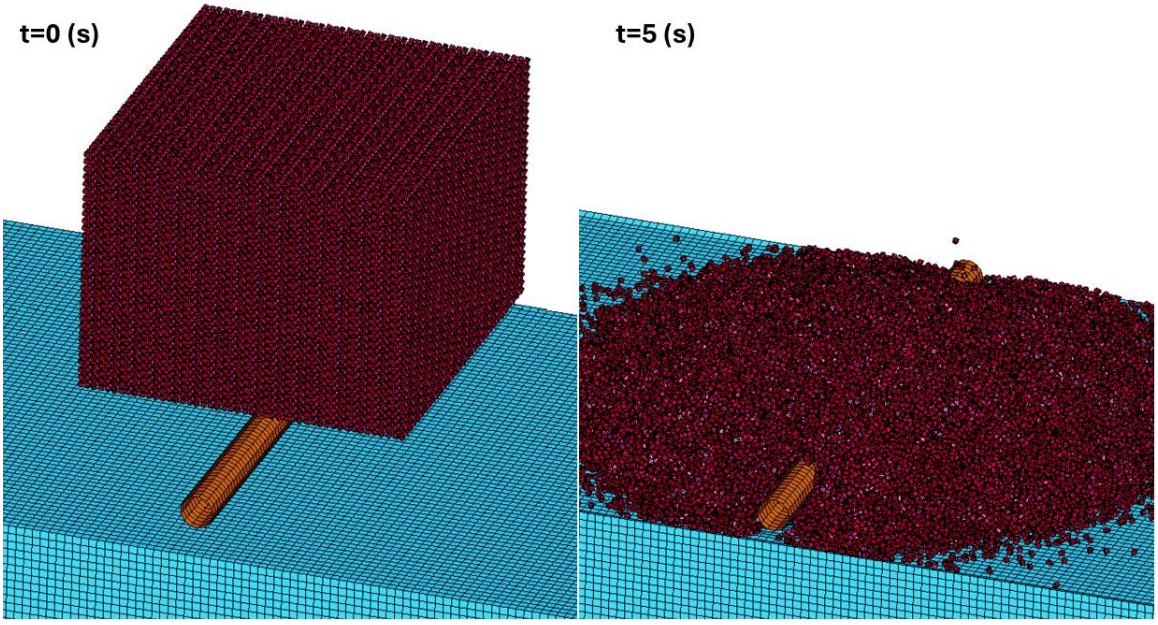

Figure B.2: Rock dumping with the help of gravity

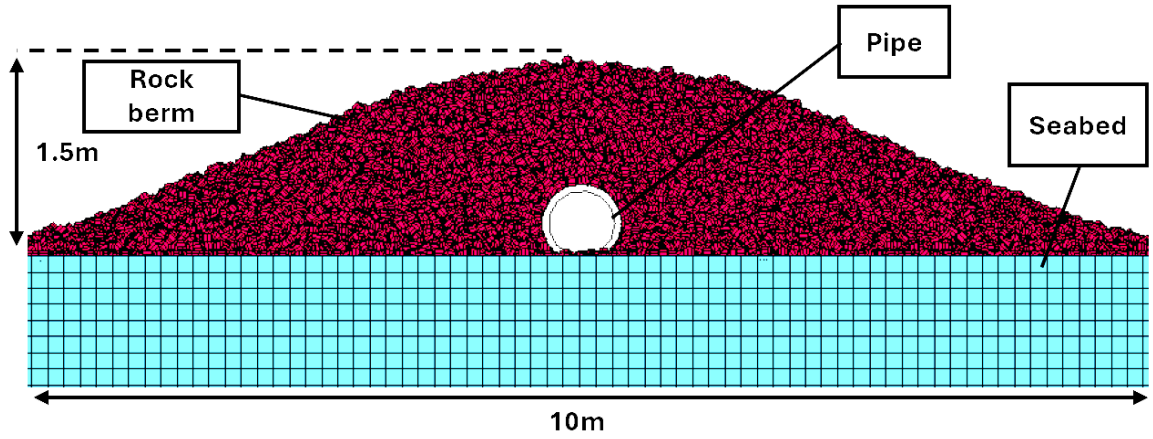

Figure B.3: Rock berm

Figure B.4 presents a test model analyzing the effectiveness of rock berms in protecting pipelines from dragged anchors. The figure demonstrates that as the anchor reaches the boundaries of the rock berm, it begins to lift out of the seabed, thereby proving the efficacy of the rock berm. A similar trend is illustrated in Figure B.5, which provides graphical data on the anchor's toe penetration depth in the seabed. It is

observed that the anchor starts to pull out of the seabed at t=22 and touches the pipeline at t=27. The anchor moves approximately 1 meter out of the seabed before impacting the pipeline.

Using accurate and calibrated Finite Element Analysis (FEA) models, engineers can predict the protective effectiveness of subsea pipelines against various threats. These models allow for the simulation of different scenarios and the evaluation of protective measures like rock berms, ensuring the safety and integrity of the pipeline infrastructure.

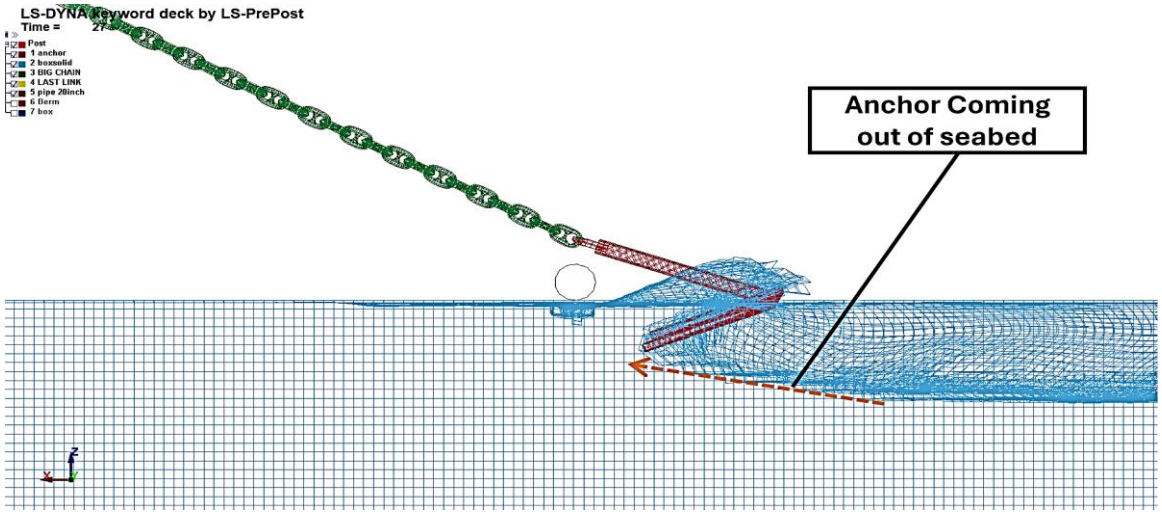

Figure B.4: Snapshot of test simulation, protection of subsea pipeline with the help of rock berm (rock berm is set to invisible)

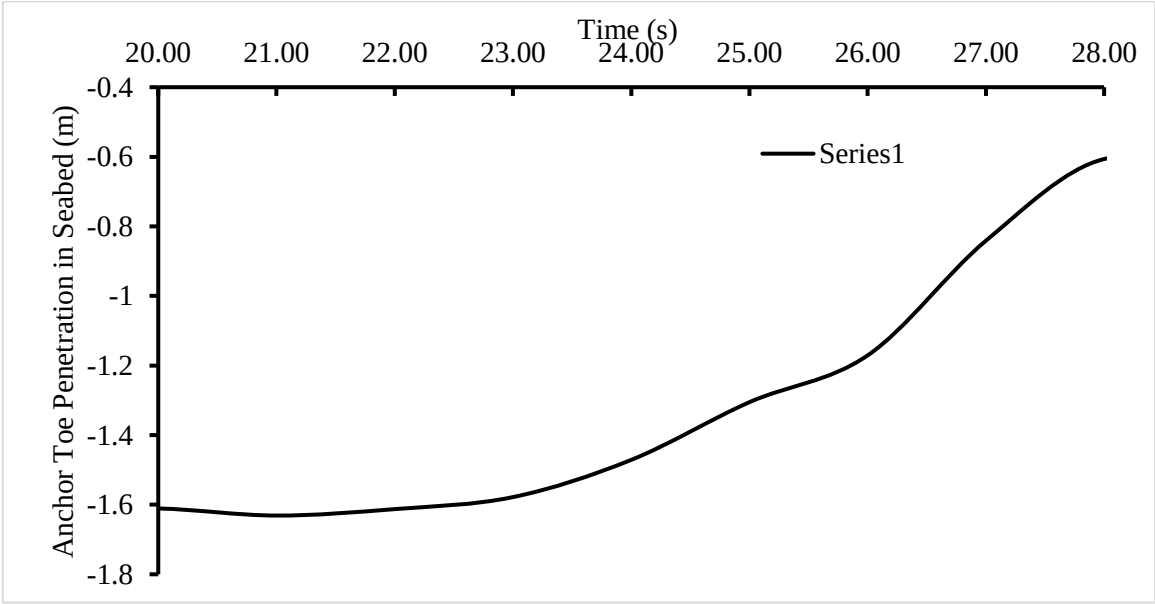

Figure B.5: Anchor toe penetration in seabed, rock berm employed